EFFECT OF VAPOR VELOCITY ON FILM CONDENSATION

James H. Webber

Library
U. S. Naval Postgraduate School
Monterey, California

EFFECT OF VAPOR VELOCITY ON FILM CONDENSATION

by

James H. Webber
U. S. Naval Academy (1949)

SUBMITTED IN PARTIAL FULFILLMENT
OF THE REQUIREMENTS FOR THE
DEGREE OF MASTER OF SCIENCE
at the
MASSACHUSETTS INSTITUTE OF TECHNOLOGY

January 17, 1955

Signature of Author ....
Department of Mechanical Engineering

Certified by ....
Thesis Supervisor

Accepted by ....
Chairman, Departmental Committee on Graduate Students

W33

Mass. Inst. of Tech.
Cambridge 39, Mass.
January 17, 1955

Professor Leicester F. Hamilton
Secretary of the Faculty
Massachusetts Institute of Technology
Cambridge 39, Massachusetts

Dear Sir:

I, hereby submit a thesis entitled "Effect of Vapor Velocity on Film Condensation" in partial fulfillment of the requirements for the degree of Master of Science in the Department of Mechanical Engineering at the Massachusetts Institute of Technology.

Respectfully yours,

James H. Webber

28996

ACKNOWLEDGEMENTS

In bringing this project to a close, it is a pleasure to express my gratitude to those people who have contributed to the work involved.

I am especially grateful to Professor Warren M. Rohsenow for providing the stimulus which initiated this investigation. As thesis supervisor, he suggested many of the basic concepts incorporated herein and his wise advice enabled many of the obstacles to be overcome. His enthusiasm and generous encouragement were primarily responsible for the successful completion of the project.

I am also indebted to Mr. Andrew T. Ling for confirmation of the theoretical work and for many of the calculations entailed in the numerical evaluations. Thanks are due Mr. Dalton Baugh of the M. I. T. Gas Turbine Laboratory for his help in the construction of the experimental equipment and Miss Margaret Tefft for her able secretarial assistance.

EFFECT OF VAPOR VELOCITY ON FILM CONDENSATION

by

James H. Webber

(Submitted to the Department of Mechanical Engineering on January 17, 1955 in partial fulfillment of the requirements for the degree of Master of Science in Mechanical Engineering.)

ABSTRACT

In a vertical plate or tube condenser, the liquid condensate layer (film) flows downward under the influence of gravity forces. Laminar flow generally exists on the upper part of the surface, but turbulent flow will exist on the lower parts if the condensation rate is sufficiently high. If the vapor velocities are appreciable, the vapor exerts a shear stress on the liquid-vapor interface, which may affect the heat transfer coefficients.

The case of laminar flow, under the influence of this vapor shear stress, has been analysed by Nusselt (1). By assuming the "universal velocity distribution" of Prandtl-Nikuradse, Seban (10) obtained analytical predictions for the turbulent film, but neglected the effect of vapor velocities. This thesis extends the previous work by developing equations which include the vapor shear stress effect on a turbulent film. Two criteria for transition are proposed. Application of these criteria permit the present results to be combined with those of Nusselt to give analytical heat transfer coefficients for the case of laminar flow on the upper portion of a plate and turbulent flow on the lower portion.

The results of the analysis are presented in the form of dimensionless plots, Figures 7 to 12, of heat transfer coefficients versus liquid Reynolds Number at the bottom of the plate and also versus plate length. Dimensionless shear stresses and liquid Prandtl Numbers are parameters in these plots. The analytical results are shown to agree closely with Colburn's correlation equation (9) in the range $N_{Pr} = 2$ to 3. However, considerable deviation exists in the very high or very low N_{Pr} range. The Prandtl Numbers covered by this analysis extend from 0.01 to 10.

An experimental set-up for investigating the hydrodynamics of a falling liquid film is described. Preliminary results indicate that

the analytical equations are able to predict film thickness quite accurately for low Reynolds Numbers. However, at higher Reynolds Numbers, some deviation was observed. It is concluded that the Prandtl-Nikuradse velocity distribution is generally adequate for the present purpose of predicting heat transfer coefficients, but that further study is necessary to verify this point.

A procedure utilizing a hot wire anemometer is described, which appears to hold promise in determining transition points in the liquid film.

Thesis Supervisor: Warren M. Rohsenow

Title: Associate Professor of Mechanical Engineering

TABLE OF CONTENTS

Page

Letter of Transmittal

Acknowledgements

Abstract

Table of Contents

List of Figures

List of Symbols

Part I Analytical Investigation of the Effect of a Vapor Shear Stress on Laminar and Turbulent Film Condensation

A. Introduction 2
B. Laminar Analysis 4
C. Transition, Laminar to Turbulent Flow 12
D. Turbulent Analysis 19
E. Discussion of Analytical Results 41
F. Sample Problems 51

Part II Experimental Investigation of Co-Current Liquid-Vapor Flow in a Vertical Tube

A. Survey of the Literature 56
B. Description of Experimental Equipment 60
C. Film Thickness Measurements 70
D. Preliminary Results of Transition Investigation with Hot Wire Anemometer 85
E. Recommendations for Further Experimental Effort 88

Appendices

A. Numerical Evaluation of Analytical Heat Transfer Coefficients 91
B. Calibration of Water Flow Orifice 99
C. Data and Calculations for Film Thickness Measurements 101
D. Bibliography 110

LIST OF FIGURES

Page

1 System Analysed, Force Balance 4

2 Shear Stress Distribution in Liquid Film 5

3 Control Volume for Energy Balance, Laminar Temperature Distribution 7

4 Criteria for Transition, Laminar to Turbulent Flow 18

5 Control Volume for Energy Balance, Turbulent Temperature Distribution 24

6 Regions of Flow, Prandtl-Nikuradse Velocity Distribution 27

7 Analytic Heat Transfer Coefficients vs. z^*, $N_{Pr} = 0.01$ 35

8 Analytic Heat Transfer Coefficients vs. N_{Re}, $N_{Pr} = 0.01$ 36

9 Analytic Heat Transfer Coefficients vs. z^*, $N_{Pr} = 1$ 37

10 Analytic Heat Transfer Coefficients vs. N_{Re}, $N_{Pr} = 1$ 38

11 Analytic Heat Transfer Coefficients vs. z^*, $N_{Pr} = 10$ 39

12 Analytic Heat Transfer Coefficients vs. N_{Re}, $N_{Pr} = 10$ 40

13 Comparison of Analytic Heat Transfer Coefficients with Colburn's Correlation Equation 44

14 Control Volume of Vapor for Evaluating Pressure Gradient 45

15 Test Section 61

16 Probe Port Details 63

17 Photograph of Micrometer Probe 64

18 Schematic of Experimental Apparatus 67

19 Photograph of Experimental Apparatus 68

20 Control Volume of Liquid in Round Tube 70

21 Experimental Film Thickness, $N_{Re} = 338$ 75

22 Experimental Film Thickness, $N_{Re} = 455$ 76

23 Experimental Film Thickness, $N_{Re} = 581$ 77

24 Experimental Film Thickness, $N_{Re} = 641$ 78

25 Experimental Film Thickness, $N_{Re} = 747$ 79

26 Experimental Film Thickness, $N_{Re} = 833$ 80

27 Experimental Film Thickness, $N_{Re} = 2680$ 81

28 Water Orifice Calibration Curve 100

LIST OF SYMBOLS

a	thermal diffusivity, $k/\rho c_p$, ft^2/hr
B	$\frac{\nu}{\nu^+} = \sqrt{\frac{g_o \tau_o}{\rho}}$, Equation (44)
c_p	specific heat, BTU/lbm - °F.
D_e	hydraulic diameter, 4S/Y, ft
F_1	function of film thickness, Equation (51)
F_2	function of film thickness, Equation (47)
g	local acceleration of gravity, ft^2/hr
g_o	universal gravity coefficient, 4.16×10^8 lbm ft/lbf hr^2
G	mass velocity, lbm/hr ft^2
h	local heat transfer coefficient, BTU/hr ft^2 °F.
h_m	mean or average heat transfer coefficient, BTU/hr ft^2 °F.
h_{fg}	latent heat of vaporization, BTU/lbm
h'_{fg}	equivalent latent heat of vaporization, to include subcooling, $h_{fg} + 3/8\, c_p \Delta t$, BTU/lbm
k	thermal conductivity, BTU/hr ft °F.
L	overall length of plate or tube, ft
M	$\frac{1}{(1+\tau_w^*/x_o^*)}$, Equation (45a)
N_{Pr}	Prandtl Number, $c_p \mu/k$
N_{Re}	Reynolds Number, $4\Gamma/\mu$
p	pressure, lbf/ft^2
q	heat transfer rate, BTU/hr
r	distance in a tube from the centerline, ft
r_i	radius of liquid-vapor interface, ft
r_o	outer radius of liquid layer, or inner radius of tube, ft
S	cross-sectional area of flow, ft^2
t	temperature, °F
t_{sat}	saturation temperature, °F
t_f	mean or average film temperature, °F
t_w	plate or tube wall temperature, °F
Δt	temperature difference across condensate film, $t_{sat}-t_w$, °F

u	velocity of vapor, ft/hr
v	velocity of liquid, ft/hr
v_z	velocity of liquid in z-direction, ft/hr
v^+	dimensionless velocity, Equation (38)
w	weight rate of liquid flow, lbm/hr
x	distance from wall, ft
x_o	thickness of condensate film, ft
x^*, x_o^*	dimensionless distances, Equation (15)
x^+, x_o^+	dimensionless distances, Equation (38)
Y	unit width, measured perpendicular to flow direction, ft
z	linear distance, measured from top of plate or tube downward, ft
z^*	dimensionless length, Equation (16)
ρ	density of liquid, lbm/ft^3
ρ_v	density of vapor, lbm/ft^3
μ	viscosity, lbm/ft hr
ν	kinematic viscosity, μ/ρ, ft^2/hr
τ	shear stress, lbf/ft^2
τ_o	wall shear stress, lbf/ft^2
τ_v	vapor shear stress at interface, lbf/ft^2
τ_v^*	dimensionless vapor shear stress, Equation (17)
Γ	flow rate per unit perimeter or width, w/Y, lbm/hr ft
ε_m	momentum eddy diffusivity
ε_h	heat eddy diffusivity

Subscripts

m	mean value over $z = 0$ to L
t	transition point
v	vapor (properties without subscript generally refer to liquid)
z	local value at z, or in z-direction

PART I

ANALYTICAL INVESTIGATION OF THE EFFECT OF A VAPOR SHEAR STRESS ON LAMINAR AND TURBULENT FILM CONDENSATION

PART I

SECTION A - INTRODUCTION

The influence of a vapor shearing stress on condensing film heat transfer coefficients has been shown by several investigators (1, 2, 3, 4) to be quite significant. However, this variable is often neglected in the interest of a manageable theoretical analysis with the result that experimentally determined values of heat transfer coefficients have often differed from predicted values by several fold. The deviation has been much more noticeable in the case of vertical tube condensers where the condensate flows in film form on the inside of the tubes. This seems reasonable when one considers the fact that high vapor velocities are more easily attainable in this case than in the case of horizontal tube condensers or vertical condensers with the condensate in the shell.

Although higher film condensate coefficients can be obtained with high vapor velocities it must be remembered that for vertical tube condensers, the price of this increase in heat transfer ability is an added pressure drop in the condensing section. In the case of steam condensers it is also to be noted that the cooling water side coefficient is usually controlling and little can be gained in overall heat transfer coefficients by decreasing the condensate resistance to heat flow. However, many industrial applications involving the condensation of organic

vapors are concerned with condensate coefficients as high as, or higher than the cooling water coefficients. It is in cases such as these that reductions in size and weight may be possible through the judicious use of this vapor shear effect.

A condensate film flowing vertically under the influence of gravity and a vapor shear stress lends itself remarkably well to theoretical attack. It is the purpose of this thesis, therefore, to attempt to further the previous analyses by deriving expressions for average heat transfer coefficients which include both laminar and turbulent condensate layers under the influence of a vapor shear stress. To simplify the resulting expressions, and at the same time give results of universal applicability, the case of a flat plate is considered. The equations may also be applied to tubes as long as the thickness of the condensate film is small compared to the tube radius, and as long as the effects of a pressure gradient may be neglected.

SECTION B - LAMINAR FILM

In the following analysis the case of a flat vertical plate, Figure 1, is considered. Condensation is of a pure, saturated vapor with no noncondensible gases present. Assumptions include constant wall temperature and constant fluid properties. The specific heat, c_p, density, ρ, and thermal conductivity, k, may be determined at the arithmetic average film temperature. The viscosity, μ, however, should be determined at the special average film temperature recommended by Colburn (5), and defined by

$$t_f = t_v - 3/4 \Delta t \qquad (1)$$

The vapor shear stress, τ_v, is considered as being directly downward, and being constant along the length of the plate.

The laminar analysis essentially follows that of Nusselt (1), where the film is in streamline motion and is under the influence of a vapor shear stress, τ_v, as shown in Figure 1.

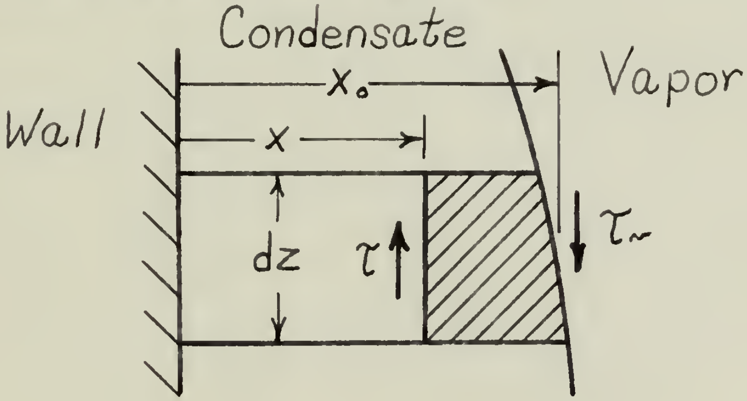

FIGURE 1

By assuming steady flow and neglecting momentum changes, a force balance for the shaded element shown gives,

$$\tau - \frac{g}{g_o}(\rho - \rho_v)(x_o - x) - \tau_v = 0 \qquad (2)$$

This gives the linear distribution of shear stress shown in Figure 2. Since $\tau = \tau_o$ at $x = 0$, the wall shear stress is given by

$$\tau_o = \frac{g}{g_o}(\rho - \rho_v)\, x_o + \tau_v \qquad (3)$$

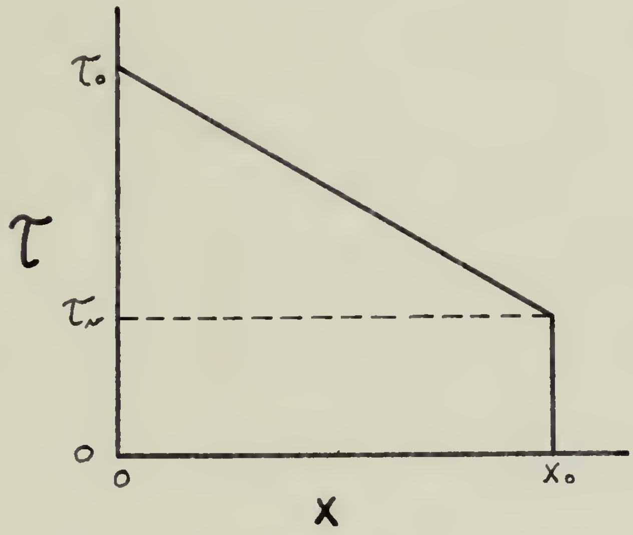

FIGURE 2

The effect of the momentum crossing the element faces within the liquid is quite small. To include the momentum effect at the liquid-vapor interface the term which should be added to Equation (2) is $(1/g_o)v_{z,x_o}\, d\Gamma$. This represents the z direction velocity of the vapor crossing the liquid-vapor interface, which is very nearly equal to the liquid surface

velocity, v_{z,x_o}, and not the velocity of the vapor flow in the main vapor stream. This momentum term also is usually quite small.

From Newton's definition of viscosity, we have for laminar flow,

$$\tau = \frac{\mu}{g_o} \frac{dv_z}{dx} \qquad (4)$$

Substituting in Equation (2) for τ gives,

$$dv_z = \frac{g}{\mu} (\rho - \rho_v)(x_o - x)dx + \frac{g_o}{\mu} \tau_v dx \qquad (5)$$

This expression may be integrated across the film with τ_v constant, giving the velocity profile as

$$v_z = \frac{g}{\mu} (\rho - \rho_v) (x_o x - x^2/2) + \frac{g_o}{\mu} \tau_v x \qquad (6)$$

The mass rate of flow per unit width of the vertical plate, Γ, may be found by

$$\Gamma = \int_0^{x_o} \rho\, v_z\, dx \qquad (7)$$

Carrying out this integration gives Γ in terms of film thickness, x_o,

$$\Gamma = \frac{\rho}{\mu} \left[g(\rho - \rho_v) \frac{x_o^3}{3} + \frac{g_o \tau_v x_o^2}{2} \right] \qquad (8)$$

Equation (8) may be differentiated with respect to x_o to give a relationship between the change in mass flow rate per unit width and the change in film thickness,

$$d\Gamma = \frac{\rho}{\mu} \left[g(\rho - \rho_v) x_o^2 + \frac{g_o \tau_v x_o}{\mu} \right] dx_o \qquad (9)$$

A linear temperature gradient may be assumed to exist within the condensate film without introducing serious error. Reference (6) gives

a complete treatment of the magnitudes involved in this assumption. Consider the control volume shown in Figure 3.

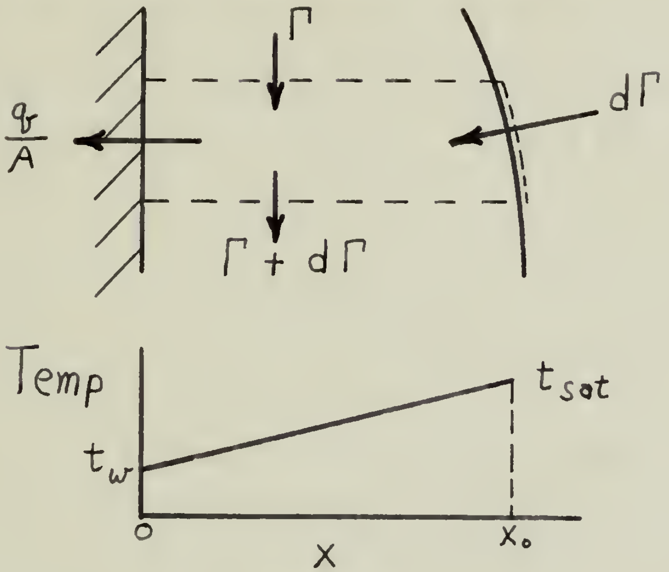

FIGURE 3

If the enthalpy of Γ entering through the upper surface of the control volume is taken at a mean film temperature, it can be seen that the Γ leaving through the lower surface of the control volume will also be at this same film temperature and hence will not enter into an energy balance. It is also evident that the enthalpy change of the increment of condensate, $d\Gamma$, will be equal to the enthalpy difference between saturated vapor and a liquid at the mean film temperature. This may be designated h'_{fg} and has been evaluated by Colburn, Millar, and Westwater (7) as $h'_{fg} = h_{fg} + 3/8\, c_p \Delta t$. On the basis of the previous discussion an energy balance for the control volume shown in Figure 3 may be made by equating the heat transfer to the change in enthalpy of the incremental increase in condensate, $h'_{fg}\, d\Gamma$,

$$\frac{q}{A}\,dz = h'_{fg}\;d\Gamma \qquad (10)$$

Since the film considered is in laminar motion, the heat transfer coefficient may be taken as the thermal conductivity of the fluid divided by the film thickness,

$$\frac{q}{A} = h\,\Delta t = \frac{k}{x_o}\,\Delta t \qquad (11)$$

Eliminating q/A between Equations (10) and (11) and substituting for $d\Gamma$ its equivalent from Equation (9), we have a differential expression containing only dz and dx_o as variables,

$$\frac{k\,\Delta t}{h'_{fg}}\,dz = \left[\frac{g}{\mu}\,\rho(\rho - \rho_v)x_o^{3} + \frac{g_o}{\mu}\,\rho\;\tau_v x_o^{2}\right]\,dx_o \qquad (12)$$

Equation (12) may be integrated from the top of the plate where $x_o = 0$ when $z = 0$, to a point x_o, z.

$$\frac{k\Delta t}{h'_{fg}}\,z = \frac{g}{\mu}\,\rho(\rho - \rho_v)\,\frac{x_o^{4}}{4} + \frac{g_o}{\mu}\,\rho\;\tau_v\,\frac{x_o^{3}}{3} \qquad (13)$$

By rearranging and substituting the Prandtl number, $N_{pr} = c_p\mu/k$, the resulting expression is obtained,

$$\frac{4z\,\Delta t}{N_{Pr}}\;\frac{c_p}{h'_{fg}}\left(\frac{g}{\mu^2}\right)^{1/3}\frac{1}{\left(1-\frac{\rho_v}{\rho}\right)} = \frac{X_o^{4}}{\left(\frac{\mu^2}{g}\right)^{4/3}} + \frac{4}{3}\;\frac{g_o\,\tau_v}{g\,(\rho-\rho_v)}\;\frac{X_o^{3}}{\left(\frac{\mu^2}{g}\right)^{4/3}} \qquad (14)$$

The following dimensionless lengths may be defined as

$$x_o^{*} \equiv \frac{x_o}{(\mu^2/g)^{1/3}} \qquad (15)$$

$$z^{*} \equiv \frac{4z\,\Delta t}{N_{Pr}}\;\frac{c_p}{h'_{fg}}\left(\frac{g}{\mu^2}\right)^{1/3}\frac{1}{\left(1-\frac{\rho_v}{\rho}\right)} \qquad (16)$$

Further define a dimensionless vapor shear stress, τ_v^*, as

$$\tau_v^* \equiv \frac{g_o \tau_v}{g(\rho-\rho_v)\left(\frac{\nu^2}{g}\right)^{1/3}} \tag{17}$$

Substituting these definitions in Equation (14) gives a simple and convenient expression for the variation of film thickness with length of the plate, z^*.

$$z^* = (x_o^*)^4 + 4/3 \ \tau_v^* (x_o^*)^3 \tag{18}$$

The usefulness of the dimensionless quantities defined by Equations (15), (16), and (17) may be more fully realized by deriving expressions for the film Reynold's Number and mean heat transfer coefficient as follows.

Define a film Reynold's Number, N_{Re}, by

$$N_{Re} = \frac{(w/S)\,D_e}{\mu} = \frac{(w/S)(4S/Y)}{\mu} = \frac{4\Gamma}{\mu} \tag{19}$$

By making use of Equation (8) for Γ, we may write

$$N_{Re} = \frac{4\Gamma}{\rho\nu} = \frac{4}{\rho\nu}\,\frac{1}{\nu}\left[g(\rho-\rho_v)\frac{x_o^3}{3} + g_o\tau_v\frac{x_o^2}{2}\right] \tag{20}$$

Rearranging the above expression, we have,

$$\frac{N_{Re}}{\left(1-\frac{\rho_v}{\rho}\right)} = \frac{4}{3}\,\frac{x_o^3}{\left(\frac{\nu^2}{g}\right)} + 2\,\frac{g_o}{g}\,\frac{\tau_v x_o^2}{\left(\frac{\nu^2}{g}\right)(\rho-\rho_v)} \tag{21}$$

Now by substituting the previously defined values of x_o^* and τ_v^*

$$\frac{N_{Re}}{\left(1-\frac{\rho_v}{\rho}\right)} = \frac{4}{3}\,(x_o^*)^3 + 2\,\tau_v^*\,(x_o^*)^2 \tag{22}$$

The original Nusselt relation gave only point values of the heat transfer coefficient and was difficult to apply in an actual design study as it involved a function of the condensate flow rate. This difficulty can be avoided, however, if a mean or average heat transfer coefficient is defined as,

$$h_m \equiv \frac{\Gamma\, h'_{fg}}{z\, \Delta t} \qquad (23)$$

By substituting Equation (8) for Γ in Equation (23) we have

$$h_m = \frac{h'_{fg}}{z\,\Delta t}\,\frac{1}{\nu}\left[g(\rho-\rho_v)\frac{x_o^3}{3} + g_o\,\tau_v\,\frac{x_o^2}{2}\right] \qquad (24)$$

Introducing the Prandtl Number and rearranging,

$$\frac{h_m}{k}\left(\frac{\nu^2}{g}\right)^{1/3} = \frac{N_{Pr}}{4}\,\frac{h'_{fg}}{c_p}\,\frac{1}{z\Delta t}\left(1-\frac{\rho_v}{\rho}\right)\left(\frac{\nu^2}{g}\right)^{1/3}\frac{4}{\nu^2}\left[\frac{1}{3}\,\frac{x_o^3}{\left(\frac{\nu^2}{g}\right)} + \frac{1}{2}\,\frac{g_o}{g}\,\frac{\tau_v\,x_o^2}{(\rho-\rho_v)\left(\frac{\nu^2}{g}\right)}\right] \qquad (25)$$

Making use of the dimensionless terms z^*, x_o^*, and τ_v^*, this reduces to

$$\frac{h_m}{k}\left(\frac{\nu^2}{g}\right)^{1/3} = \frac{4}{3}\,\frac{(x_o^*)^3}{z^*} + 2\,\tau_v^*\,\frac{(x_o^*)^2}{z^*} \qquad (26)$$

Equations (18), (22), and (26) completely define the results for the laminar region. For given values of the dimensionless shear stress, τ_v^*, either the mean heat transfer coefficient group, or the N_{Re} can be plotted as a function of the dimensionless length of the plate, z^*. This involves assuming values of x_o^* and then solving for z^* from

Equation (18), N_{Re} from Equation (22), and $\frac{h_m}{k}\left(\frac{\nu^2}{g}\right)^{1/3}$ from Equation (26). This has been done for various N_{Pr} and forms the basis for the curves to the left of the transition points in Figures 7 to 12. The use of these curves in a design case will be discussed in a later section, where the results of a turbulent film as well as the laminar film have been derived, and are plotted in terms of these same variables.

SECTION C - TRANSITION

For a liquid flowing in film form down a vertical surface it seems reasonable to postulate that there will be transition from laminar flow to turbulent flow at a critical Reynolds number, in much the same manner that transition occurs in a pipe full of fluid. When we speak of a critical Reynolds number it is to be remembered that this is not a definite, distinct point at which transition will occur in all cases. Rather it represents some sort of a mean value where the turbulence is sufficiently developed to materially affect the velocity profile within the film and where turbulent velocity fluctuations will be evident to the extent of affecting such characteristics of the film as the heat transfer coefficient.

Before proceeding with a discussion of transition, it becomes necessary to define a Reynolds number to give a common basis of comparison. In the case under consideration it has become accepted to define the Reynolds number in terms of the mass rate of flow per unit cross-sectional area, (w/S), the average fluid viscosity, μ, and an equivalent hydraulic diameter commonly taken as $(4S/Y)$, where Y is the unit width of the plate down which the fluid is flowing. In terms of these quantities, the Reynolds number may be defined as,

$$N_{Re} = \frac{(w/S)\,D_e}{\mu} = \frac{(w/S)(4S/Y)}{\mu} = \frac{4\Gamma}{\mu} \qquad (27)$$

Although there has been little experimental work with the specific

aim of determining the transition point of a freely falling vertical film, certain points may be inferred from heat transfer data. In references (12) and (13) on the basis of somewhat limited data it is recommended that a Reynolds number of 1800 be taken as the transition point for the case of zero vapor shear stress. It will be shown later that considerable doubt exists as to this value, however from the present extent of knowledge no more precise value can be predicted. Therefore, for the purposes of the analysis, this criterion for transition will be adopted. One of the objectives of the experimental work undertaken as part of this thesis will be to determine more adequate information on transition.

Although we have adopted a critical Reynolds number of 1800 for zero vapor shear stress, there remains the considerable problem of considering how a shear stress may modify this value. Carpenter (3) has suggested that under the influence of a vapor shear stress, transition will occur at a given value of wall shear stress. This may be more readily visualized by considering the layer of fluid next to the wall. In laminar flow the sole effect of the outer layers on this inner layer will be a shear stress exerted on it. In effect, all the inner layer "sees" of the outer layer is a transmitted shear stress. If we first consider the case of zero vapor flow, but increasing liquid flow, this inner layer next to the wall will trip over to turbulent motion when the Reynolds number attains the value 1800. However, all the inner layer "knows" of this condition is a certain value of transmitted shear stress.

Now, considering the case of a finite vapor shear stress, it is reasonable to assume that the layer next to the wall will change to turbulent flow whenever this "critical" shear stress is exerted on it, whether by outer layers of liquid or by an outer layer of vapor. Taking the wall shear stress, τ_o, as the most convenient to which to apply this criterion of critical shear stress, we may find its value from the known case of transition at a Reynolds number of 1800 with zero vapor shear stress. From Equation (3), τ_o can be expressed in terms of x_o for $\tau_v = 0$,

$$\tau_o = \frac{g}{g_o} (\rho - \rho_v)\, x_o$$

Similarly Γ, and hence Reynolds number, $\frac{4\Gamma}{\mu}$, may also be expressed in terms of x_o from Equation (8),

$$\left(\frac{4\Gamma}{\mu}\right)_{tran} = 1800 = 4/3\, \frac{g}{\nu^2} (1 - \rho_v/\rho)\, x_o^3$$

Eliminating x_o between these two equations we are able to arrive at an expression for the critical wall shear stress, designated by $(\tau_o)_{tran}$,

$$(\tau_o)_{tran} = \frac{g}{g_o} (\rho - \rho_v) \left[\frac{1350\ (\nu^2/g)}{(1 - \rho_v/\rho)} \right]^{1/3} \qquad (28)$$

For the more general case where $\tau_v \neq 0$, we apply our postulation that transition will still occur at this value of a critical wall shear stress derived above. From equation (3) we have an expression for τ_o in the presence of a vapor shear stress. By introducing the value of wall shear stress obtained in Equation (28) and rearranging, the following expression for the dimensionless film thickness at transition can be obtained,

$$(x_o^*)_{tran} = \frac{11.05}{(1 - \rho_v/\rho)^{1/3}} - \tau_v^* \qquad (29)$$

Substituting this value in Equation (22) gives an equation for the transition Reynolds numbers in terms of the only variable, τ_v^*.

$$\left(\frac{4\Gamma}{\mu}\right)_{tran} = 1800 - 246(1-\rho_v/\rho)^{1/3}\,\tau_v^* + 0.667(1 - \rho_v/\rho)\,(\tau_v^*)^3 \qquad (30)$$

This function is plotted in Figure 4 from a value of $\tau_v^* = 0$ to $\tau_v^* = 9.2$.

Inspection of Equation (29) will reveal that whenever $\tau_v^* > \frac{11.05}{(1-\rho_v/\rho)^{1/3}}$, the dimensionless film thickness, x_o^*, will be negative at transition. Obviously this is impossible physically and represents a limit to the applicability of the previously discussed criterion for transition. In the higher ranges of vapor shear stress, we must, therefore, develop a new criterion.

For the higher values of τ_v^* it is quite possible that the film thickness at transition approaches a limiting value, perhaps that of the laminar sublayer thickness which exists in ordinary pipe flow. Carpenter (3) suggests the following magnitude for this thickness:

$$(x_o^+)_{tran} = \frac{x_o}{\nu}\sqrt{\frac{g_o\,\tau_o}{\rho}} = 6 \qquad (31)$$

Ordinarily a magnitude of 5 expresses the laminar sublayer thickness. Actually an appropriate value is somewhere between 5 and perhaps 10. The value of 6 is arbitrarily chosen.

If Equation (31) is solved for τ_o and this expression substituted in Equation (3), the following cubic equation relating film thickness

and vapor shear stress is obtained,

$$(x_{o\,t}^{*})^3 + (x_{o\,t}^{*})^2 \, \tau_v^* = \frac{36}{1 - \rho_v/\rho} \qquad (32)$$

For a given value of τ_v^*, x_o^* may be found from this equation through a trial and error process. With this value of x_o^* and the given value of τ_v^*, the Reynolds number may be found through the use of Equation (22). The resulting plot is shown in Figure 4 for values of $\tau_v^* > 9.2$. It can be seen that the assumption of transition at $x_o^+ = 6$ is almost equivalent to the assumption of transition at a Reynolds number of about 70 to 80, there being little variation of Reynolds number with vapor shear stress.

This appears on first observation to be a somewhat startingly low Reynolds number at which to expect transition, however, there is a logical basis for its selection. There is very little good data available to establish conditions under which transition occurs when there is a significant vapor shear stress. A single point can be obtained from the enthanol data of Carpenter (3) by plotting his experimental points and noting the region of departure from the Nusselt laminar prediction. This transition point at a $\tau_v^* = 110$ and Reynolds number of 96.5 agrees fairly well with the transition Reynolds number of 71.8 predicted under the present analysis. In terms of x_o^+ the transition data have the value of 6.9 which is close to the 6 of Equation (31).

Although the criteria for transition as portrayed by Figure 4 have not been adequately substantiated, the results are nevertheless quite reasonable and are probably not seriously in error. This entire

phenomenon of transition as affected by vapor shear stress must be investigated by obtaining much more experimental data. In spite of lack of adequate substantiation it seems reasonable to select the transition criteria as shown in Figure 4 for use in the present analysis.

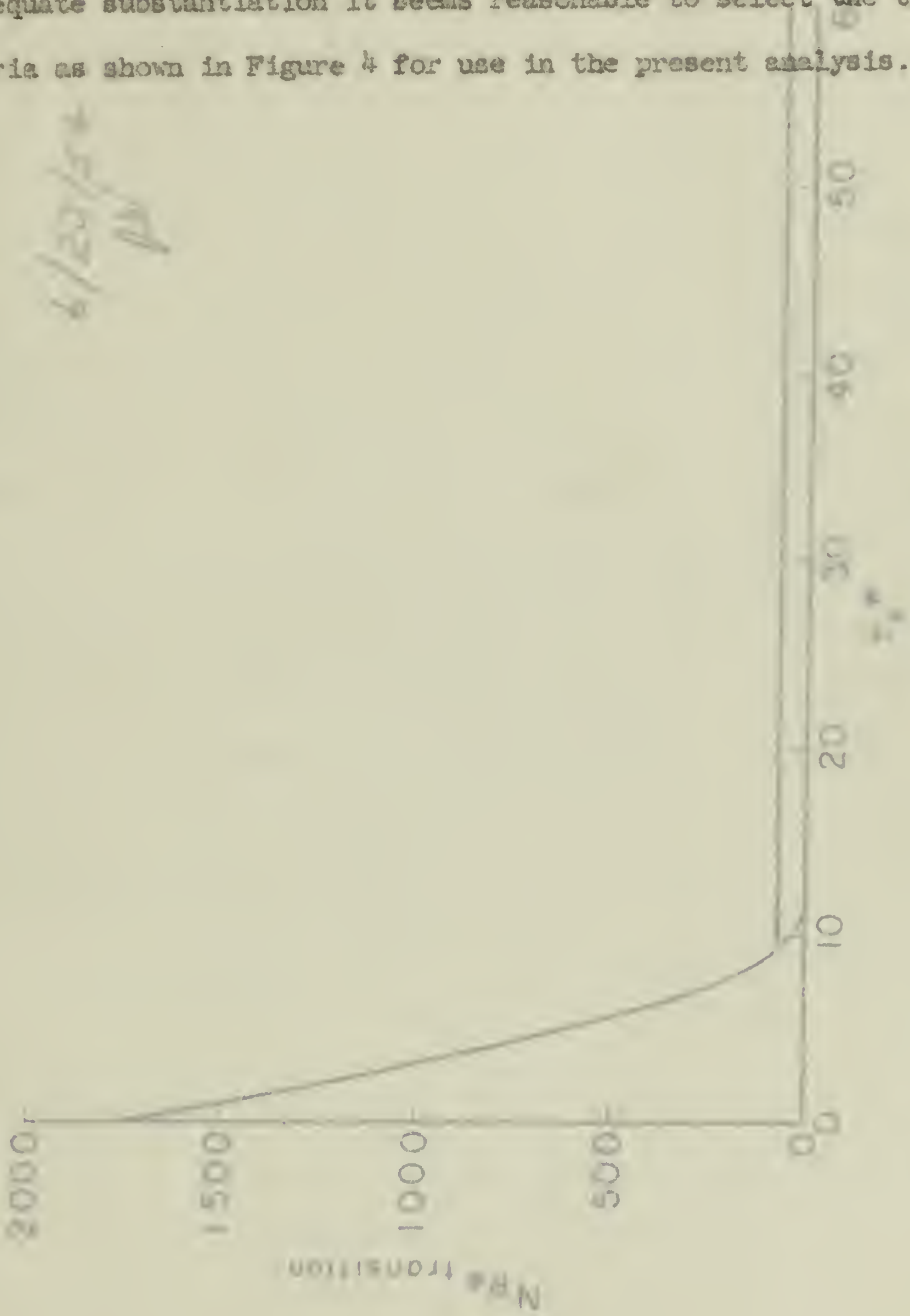

FIGURE 4

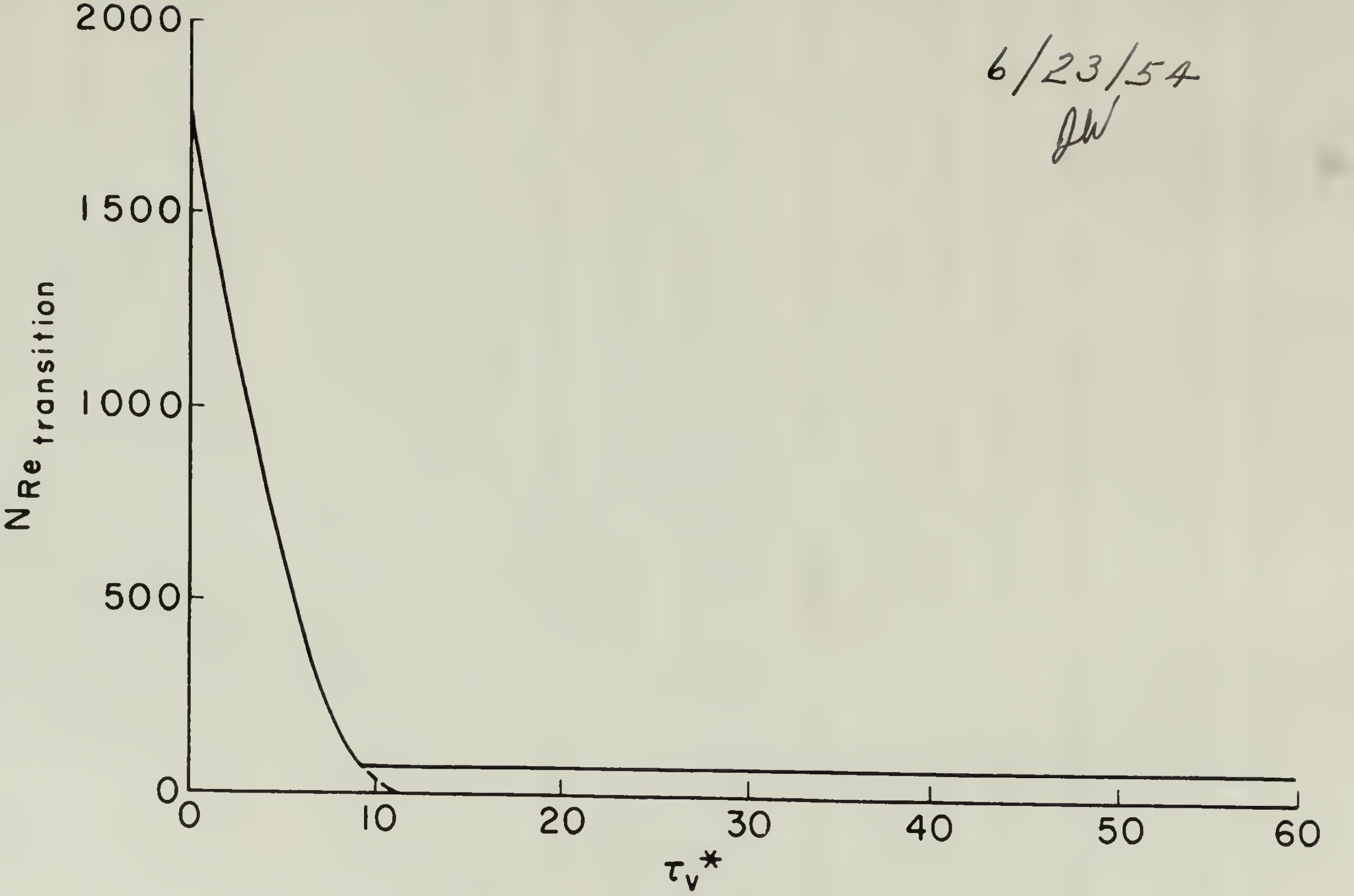

6/23/54
JW

FIGURE 4

SECTION D - TURBULENT ANALYSIS

When condensate flow rates become large, it seems reasonable to predict that turbulent flow will result, with considerable effect on the heat transfer coefficients. It was observed experimentally by Kirkbride (2) that, in the case of vapor condensing on the outside of vertical tubes, measured heat transfer coefficients differed considerably from those predicted by the Nusselt laminar analysis. In these investigations there was evidently no appreciable vapor shear stress.

Colburn (8) reviewed the results of Kirkbride and, by assuming that the sole resistance to heat transfer lay in the laminar sublayer, was able to derive heat transfer equations for a turbulent condensate layer. The Prandtl-Nikuradse velocity distribution was assumed, and by selecting the thickness of the laminar sublayer at about $x^+ = 10$, a satisfactory correlation of the data was obtained. This equation, as presented by Colburn (8) is

$$\frac{h}{k}\left(\frac{\mu^2}{g}\right)^{1/3} = 0.056\,(N_{Pr})^{1/3}\left(\frac{4\Gamma}{\mu}\right)^{0.2} \tag{33}$$

It is to be noted that the Prandtl number enters here, while it did not in the laminar analysis. This does not seem unusual when one considers the correlation equations for heat transfer in pipes with no phase change. However, it should also be noted that this correlation was applied principally to Kirkbride's data, with only small variation of N_{Pr} in the range of 2 to 5.

The above analysis was extended by Carpenter and Colburn (3,9) to include the effect of a vapor shear stress. In reference (3) heat transfer coefficients were investigated in a 5/8 inch copper tube 9 feet long. Special effort was made to accurately measure pressure drop, from which the magnitude of the vapor shear stress could be obtained. As the result of the experimental work and theoretical investigations, the following correlation equation for point values of heat transfer coefficients was obtained:

$$\frac{h\mu}{k\rho^{1/2}} = 0.043\,(N_{Pr})^{1/2}\;\tau_v^{\,1/2} \tag{34}$$

By integrating over the length of the tube, an equation for mean heat transfer coefficients was also obtained

$$\frac{h_m\mu}{k\rho^{1/2}} = 0.065\,(N_{Pr})^{1/2}\;\tau_v^{\,1/2} \tag{35}$$

By the introduction of the dimensionless vapor shear stress defined in Equation (17), this equation may readily be converted into the form

$$\frac{h_m}{k}\left(\frac{\nu^2}{g}\right)^{1/3} = 0.065\,(N_{Pr})^{1/2}\,(\tau_v^{*})^{1/2} \tag{36}$$

The question of properly evaluating the vapor shear stress becomes somewhat complex when it is realized that, as condensation is taking place along the length of the tube, the vapor velocity is continually

decreasing. For convenience in making calculations, Carpenter and Colburn recommend taking a mean vapor shear stress, evaluated from the usual plots of friction factor for one component flow at a vapor mass velocity,

$$G_m = \left(\frac{G_1^2 + G_1G_2 + G_2^2}{3} \right)^{1/2} \tag{37}$$

where G_1 is the value of G at the top of the tube, and G_2 is its value at the bottom. It is felt that this represents somewhat of an oversimlification and that the friction factor should at least be evaluated from the limited data on concurrent two phase flow available (11). In reference (11) it is shown that there is considerable variation of friction factor from the smooth pipe data, mainly due to the fact that the liquid layer presents a rough surface to the flowing vapor.

One point especially worthy of comment in connection with the work of Carpenter and Colburn is their consideration of the momentum flux across the liquid-vapor interface. In their derivation they evaluate this term as the product of the increment of condensate, $d\Gamma$, and the main stream vapor velocity. This in effect assumes one dimensional flow of the vapor. In view of the fact that a vapor shear stress is also considered, it seems somewhat contradictory to assume, when evaluating the momentum term, that a zero velocity gradient exists at the interface, and, when considering the vapor shear stress, to assume a finite velocity gradient. It seems more realistic to visualize the

layer of vapor immediately next to the interface as flowing with essentially the same velocity as the interface itself. In this case it can be readily seen that such momentum terms will be small. It is through this line of reasoning that this momentum term has been neglected in the present analysis.

Quite recently Seban (10) has applied analogy calculations of the Prandtl-Karman type to a turbulent condensate layer, assuming the "universal velocity distribution" of Prandtl-Nikuradse. The improvement over previous analyses lies in the fact that the resistence to heat transfer of the complete condensate layer is considered, rather than just the resistance of the laminar sublayer. Seban's analytical results extend over the considerable range of N_{Pr} of 0.01 to 5 and agree well with the empirical results of Colburn (8) in the range $N_{Pr} = 2$ to 5. In the derivation Seban neglected the possible effects of a vapor shear stress. It is the purpose of the present analysis to extend Seban's results to include this effect and to complete the story by obtaining mean heat transfer coefficients which include a laminar region at the top of the plate, followed by a turbulent range over the lower regions.

Turbulence has no effect on the force balance for a control volume in the condensate film if we think of the shear stress as an apparent τ rather than the Newtonian viscous shear stress. Therefore, the resulting force balance equation will be identical with that for the laminar case, and is given by Equations (2) and (3). The same linear distribution of shear stress within the film will exist.

$$\tau = \frac{g}{g_o}(\rho - \rho_v)(x_o - x) + \tau_v \qquad (2)$$

$$\tau_o = \frac{g}{g_o}(\rho - \rho_v)\,x_o + \tau_v \qquad (3)$$

Since Newton's law of viscous shear will not hold in the turbulent region, it is impossible to obtain analytically an expression for the velocity distribution within the condensate film. This analysis will be based on the assumption that the velocity distribution will be that of the Prandtl-Nikuradse formulation as given in reference (12) .

For $0 < x^+ < 5$ $\qquad v^+ = x^+$

$5 < x^+ < 30$ $\qquad v^+ = -3.05 + 5.0 \ln x^+$

$30 < x^+$ $\qquad v^+ = 5.5 + 2.5 \ln x^+$

where:

$$x^+ \equiv \frac{x}{\nu}\sqrt{\frac{g_o\tau_o}{\rho}} \qquad v^+ \equiv v\sqrt{\frac{\rho}{g_o\tau_o}} \qquad (38)$$

The apparent shear stress, τ , for turbulent flow may be expressed as the sum of the viscous shear stress and the eddy diffusivity times the velocity gradient.

$$\tau = \left(\mu + \frac{\rho}{g_o}\,\varepsilon_m\right)\frac{dv}{dx} \qquad (39)$$

where ε_m is the eddy diffusivity.

Rearranging, $\dfrac{g_o\tau}{\rho} = (\nu + \varepsilon_m)\dfrac{dv}{dx}$

Substituting for τ from Equation (2)

$$\frac{g_o}{\rho}\left[\frac{g}{g_o}(\rho - \rho_v)(x_o - x) + \tau_v\right] = (\nu + \varepsilon_m)\frac{dv}{dx}$$

Considering the region in the film where $30 < x^+ < x_o^+$, it may be assumed that $\nu \ll \varepsilon_m$. Solving for ε_m/ν,

$$\frac{\varepsilon_m}{\nu} = \frac{\dfrac{g_o \tau_w}{\rho \nu} + \dfrac{g(1-\rho_v/\rho)(x_o - x)}{\nu}}{\dfrac{dv}{dx}} \tag{40}$$

The term dv/dx may be evaluated for the region under consideration ($30 < x^+ < x_o^+$) from the assumed universal velocity distribution,

$$v^+ = 5.5 + 2.5 \ln x^+$$

$$v = \sqrt{\frac{g_o \tau_o}{\rho}}\left[5.5 + 2.5 \ln\left(\frac{x}{\nu}\sqrt{\frac{g_o \tau_o}{\rho}}\right)\right]$$

$$dv/dx = 2.5\sqrt{\frac{g_o \tau_o}{\rho}}\;\frac{1}{x} \tag{41}$$

The control volume for the energy balance is shown in Figure 5. Also shown is the type of temperature distribution to be expected for turbulent flow.

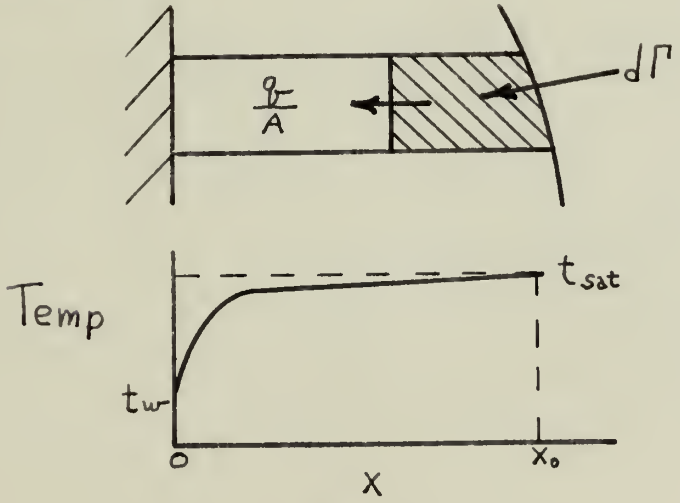

FIGURE 5

For the shaded control volume it can be seen that there will be no enthalpy change for the portion of condensate entering through the upper surface and leaving through the lower surface. Further, it is apparent that the enthalpy change of the increment of condensate will be essentially that from saturated vapor to saturated liquid. Therefore, an energy balance will be of the form,

$$\frac{q}{A}\,dz = h_{fg}\;d\Gamma$$

As the left side of the control surface is moved across the film toward the wall, the above statements will hold true except for the thin layer next to the wall where the temperature distribution experiences a sharp change in slope. Since this layer is thin, the effect of subcooling may be neglected for the turbulent film and q/A will equal $(q/A)_o$, or the heat transfer per unit area at the wall. Introducing this into the energy balance, we have

$$\left(\frac{q}{A}\right)_o = \frac{q}{A} = h_{fg}\,\frac{d\Gamma}{dz} \tag{42}$$

The equation for heat transfer across a turbulent film may be written in the form

$$\frac{(q/A)}{\rho\, c_p} = (a + \varepsilon_h)\,\frac{dt}{dx} \tag{43}$$

where $a = \dfrac{\nu}{N_{Pr}}$ = thermal diffusion coefficient

ε_h = eddy diffusion coefficient

Through the application of the heat - momentum transfer analogy that $\varepsilon_h = \varepsilon_m$, and knowing the velocity gradients throughout the film

from the assumed velocity distribution, we are able to obtain an expression for the temperature gradients. By substituting ε_h for ε_m in Equation (40) and the velocity gradient from Equation (41), we obtain

$$\frac{\varepsilon_h}{\nu} = \frac{\dfrac{g_0 \tau_w}{\rho \nu} + \dfrac{g(1-\rho_v/\rho)(X_0 - x)}{\nu}}{2.5\sqrt{\dfrac{g_0 \tau_0}{\rho}}\;\dfrac{1}{x}}$$

Substituting this expression in Equation (43), the desired expression involving dt/dx and x as the only variables is obtained.

$$\frac{(q/A)}{\rho\, c_p\, \nu} = \left[\frac{1}{N_{Pr}} + \frac{\dfrac{g_0 \tau_w}{\rho \nu} + \dfrac{g(1-\rho_v/\rho)(X_0 - x)}{\nu}}{2.5\,\dfrac{1}{x}\sqrt{\dfrac{g_0 \tau_0}{\rho}}}\right]\frac{dt}{dx}$$

Solving for dt and introducing, for convenience sake, the following notation, $B \equiv \dfrac{v}{v^+} = \sqrt{\dfrac{g_0 \tau_0}{\rho}} = \sqrt{\dfrac{g_0 \tau_w}{\rho} + g(1-\rho_v/\rho)\,X_0}$

$$dt = \frac{(q/A)}{\rho\, c_p\, \nu}\;\frac{dx}{\dfrac{1}{N_{Pr}} + \dfrac{1}{2.5\nu}\,Bx - \dfrac{g(1-\rho_v/\rho)\,x^2}{2.5\,\nu\, B}} \tag{44}$$

The condensate film may be divided into the following regions:

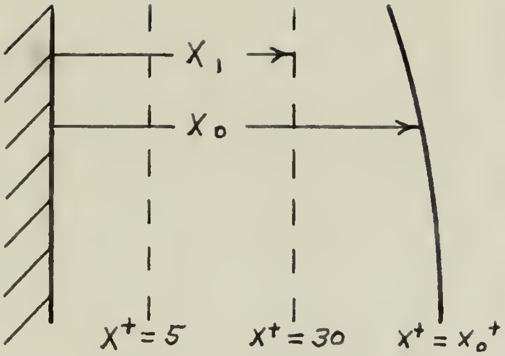

FIGURE 6

Equation (44) contains only two variables, t and x, since we have shown that q/A will be constant across the film. This equation may then be integrated between the limits t_{x_1} to t_{x_0} and x_1 to x_0. After considerable algebraic manipulation and simplification, the result of this integration across the film may be expressed as,

$$\frac{(t_{x_0}-t_{x_1})}{(q/A)}\,\rho C_p\sqrt{\frac{g(1-\rho_v/\rho)x_0}{M}} = \frac{2.5}{\sqrt{1+\frac{10}{N_{Pr}X_0^+}M}}\;\ln\left[\frac{2M-1+\sqrt{1+\frac{10}{N_{Pr}X_0^+}M}}{2M-1-\sqrt{1+\frac{10}{N_{Pr}X_0^+}M}}\cdot\frac{\frac{60}{X_0^+}M-1-\sqrt{1+\frac{10}{N_{Pr}X_0^+}M}}{\frac{60}{X_0^+}M-1+\sqrt{1+\frac{10}{N_{Pr}X_0^+}M}}\right] \tag{45}$$

$$\text{where } M \equiv \frac{1}{\frac{g_0\tau_v}{g(\rho-\rho_v)x_0}+1} = \frac{1}{1+\frac{\tau_v^*}{X_0^*}} \tag{45a}$$

Equation (45) gives an expression for the temperature drop across the highly turbulent core of the condensate film. By utilizing the results of a previous analysis by Von Karman (14) for the temperature difference between the wall and the outer edge of the buffer layer ($x^+ = 30$), we can obtain an expression for the total temperature difference from the liquid-vapor interface to the wall. Von Karman's results may be put in the form

$$\frac{(t_{x_1} - t_w)}{(q/A)} \rho C_p \sqrt{\frac{g(1-\rho_v/\rho)X_0}{M}} = 5 N_{Pr} + 5 \ln(1 + 5 N_{Pr}) \tag{46}$$

Adding Equations (45) and (46) to obtain the total temperature drop across the film,

$$\frac{(t_{x_0} - t_w)}{(q/A)} \rho C_p \sqrt{\frac{g(1-\rho_v/\rho)X_0}{M}} = \left[5 N_{Pr} + 5 \ln(1 + 5 N_{Pr})\right] + \frac{2.5}{\sqrt{1 + \frac{10}{N_{Pr} X_0^+} M}} \ln \left[\frac{2M - 1 + \sqrt{1 + \frac{10}{N_{Pr} X_0^+} M}}{2M - 1 - \sqrt{1 + \frac{10}{N_{Pr} X_0^+} M}} \quad \frac{\frac{60}{X_0^+} - 1 - \sqrt{1 + \frac{10}{N_{Pr} X_0^+} M}}{\frac{60}{X_0^+} - 1 + \sqrt{1 + \frac{10}{N_{Pr} X_0^+} M}} \right] \tag{47}$$

Let the right hand side of Equation (47) equal F_2, then this expression may be written

$$\frac{\Delta t}{(q/A)} \rho C_p \sqrt{\frac{g(1-\rho_v/\rho)X_0}{M}} = F_2 \tag{47a}$$

For $x_o^+ > 30$

$$\Gamma = \rho\nu(-64 + 3x_o^+ + 2.5x_o^+ \ln x_o^+)$$

For $5 < x_o^+ < 30$

$$\Gamma = \rho\nu(12.55 - 8.05\, x_o^+ + 5\, x_o^+ \ln x_o^+)$$

$$(49)$$

Differentiating with respect to x_o^+ gives,

For $x_o^+ > 30$

$$\frac{d\Gamma}{dx_o^+} = \rho\nu(5.5 + 2.5 \ln x_o^+)$$

For $5 < x_o^+ < 30$

$$\frac{d\Gamma}{dx_o^+} = \rho\nu(-3.05 + 5 \ln x_o^+) \qquad (50)$$

For convenience define F_1 as follows,

For $x_o^+ > 30$ $\quad F_1 \equiv 5.5 + 2.5 \ln x_o^+$

For $5 < x_o^+ < 30$ $\quad F_1 \equiv -3.05 + 5 \ln x_o^+ \qquad (51)$

Then Equation (50) may be written as

For $x_o^+ > 30$ $\quad \frac{d\Gamma}{dx_o^+} = \rho\nu F_1$

For $5 < x_o^+ < 30$ $\quad \frac{d\Gamma}{dx_o^+} = \rho\nu F_1$

$$(50a)$$

Equation 42 gives the results of the energy balance in the form

$$\left(\frac{q}{A}\right)_o = h_{fg} \frac{d\Gamma}{dz}$$

This may be written as

$$\left(\frac{q}{A}\right)_o = h_{fg} \frac{d\Gamma}{dx_o^+} \frac{dx_o^+}{dz} \qquad (52)$$

From Equation (47a) we have an expression for (q/A) as a function of film thickness, which may be rearranged in the form

$$\frac{q}{A} = \frac{\Delta t \, \rho \, c_p \, (x_o^+)^{1/3} \left[\frac{(1 - \rho_v/\rho)}{M}\right]^{1/3} \left(\frac{g}{\nu^2}\right)^{1/3} \nu}{F_2} \tag{53}$$

Since it has been shown that $(q/A) = (q/A)_o$, this term may be eliminated between Equations (52) and (53). Substituting for $\frac{d\Gamma}{dx_o^+}$ from Equation (50a), we obtain an expression containing, as the only variables, x_o^+, dx_o^+, and dz.

$$\frac{F_1 F_2}{(x_o^+)^{1/3}} \left[\frac{M}{(1 - \rho_v/\rho)}\right]^{1/3} dx_o^+ = \Delta t \left(\frac{c_p}{h_{fg}}\right) \left(\frac{g}{\nu^2}\right)^{1/3} dz$$

This may be integrated between the limits x_{ot}^+ to x_o^+ and z_t to z, where x_{ot}^+ and z_t indicate the values at the transition from laminar to turbulent flow. The resulting equation may be put into the convenient form

$$(z - z_t)\,\Delta t = \frac{\int_{x_{ot}^+}^{x_o^+} \frac{F_1 F_2}{(x_o^+)^{1/3}} \left[\frac{M}{(1 - \rho_v/\rho)}\right]^{1/3} dx_o^+}{\left(\frac{c_p}{h_{fg}}\right) \left(\frac{g}{\nu^2}\right)^{1/3}} \tag{54}$$

Equation (54) now gives the desired expression for the distance down the plate, z, as a function of film thickness. In solving for this distance, the value of x_o^* at the transition point must first be solved for from either Equation (29) or (32) and then the distance to the transition point, z_t, found from Equation (18). The distance from the

transition point to the point under consideration may then be calculated from Equation (54) by evaluating the integral. This must be done numerically.

While point values of the heat transfer coefficient as given in Equation (48) are of academic interest, they do not give answers readily usable by the designer. To predict the heat transfer characteristics of a condenser or to enable rational design, it becomes necessary to predict mean heat transfer coefficients which can be applied to the condenser as a whole rather than at just one point. Accordingly it is possible to define this mean heat transfer coefficient in the same manner as was done for the wholly laminar film.

$$h_m \equiv \frac{q_T}{L Y} \frac{1}{(t_{x_0} - t_w)} = \frac{\Gamma h_{fg}}{L(t_{x_0} - t_w)} \tag{55}$$

It should be noted at this point that the substitution of $q = w\, h_{fg} = \Gamma\, Y\, h_{fg}$ implicit in Equation (55) neglects the effect of subcooling of the condensate film. As has been shown previously this is very nearly true for the turbulent film, but it is not true for the laminar film. Since, in the present case, we are considering both a laminar and a turbulent film, this will introduce some error in the results. There will be no error in the laminar curves provided an equivalent h'_{fg} as defined in Equation (10) is substituted for h_{fg}. The error involved in neglecting subcooling may be somewhat evident in the region just following transition, but will become less important as more and more of the film is in turbulent motion. In most of the cases encountered

the laminar film and transition region will extend only a few inches from the top of the plate and the neglecting of the subcooling in this small area should not appreciably affect the overall results for plates whose lengths may approach several feet. It is also felt that the uncertainties of actually determining the transition point will introduce errors of at least as great a magnitude as the subcooling error, and therefore this latter point should not be belabored.

Since we have assumed a constant temperature difference, the denominator of Equation (55) may be broken into two parts.

$$h_m = \frac{\Gamma\, h_{fg}}{(t_{x_o} - t_w) z_t + (t_{x_o} - t_w)(L - z_t)} \tag{56}$$

The term $(t_{x_o} - t_w)\, z_t$ applies to the laminar portion of the condensate film, and the term $(t_{x_o} - t_w)(L - z_t)$ applies to the turbulent portion.

From Equations (16) and (18),

$$z_t(t_{x_o} - t_w) = \frac{(1 - \rho_v/\rho)\, N_{Pr}\, h'_{fg} \left(\frac{\mu^2}{g}\right)^{1/3}}{4\, c_p} \left[(X^*_{ot})^4 + \frac{4}{3}\, \tau^*_v\, (X^*_{ot})^3 \right] \tag{57}$$

Equation (54) gives the expression for the turbulent length. Substituting these two values into Equation (56) yields the final equation for the mean heat transfer coefficient in terms of functions of the film thickness,

$$\frac{h_m}{k}\left(\frac{\nu^2}{g}\right)^{1/3} = \frac{\frac{\Gamma}{\rho\nu}\; N_{Pr}}{\int_{x_{0t}^+}^{x_{0L}^+} \frac{F_1 F_2}{(x_0^+)^{1/3}} \left[\frac{M}{(1-\rho_v/\rho)}\right]^{1/3} dx_0^+ \; + \left(1-\frac{\rho_v}{\rho}\right) N_{Pr}\left[\frac{1}{4}\left(x_{0t}^*\right)^4 + \frac{\tau_v^*}{3}\left(x_{0t}^*\right)^3\right]} \tag{58}$$

The Reynolds Number at the bottom of the plate is of some interest as it is a direct measure of the amount of vapor that has been condensed. This $N_{Re} = \frac{4\Gamma}{\rho\nu}$ and may be readily evaluated from Equations (49)

For $x_{0L}^+ > 30$

$$N_{Re} = -256 + 12\, x_{0L}^+ + 10\, x_{0L}^+ \ln x_{0L}^+$$

For $5 < x_{0L}^+ < 30$

$$N_{Re} = 50.2 - 32.2\, x_{0L}^+ + 20\, x_{0L}^+ \ln x_{0L}^+ \tag{59}$$

Equations (54), (58), and (59) represent the results of the turbulent analysis in much the same way that Equations (18), (26), and (22) represent the results of the laminar analysis. The same forms of plotting are therefore used, the turbulent plots merely being continuations of the laminar curves. A description of the numerical evaluations of these equations is contained in the Appendix A.

6/23/54 JW

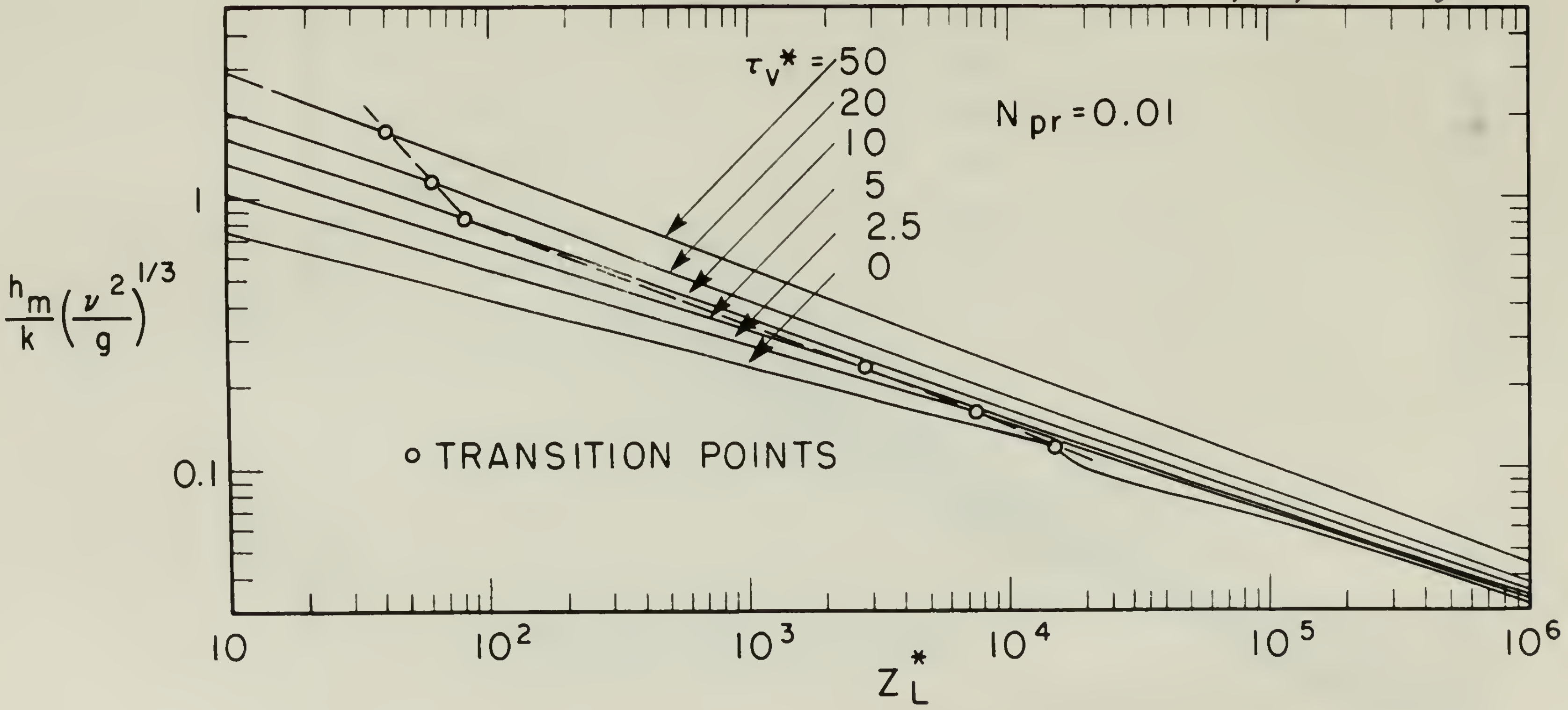

FIG. 7

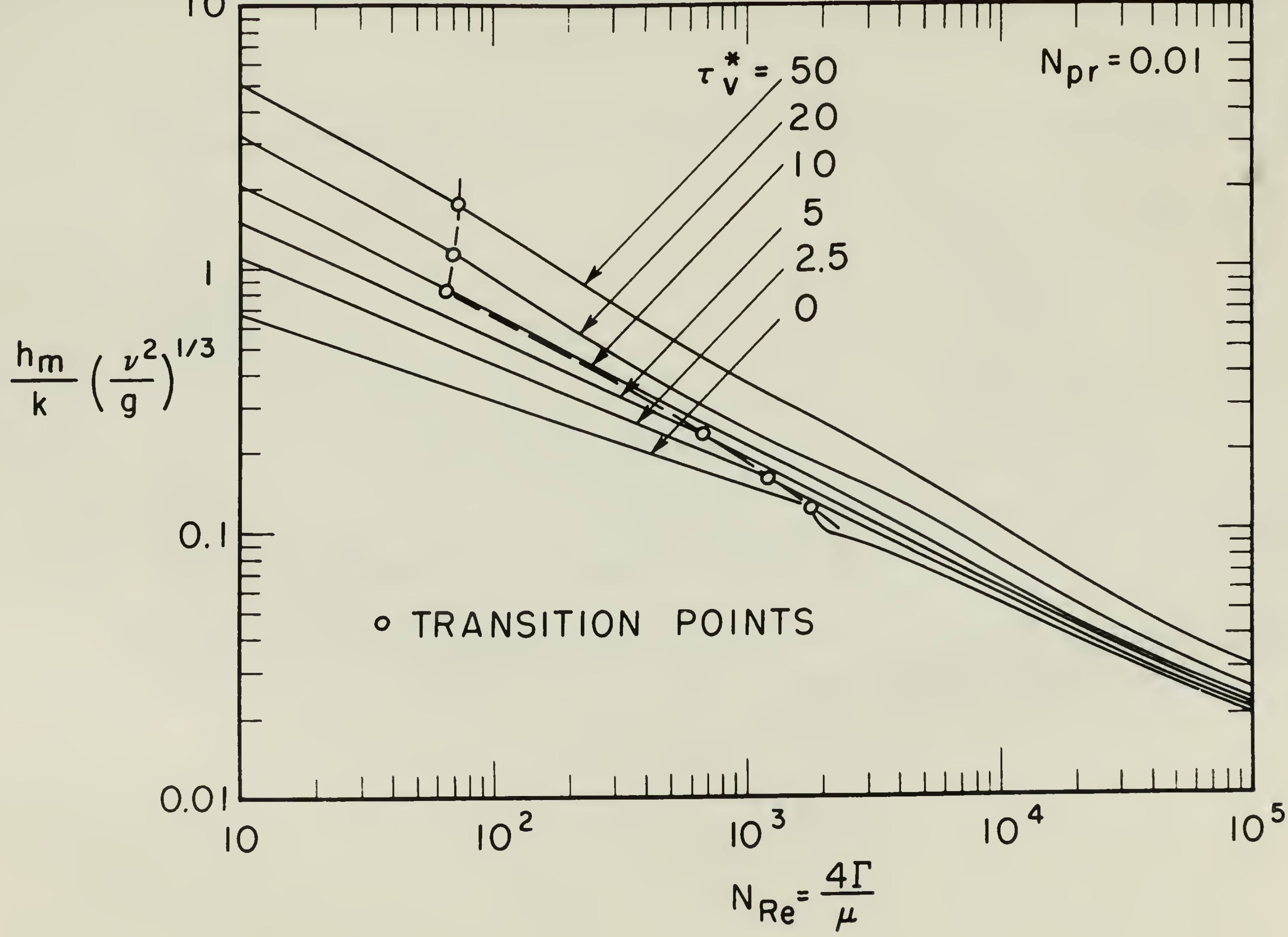

6/23/54 JW

FIG. 8

6/23/54 JW

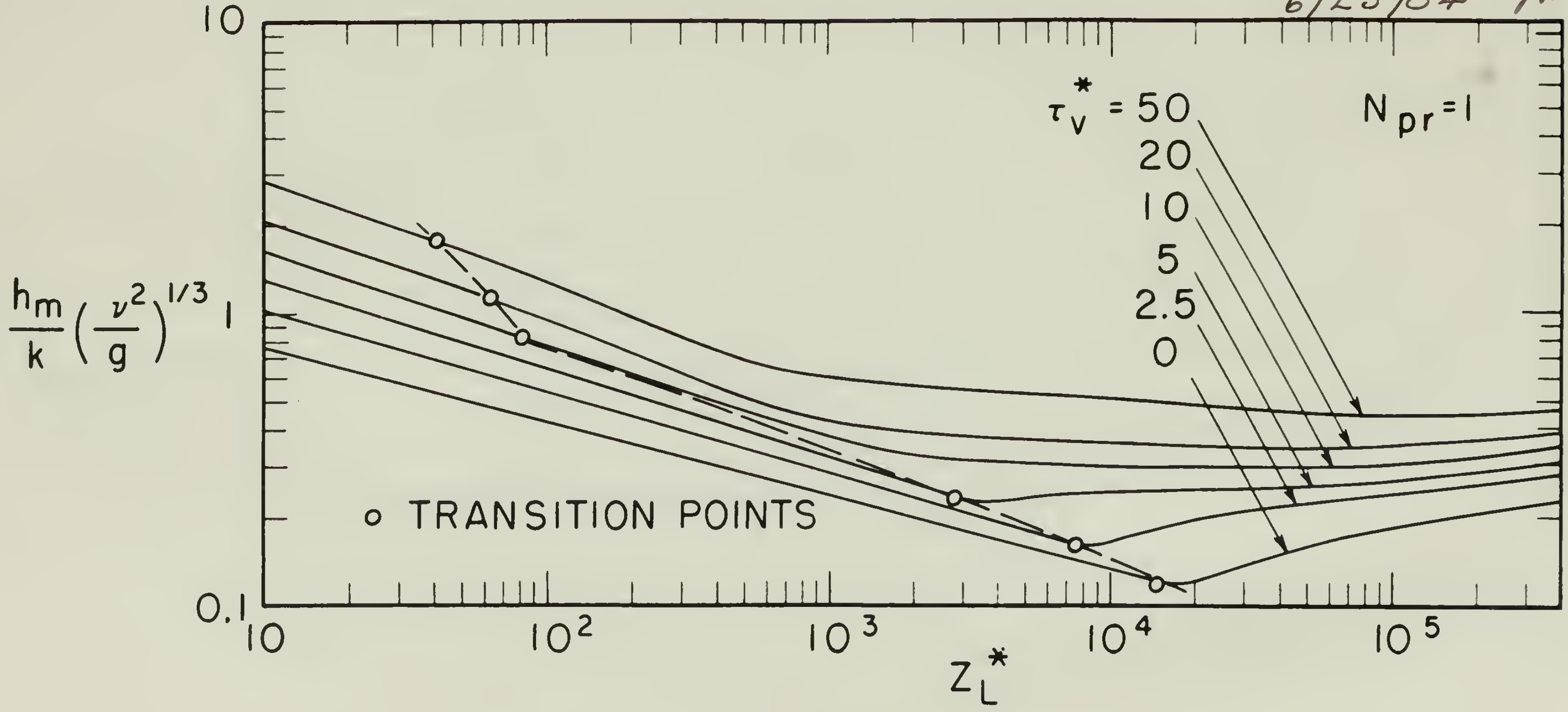

FIG. 9

6/23/54 JW

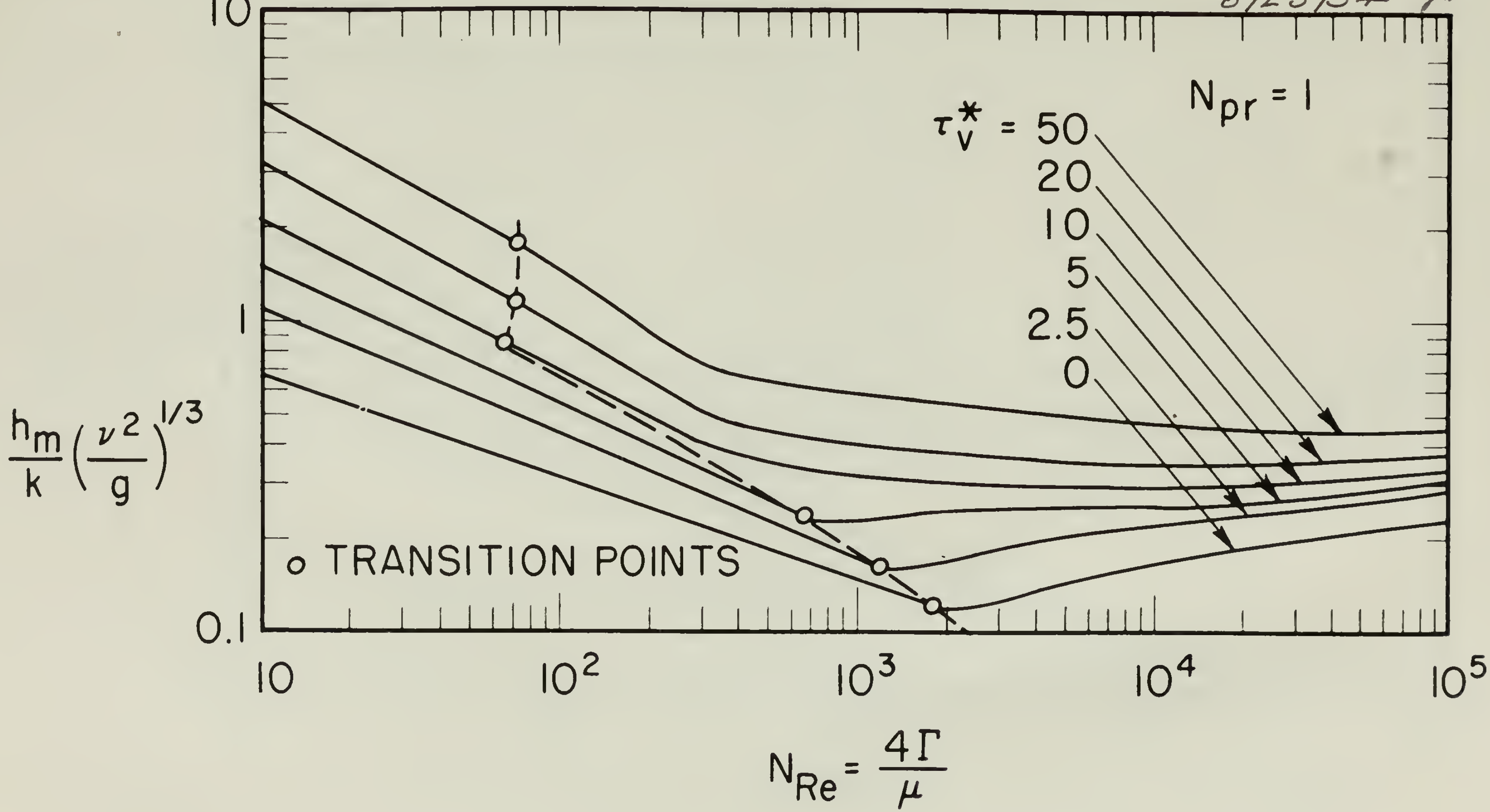

FIG. 10

6/23/54 JW

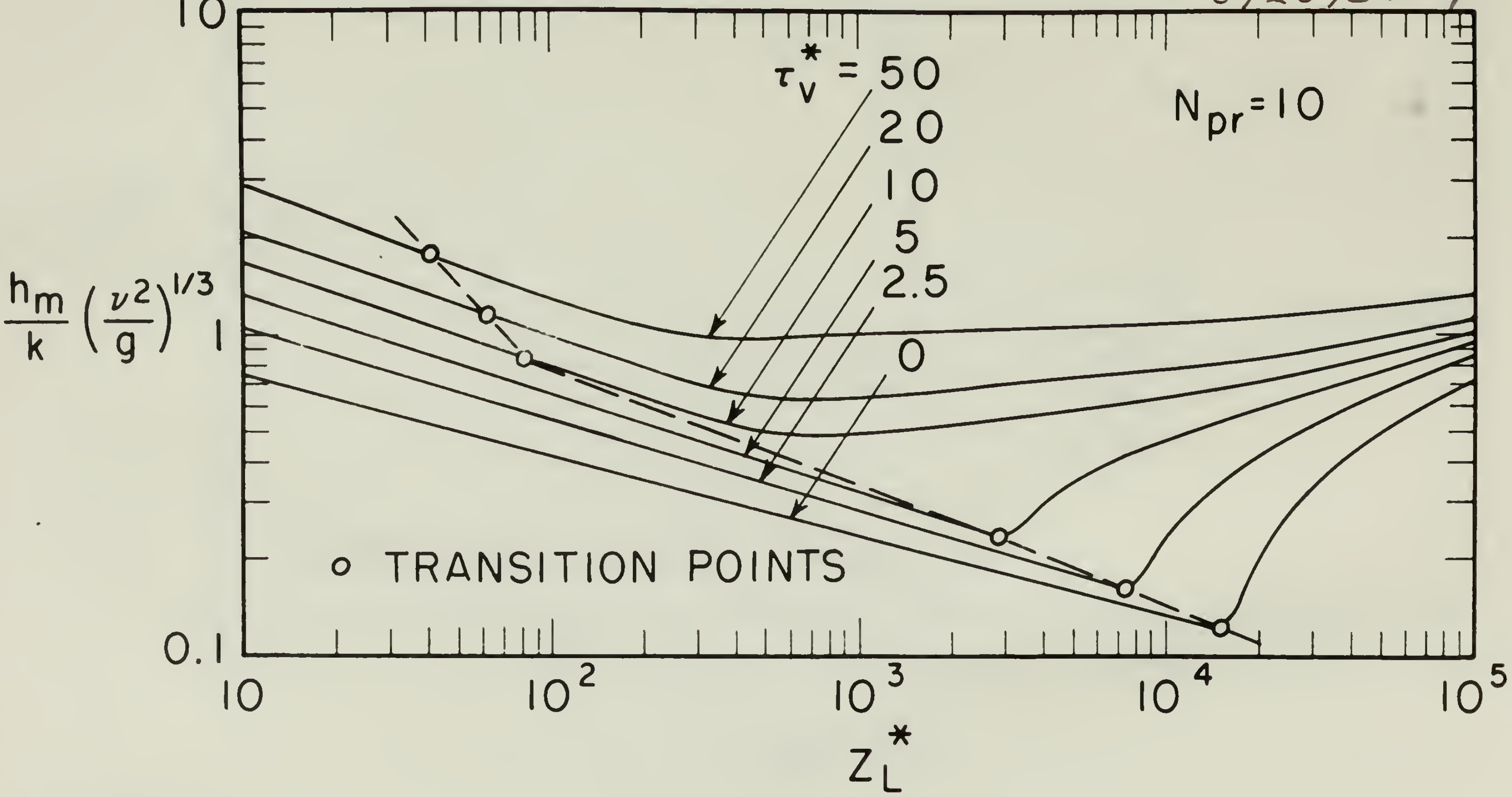

FIG 11

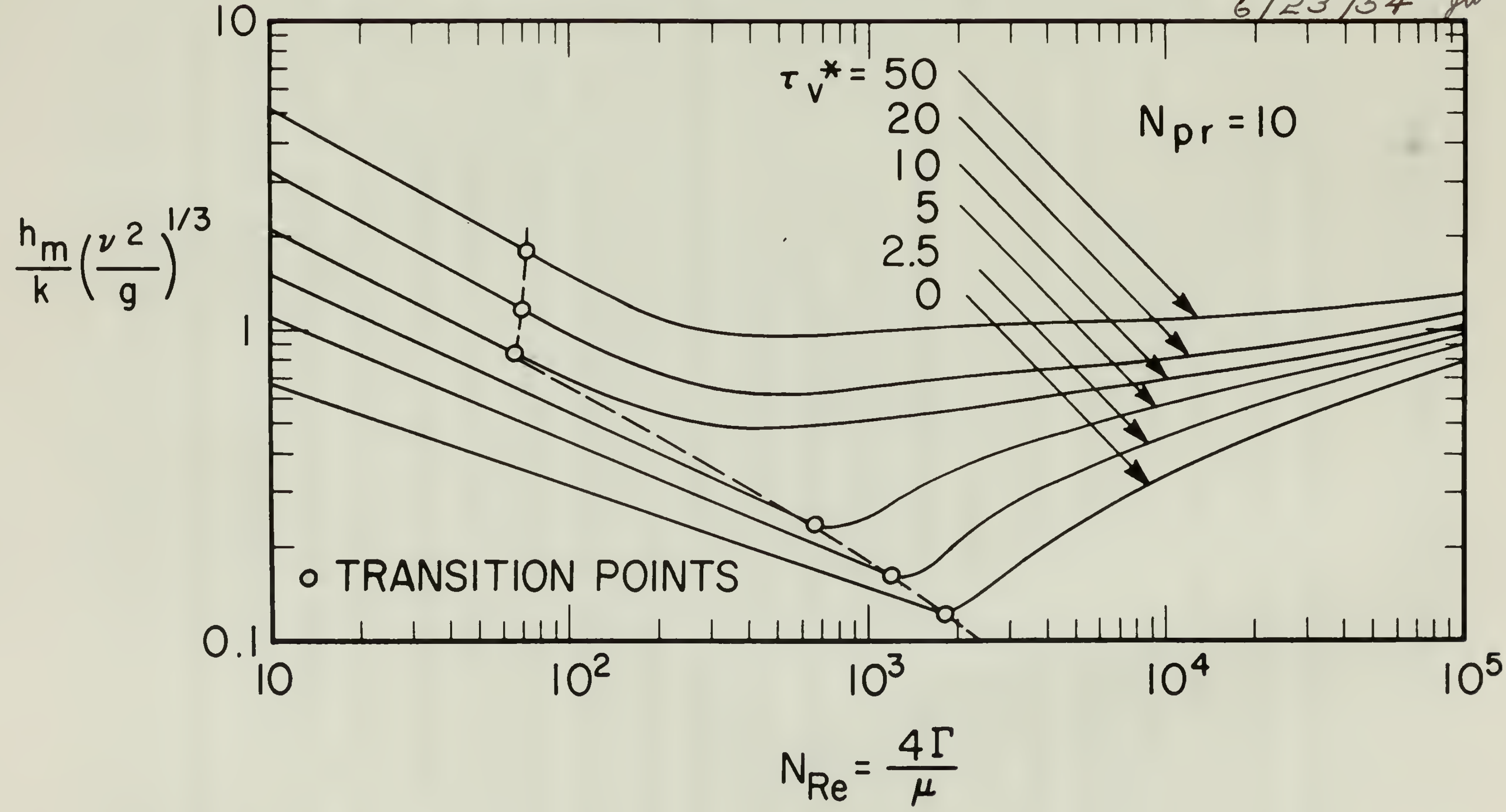

6/23/54 JW

FIG. 12

SECTION E - DISCUSSION OF ANALYTICAL RESULTS

The results of the analysis presented in this thesis are contained in Figures 7 through 12. These curves are based on a rational approach, and show the effect of a vapor shear stress on heat transfer in laminar and turbulent film condensation for a wide range of N_{Re} and N_{Pr}. The use of these curves will be illustrated later by a sample problem.

It is significant that the plotted values of mean or average heat transfer coefficient include the effect of a laminar condensate film on the upper part of the plate and a turbulent film on the lower regions, if one exists. To use these plots it is not necessary to first investigate whether or not turbulent flow exists, this determination having already been made in the preparation of the plots. The values given are universally applicable and are not dependent on the geometry of the system or the fluid properties except as they enter into the determination of the dimensionless quantities needed to enter the curves.

Inspection of Figures 7 through 12 reveal several interesting points concerning the mechanism of film condensation. First, the significant effect of a vapor shear stress is apparent. This effect is more pronounced in the lower N_{Re} range, giving an increase in heat transfer coefficients of several fold in some cases. At higher N_{Re} the effect is less. The effect on h_m of the exact location of the transition point, as influenced by the vapor shear stress, becomes less significant as the value of N_{Re} at the bottom of the surface increases and is practically

insignificant for N_{Re} greater than 10,000.

The effect of turbulence in the film is illustrated by the change in slope following the transition points. It can be seen that the turbulence effect on the heat transfer coefficients is greater for increasing N_{Re} and for increasing N_{Pr}. The Reynolds Number effect might be expected, as larger N_{Re} will result in a greater degree of turbulence and hence a greater portion of heat transfer by the mechanism of turbulent mixing. The Prandtl Number effect is best seen by comparing the heat transfer plots for the very low $N_{Pr} = 0.01$, representative of liquid metals, and the plot for the high $N_{Pr} = 10$. The curves show that turbulence has a greater role in increasing the heat transfer characteristics for the higher N_{Pr}. In fact the low Prandtl number curves for the turbulent portion actually lie below an extension of the laminar curves. This may be explained once it is realized that for these liquids, the thermal conductivity is so large that it becomes the principal means of heat transfer, rather than turbulent mixing. Since the assumed velocity distribution results in a thicker condensate film than would exist for laminar flow, it can be seen that this thicker film offers a greater resistance to heat flow through conduction than would the laminar film.

It would be desirable to compare the present analysis directly with experimental results. However, experimental data on film condensation in which the vapor shear stress has been accurately determined was not readily available. There does exist a correlation equation based on considerable experimental data, which has already been mentioned,

and is given by Equation (36). In order to compare the analytical results with this correlation equation, the curves in Figures 8, 10, and 12 have been cross plotted at a Reynolds Number of 5000 and are presented as curves of mean heat transfer coefficient versus τ_v^*. These plots are represented by the solid lines in Figure 13 for various Prandtl Numbers. The correlation equation in the form given by Equation (36) has also been plotted, and is shown by the dotted lines. As can be seen, the agreement is quite good for $N_{Pr} = 2$ to 3, which lies within the range of 2 to 5 of the liquids actually tested and on which the correlation equation is based. There is considerable deviation outside this range, as evidenced by the curves for $N_{Pr} = 10$ and 0.01. This indicates that caution should be employed when using the correlation equation outside the range for which it was proposed.

Figure 13 also graphically illustrates the considerable effect that a vapor shear stress may have on the heat transfer coefficients. For example, the h_m group for $N_{Pr} = 10$ and $\tau_v^* = 50$ is about 1.00, or four times the value of 0.25 given for $\tau_v^* = 0$.

In the force balance given by Equation (2) the only pressure gradient in the z direction considered was that due to the height of the vapor and is represented by the $\frac{g}{g_0} \rho_v$ term. While this assumption was valid for the case of a flat plate in an infinite atmosphere which we considered, it may lose its validity when a vertical pipe is considered. For pipe flow, the existance of a vapor shear stress is intimately connected with a pressure gradient in the z direction. To include this

6/23/54 JW

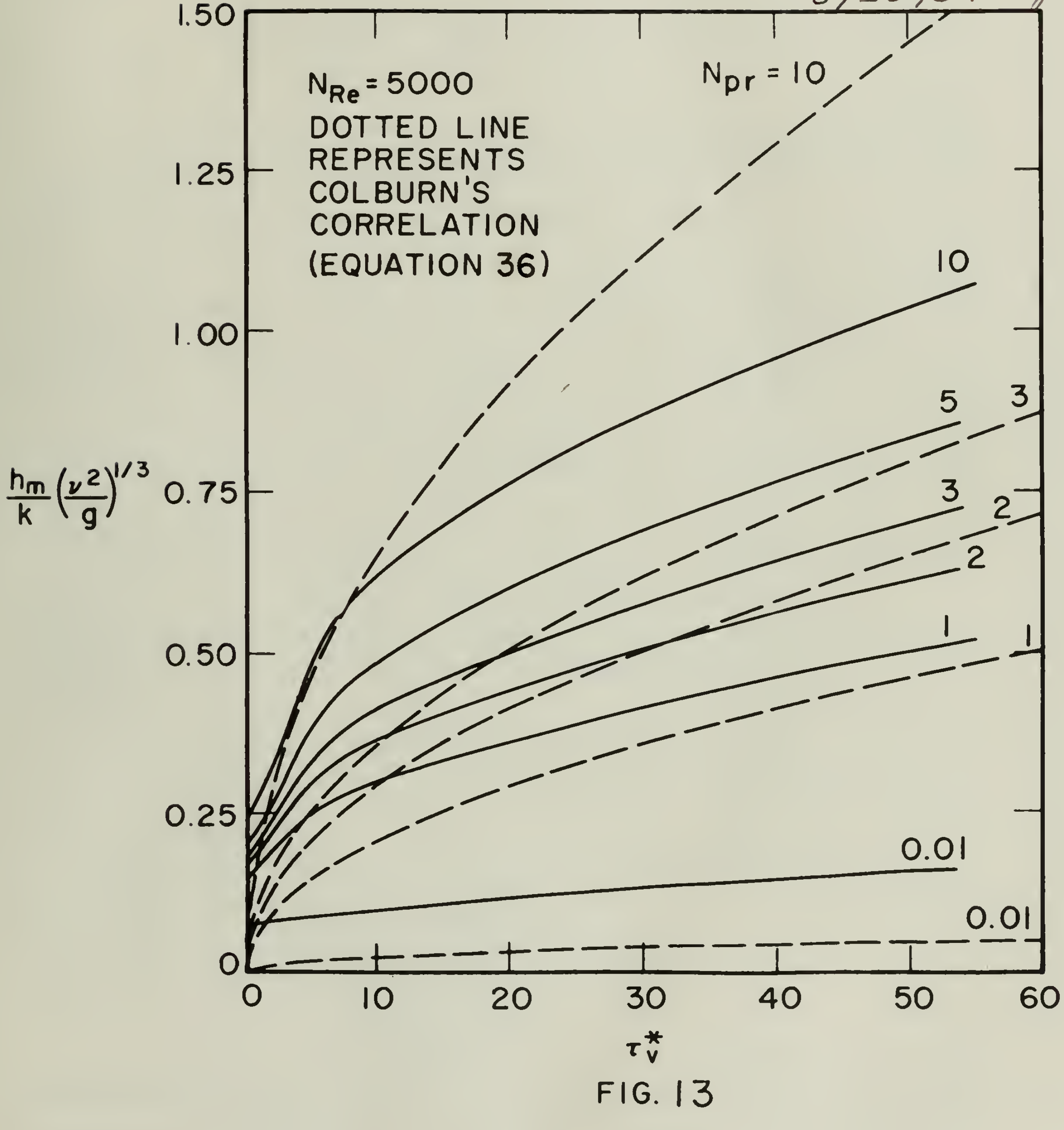

FIG. 13

effect, it is necessary to rewrite the force balance, Equation (2) in the form

$$\tau - \left(\frac{g}{g_0}\rho - \frac{\partial p}{\partial z}\right)(X_0 - X) - \tau_v = 0 \tag{60}$$

To evaluate $\frac{\partial p}{\partial z}$, consider a control volume containing the vapor in the core of a vertical pipe, as shown in Figure 14.

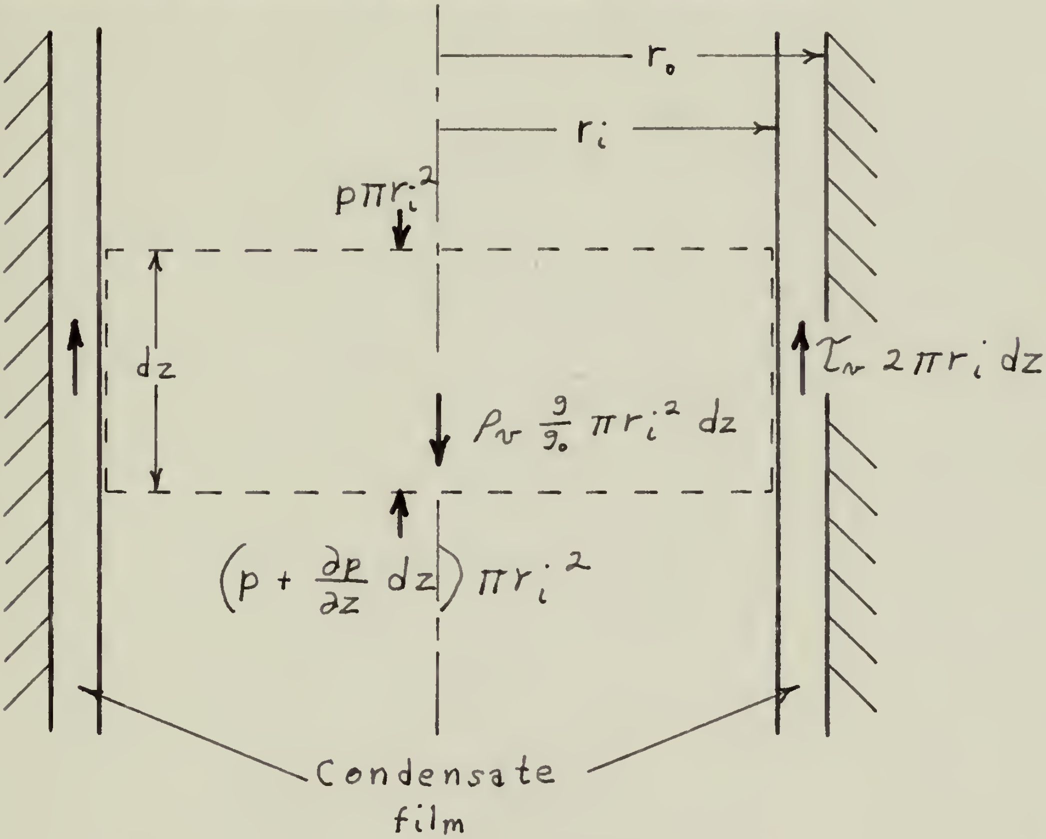

r_o
r_i
$p\pi r_i^2$
dz
$\tau_v 2\pi r_i dz$
$\rho_v \frac{g}{g_0} \pi r_i^2 dz$
$\left(p + \frac{\partial p}{\partial z} dz\right) \pi r_i^2$
Condensate film

FIGURE 14

Considering the vapor flow as one dimensional and including the change in momentum, the pressure gradient may be evaluated from a force balance on the control volume as,

$$\frac{dp}{dz} = \frac{g}{g_0} \rho_v - 2 \frac{\rho_v}{g_0} u \frac{du}{dz} - \frac{2 \tau_v}{r_i} \tag{61}$$

where u represents the vapor velocity.

The weight rate of flow of the vapor, $w_v = \rho_v u \pi r_i^2$, which may be differentiated to give,

$$\frac{dw_v}{dz} = \rho_v \pi r_i^2 \frac{du}{dz}$$

The weight rate of flow of the liquid condensate, $w = 2 \pi r_o \Gamma$ which may also be differentiated to give,

$$\frac{dw}{dz} = 2 \pi r_o \frac{d\Gamma}{dz}$$

Since $\frac{dw_v}{dz} = - \frac{dw}{dz}$, we may solve between these two equations for the velocity gradient,

$$\frac{du}{dz} = - \frac{2}{\rho_v r_i} \frac{d\Gamma}{dz} \frac{r_o}{r_i}$$

Substituting this expression in Equation (61) gives the pressure gradient as

$$\frac{dp}{dz} = \frac{g}{g_0} \rho_v + \frac{4}{g_0} \frac{u}{r_i} \frac{d\Gamma}{dz} \frac{r_o}{r_i} - \frac{2 \tau_v}{r_i} \tag{62}$$

Previously, in the case of the flat plate, we had taken the pressure gradient = $(g/g_o) \rho_v$. However, for the case of the vertical pipe condenser we may take an equivalent vapor density

$$\rho_v' = \rho_v + \frac{4}{g} \frac{u}{r_i} \frac{r_o}{r_i} \frac{d\Gamma}{dz} - 2 \frac{g_0}{g} \frac{\tau_v}{r_i} \tag{63}$$

This equivalent vapor density, which takes into account the pressure gradient for a vertical pipe, contains two terms which are dependent

on r_i, the radius of the condensate layer interface. For a given tube, the equations presented in the analysis can be evaluated in a manner analogous to that for the flat plate. Since $\frac{d\Gamma}{dz}$ and u will vary down the length of the tube, these must be determined from the given conditions at each step in the stepwise numerical integration. It is apparent that the solutions so obtained will apply to only the particular geometry for which they were calculated and for the particular vapor velocity which was considered. In this procedure, the advantage of the universality which was obtained for the flat plate will be lost.

In Equation (63) the terms containing the vapor shear stress and the vapor velocity are subtractive and may quite possibly largely cancel out. If the net magnitude of Equation (63) is small compared to the condensate density, ρ, it is then possible to apply the results obtained for the flat plate.

It is worthwhile to investigate the magnitude of the pressure gradient correction for a specific case. Consider a 1 inch diameter tube, in which water is condensing. Saturated vapor temperature will be taken as 120° F., and the tube wall temperature as 60° F. To take an extreme case, assume $\tau_v^* = 50$.

Mean film temperature, from Equation (1),

$$t_f = 120 - 3/4\ (60) = 75^\circ \text{ F.}$$

Then

$$\nu = 1.000 \times 10^{-5} \text{ ft}^2/\text{sec}$$

$$\left(\frac{\nu^2}{g}\right)^{1/3} = 1.46 \times 10^{-4} \text{ ft.}$$

Since $\rho_v << \rho$

$$\tau_v = \tau_v^* \rho \left(\frac{\mu^2}{g}\right)^{1/3} = .455 \ \mathrm{lb/ft^2}$$

From Equation (42),

$$\frac{d\Gamma}{dz} = \frac{1}{h_{fg}} \left(\frac{q}{A}\right)_0 = \frac{1}{h_{fg}} \, h \, \Delta t$$

$$\text{where } h = \frac{k}{\left(\frac{\mu^2}{g}\right)^{1/3}} \; \frac{N_{Pr}}{F_2} \; (x_0^+)^{1/3} \left[\frac{(1-\rho_v/\rho)}{M}\right]^{1/3}$$

Consider a point in the tube where $x_0^* = 50$. Then $x_0^+ = 500$ and

$$\left[\frac{M}{X_0^+}\right]^{1/3} = 0.1$$

At 75° F., the Prandtl Number of water is 6.29. Proceeding in the manner outlined in the section on calculation methods, F_2 may be evaluated.

$$F_2 = 57.6$$

Then taking k of the condensate as .357 BTU/hr-ft -°F,

$$h = 2660 \ \mathrm{BTU/hr\text{-}ft^2\text{-}{}^\circ F.}$$

Substituting h, h_{fg} = 1026 BTU/lb, and Δt = 60°F.,

$$\frac{d\Gamma}{dz} = 2.59 \ \mathrm{lb/hr\text{-}ft^2}$$

Taking smooth pipe friction factors for illustrative purposes, f = .005 at a vapor Reynold's Number of 64,500. Since $\tau_v = f \frac{\rho_v u^2}{2}$ we may solve for the vapor velocity, u,

$$u = 1090 \ \mathrm{ft/sec}$$

$$(N_{Re})_v = \frac{\rho_v u D}{\mu_v} = 64{,}500$$

Substituting our computed values in Equation (63), we are able to evaluate ρ_v',

$$\rho_v' = \frac{1}{203} + 2.34 - 21.82 = -19.48 \ \mathrm{lb/ft^3}$$

Although ρ_v' is about 1/3 of the condensate density, ρ, this is not the magnitude of the error involved by neglecting this term. Referring to Equation (60), by continuing our present specific example, we can evaluate the maximum error in the shear stress, τ, which will occur when $x = 0$, or $\tau = \tau_o$. Since $x_o^* = 50$, $x_o = 50 \times 1.46 \times 10^{-4}$ ft. = .0073 ft.

$$\tau_o = \tau_v + \left(\frac{g}{g_o}\rho - \frac{dp}{dz}\right) x_o$$

$$\tau_o = .455 + (62.4 + 19.48)\,(.0073)$$

$$(\tau_o)_{corr.} = .455 + .597 = 1.052 \text{ lb/ft}^2$$

By neglecting the pressure gradient,

$$(\tau_o)_{uncorr.} = .455 + .455 = .910 \text{ lb/ft}^2$$

The final error which is introduced in this specific case is of the order of 13.5%. These calculations are included, not to exhaustively investigate the effect of the pressure gradient term, but rather to give an order of magnitude of the error which might be expected. The values chosen in the problem are felt to be representative except for the vapor velocity of 1090 ft/sec. This high value was deliberately picked to indicate an upper limit to the error involved. In any practical steam condenser, the vapor velocity will undoubtedly be much lower, with lower vapor shear stresses. It may be concluded that in many cases, the effect of the pressure gradient may be neglected, and the analytical results for the flat plate may be applied to vertical tube condensers with confidence.

In all of the calculations for Figures 7 through 12, the quantity

$(1 - \rho_v/\rho)$ was taken as unity; e.g., ρ_v/ρ small. It was also assumed that τ_v and $(t_{x_0} - t_w)$ were uniform along the plate. The equations in the analysis may be readily evaluated accounting for any value of $(1 - \rho_v/\rho)$ and for any prescribed variations of $(t_{x_0} - t_w)$ or of τ_v along the length. The effects of these variations are functions of the particular geometry and are hard to generalize.

Of the many assumptions underlying this analysis, most are sound and have considerable experimental evidence to back up their validity. The two most subject to question are the assumed velocity distribution and the criteria for transition. It will be the purpose of the second section of this thesis to investigate the hydrodynamics of a falling vertical liquid film under the influence of an appreciable shear stress at the interface. These investigations are preliminary only and will merely point out the direction to be followed in a more detailed experimental program.

SECTION F - SAMPLE DESIGN PROBLEMS

Application of the results of the analysis is conveniently made with the use of the dimensionless plots of Figures 7 through 12. Since mean or overall heat transfer coefficients are dealt with throughout, no point by point or stepwise calculations are necessary. The actual methods involved in a design calculation are illustrated by the following problems.

The two problems selected are felt to be representative of those which might be met in industrial practice. The operating conditions and tube sizes chosen correspond to two actual cases where measurements have been taken. The calculations should therefore serve the additional purpose of comparing the accuracy of the predictions made by the present analysis. The first problem utilizes the initial data for water run 191 of Carpenter's experimental program, reference (3). The second is based on an actual industrial design as reported by Wurster, reference (15).

The problem is posed in the following manner. For a given condensate weight rate of flow per tube, it is desired to determine the required length of tube to condense the amount specified, with no uncondensed vapor passing out of the bottom of the tube. In addition, it is required to compute the mean condensing side heat transfer coefficients.

In both cases the condensing vapor is steam at essentially

atmospheric pressure. The wall temperature has been taken as the arithmetic average of the wall temperatures reported in each of the references.

	No. 1	No. 2	
Tube Characteristics:	5/8",14 BWG	1",17BWG	
Inside Diameter	.459	.884	in.
Cross-Sectional Area	.00115	.00426	ft^2
Tube wall temperature, t_w	162°F	182.8° F	
Desired condensate flow rate, w	50.1	201	lb/hr

Vapor mass velocity at top of tube, G_1	43,600	47,100	lb/hr-ft^2
Since G_2=0, Eq. (37) gives G_m	25,300	27,400	lb/hr-ft^2
Specific volume of saturated vapor at 14.7 psia, v=26.8 ft^3/lb			
Mean vapor velocity, u_m	188.2	204	ft/sec
Condensate flow rate per unit perimeter at bottom of tube, $\Gamma = w/Y$	418	870	lb/hr-ft
Average condensate flow rate Γ_m	209	435	lb/hr-ft
Since water is the fluid being condensed, the ratio of surface tensions, $s_w/s = 1$.			
The density of saturated liquid at 212° F., $\rho = 59.7$			lb/ft^3
Then $\frac{\Gamma s_w}{\rho s}$	3.5	7.28	ft^2/hr
The viscosity of steam at 212° F., $\mu_v = .0303$			lb/ft-hr
The Reynolds Number of the vapor, $\frac{DG_m}{\mu_m}$	29,700	66,600	
Utilizing the two component flow friction factor data in reference (11), f	.0063	.0072	
Vapor shear stress $\tau_v = f \frac{\rho_v u_m^2}{2}$	.1296	.174	lb/ft^2

	No.1	No.2	
Mean Film Temperature, from Eq. (1), t_f	174.5°	190°	
Kinematic viscosity at t_f, ν	$.399 \times 10^{-5}$	$.362 \times 10^{-5}$	ft^2/sec
$\left(\frac{\nu^2}{g}\right)^{1/3}$	$.790 \times 10^{-4}$	$.741 \times 10^{-4}$	ft
$\tau_v^* = \dfrac{g_0 \tau_v}{g(\rho - \rho_v)\left(\frac{\nu^2}{g}\right)^{1/3}}$	27.4	39.3	
Viscosity of condensate at t_f, μ	$.754 \times 10^{-5}$	$.680 \times 10^{-5}$	lb-sec/ft^2
Condensate Reynolds Number at bottom of tube, $N_{Re} = \frac{4\Gamma}{\mu}$	1915	4420	
Prandtl Number of Condensate at t_f, N_{Pr}	2.26	2.02	
Enter Fig. 10 for $N_{Pr} = 1$ with N_{Re} and τ_v^*, get $\frac{h_m}{k}\left(\frac{\nu^2}{g}\right)^{1/3}$	.41	.47	
Enter Fig. 12 for $N_{Pr} = 10$ with N_{Re} and τ_v^*, get $\frac{h_m}{k}\left(\frac{\nu^2}{g}\right)^{1/3}$	.74	.98	
Interpolate to actual N_{Pr}, $\frac{h_m}{k}\left(\frac{\nu^2}{g}\right)^{1/3}$	.46	.53	
Thermal Conductivity of condensate at t_f, k	.386	.390	$\frac{\text{BTU}}{\text{hr-ft-}^\circ\text{F}}$
Mean heat transfer coefficient, h_m	2250	2470	
$z^* = N_{Re} / \frac{h_m}{k}\left(\frac{\nu^2}{g}\right)^{1/3}$	4160	8350	
Since $z^* = \frac{4 z \Delta t}{N_{Pr}} \frac{C_p}{h_{fg}} \left(\frac{g}{\nu^2}\right)^{1/3} \frac{1}{(1-\rho_v/\rho)}$ solve for z	3.60	10.4	ft
Actual z, as determined by experiment, (references (3) and (15))	3.6	11.7	ft

By comparing calculated and actual tube lengths, it can be seen that the analytical results will predict the performance of a condenser quite closely. Probably the greatest source of error lies in the selection of the correct average vapor shear

stress and tube wall temperature. If it was desired to predict performance within very close tolerances, the numerical integration procedure described in Appendix A could be reworked with the known variations of Δt and τ_w^* included in a stepwise approximation. However, this would involve a rather tedious and lengthy set of calculations and, for most cases, it is felt that the constant average values as used above will provide results of sufficient accuracy.

PART II

EXPERIMENTAL INVESTIGATION OF CO-CURRENT LIQUID-VAPOR FLOW IN A VERTICAL TUBE

PART II

SECTION A - LITERATURE SURVEY

Part I of this thesis is concerned with the development of analytical expressions predicting the heat transfer coefficients of a falling film condenser. Use has been made of the heat momentum transfer analogy, so that the validity of the predicted heat transfer coefficients is dependent upon a knowledge of the hydrodynamics of a falling film. Assumptions have been made regarding the behavior of such a film, based on the best knowledge available today. It is the purpose of this section, therefore, to give a brief review of the literature covering the subject of falling liquid films.

Monrad and Badger (13) discuss the onset of turbulence in a falling liquid film. Their conclusion, based on the work of other investigators, is that the critical Reynolds Number is in the range of 1800. They also cite data of Jakob and Erk (19) as showing that transition may occur at lower N_{Re} in the presence of high values of vapor velocity.

In reference (17), Hebbard and Badger measured film coefficients of heat transfer on a 1 inch O.D. vertical tube condenser 12 feet long. Reynolds Numbers of the film covered the range 500 to 3000. Results are consistently higher than those predicted by the Nusselt laminar equations, and generally lie in a line parallel to the predicted line. No measurements of the vapor shear stress were made, and it is felt by this author that the discrepancies may quite possibly be explained by this effect. No information as to the onset of turbulent flow can

be deduced from these results.

Kirkbride, reference (2), presents heat transfer data of several investigators on liquid films flowing down vertical walls. This data covers the Reynolds Number range of 700 to 20,000. By the marked difference in slope of the correlating line from the Nusselt laminar prediction, turbulent flow of the film is definitely indicated. However, there is little data for the lower N_{Re}, so it is not possible to directly infer the location of the transition point. The best correlating line through the data intersects the theoretical Nusselt prediction at a N_{Re} of about 1100. The vapor shear stress was not considered.

In addition to considering heat transfer coefficients, Kirkbride (2) presents data on measured film thicknesses for N_{Re} less than 2000. Excellent agreement with predicted thicknesses is obtained for the lower N_{Re}, however, deviations are observed for the higher N_{Re}. Surface waves are given as the explanation for the discrepancies.

Cooper, Drew, and McAdams (18) present isothermal data of six observers dealing with liquids flowing down the wetted smooth surface of vertical towers or over flat plates at slight inclinations. Film thicknesses were measured either by a micrometer, visually observing contact with the film, or by suddenly stopping the flow and measuring the quantity that drains out of the test section. In a plot of the Fanning friction factor versus N_{Re}, scatter of the data from the laminar equation starts at a N_{Re} of about 1000, with the best correlating curve indicating transition at about 2100. Data were not available for determining the possible effects of gas velocity on the liquid flow.

Considerable experimental work has been done on non-condensing heat exchangers employing vertical tubes, in which the fluid flows in film form down the tube walls, references (20) to (26). Bays in reference (22) has plotted heat transfer coefficients versus N_{Re}. A break in the curve at a N_{Re} of 1300 or 1400 may possibly indicate transition of the film from laminar to turbulent flow, however, Bays recommends a value of 1000. Leavitt's data (25) for water extends from a N_{Re} of 1000 up, with no indication of transition as low as 1000, although considerable scatter of the data is observed below $N_{Re} = 1700$. The data of Fentress (24) covers the Reynolds Number range of 850 to 20,000, with no break observed which might indicate transition. In all of these references, no vapor shear stress was present and no attempts were made to measure film thicknesses.

Dukler in reference (27) has used a film thickness measuring technique employing a capacitance measurement. This device determines film thickness by the difference in dielectric constants of air and water between two plates of a capacitor. One of the advantages of the technique is that it averages out surface waves and irregularities. All measurements were made on the film flowing down a vertical, flat plate. Film thickness readings agree well with the Nusselt prediction in the lower N_{Re} range and with the prediction from the "universal velocity distribution" in the higher N_{Re} range. As the technique is somewhat difficult to apply in a round tube, no investigations of a vapor shear stress effect were undertaken. For the flat plate with no vapor shear

stress, transition is indicated at a N_{Re} of 1000.

It is apparent that considerable variation exists in the results of the many investigators cited here. On the basis of the works covered in this survey, no difinite conclusions can be reached as to the onset of turbulence in a liquid film flowing downward under the influence of gravity. Furthermore, no investigations have been made to determine the effects of an appreciable vapor shear stress. More knowledge in this direction is urgently needed. This, therefore, will be the direction to be taken in the experimental part of the thesis.

SECTION B - EXPERIMENTAL EQUIPMENT

The purpose of the experimental program is to investigate the hydrodynamics of a liquid film flowing downward along a vertical surface under the influence of a shear stress exerted on the outer face of the liquid. In order to obtain quantitative results it is necessary to be able to directly measure the following quantities:

(1) The liquid flow rate

(2) The liquid temperature

(3) The magnitude of the interfacial shear stress

(4) The liquid film thickness

(5) In addition, it would be desirable to be able to obtain measurements which would give quantitative information as to friction factors for two component flow

Although a two dimensional set-up, with the liquid flowing down a flat plate, was considered, the necessity of accurately determining the interfacial shear stress led to the choice of a vertical tube for the test section. By introducing the liquid along the tube wall, it flows down the walls in film form. A flow of air in the core of the tube simulates the vapor flow in a vertical tube condenser and supplies the shear stress on the outer face of the liquid. By assuming no pressure drop across the liquid film, this shear stress can be easily measured by pressure drop readings along the length of the tube.

The test section is shown in Figure 15 and is a one inch diameter tube approximately 5 feet long. Pressure taps are installed at one

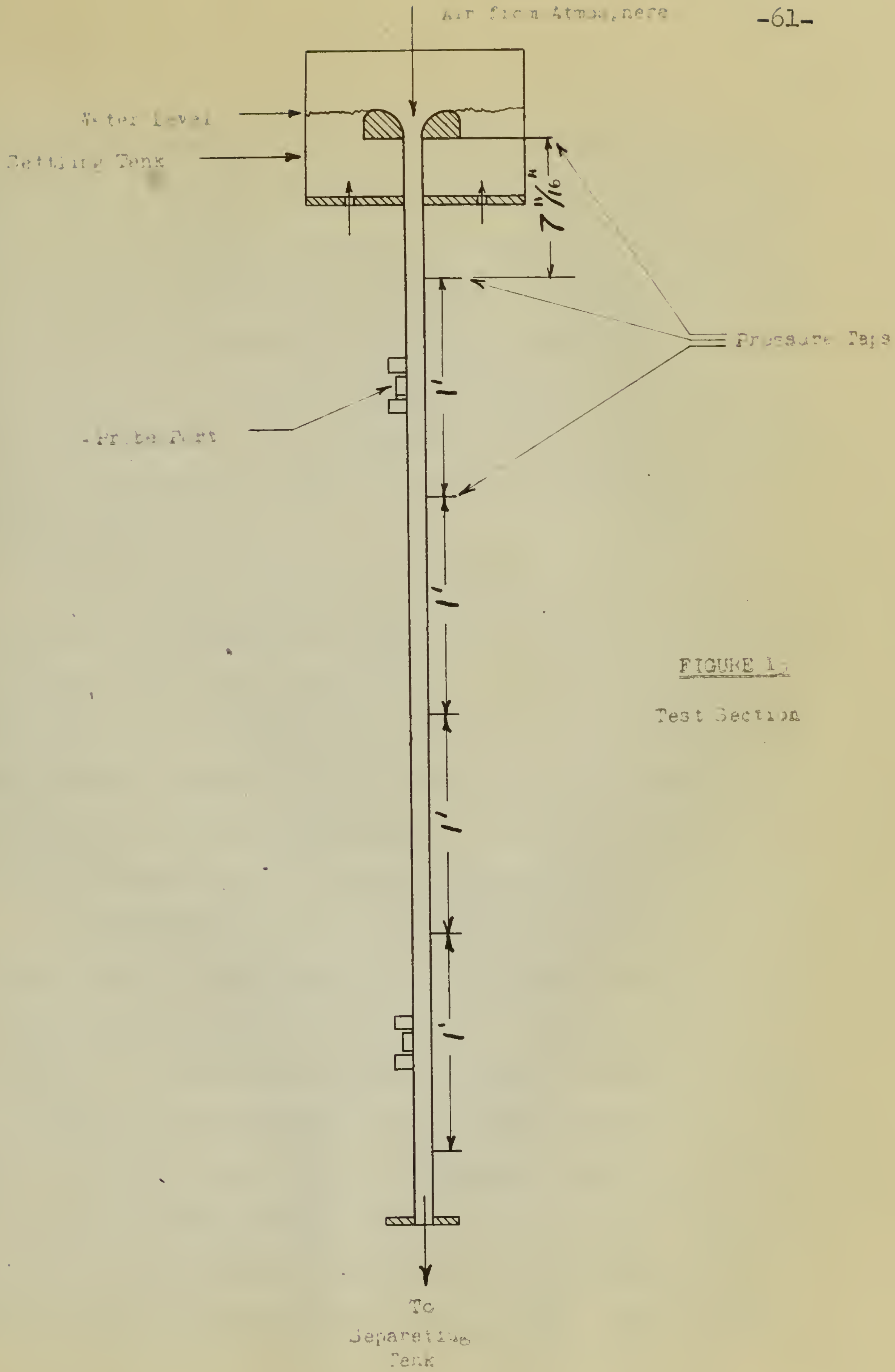

FIGURE 1

Test Section

foot intervals along its length. In order to prevent arcing over of the liquid at high flow rates, a smooth convergent nozzle is placed at the top of the tube. Surrounding the nozzle is a settling tank to damp out any turbulence or fluctuations which might exist in the liquid as it is discharged from the supply system. The nozzle acts as a weir in the settling tank to evenly distribute the liquid along the walls of the tube. The entire test section, nozzle, and settling tank are constructed of lucite to permit visual observation of flow characteristics.

Six probe ports are installed in the test section. These are arranged in two groups of three each, spaced evenly around the circumference of the tube. Details of the probe ports are shown in Figure 16. Film thickness readings are made with the modified depth gage micrometer, shown in place. Metal probe plugs, whose inner ends are flush with the test section wall, are installed to provide electrical continuity from the micrometer probe through the liquid film.

The micrometer probe is a standard depth gage micrometer with a pointed extension added to the shaft. The shaft and the extension, except for the extreme tip, are insulated. This probe is shown in Figure 17. To obtain film thickness readings, the probe is inserted in the port, with the shoulders of the micrometer held firmly on the blocks provided. A zero reading is obtained by advancing the micrometer until it touches the far wall of the test section. The probe is retracted and a sensitive ohmmeter connected between the end of the micrometer and one of the adjacent port plugs. The micrometer

FIGURE 10

Probe Port

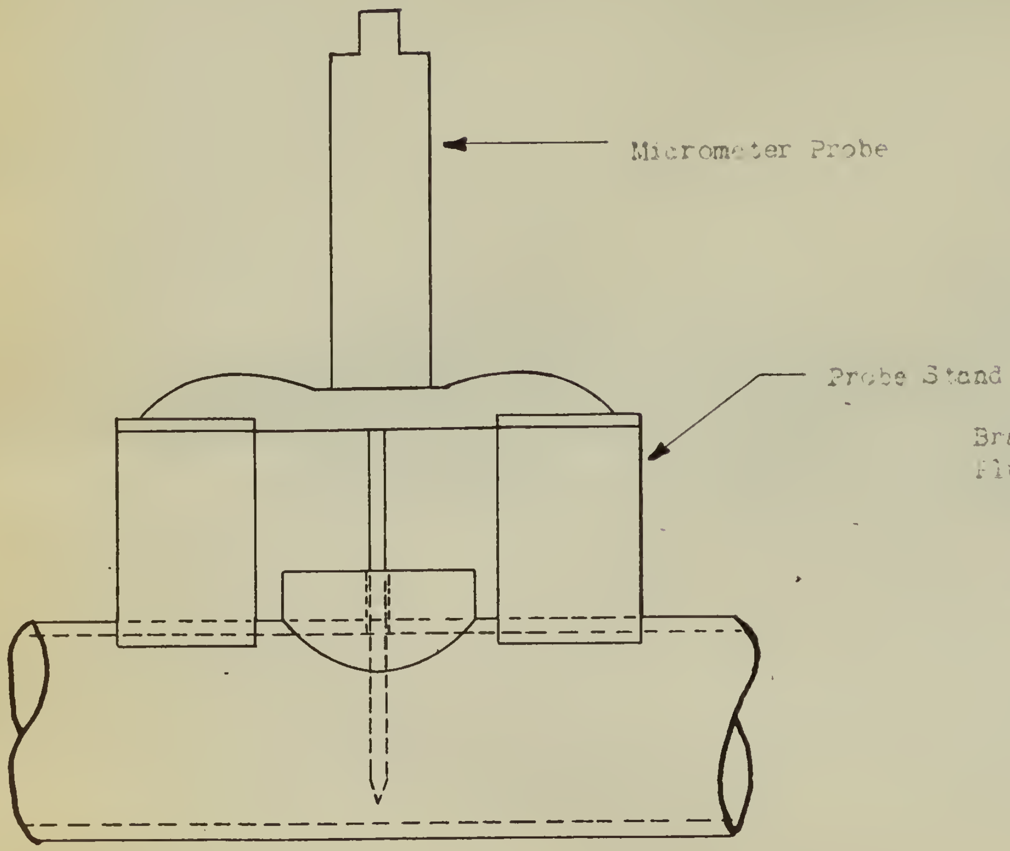

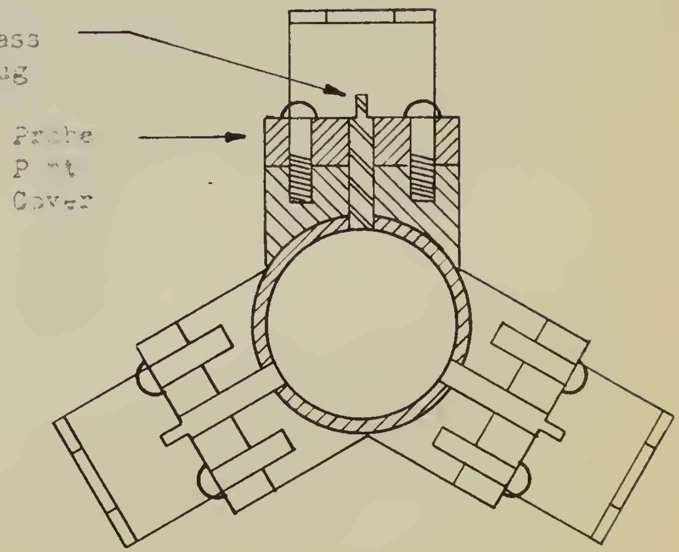

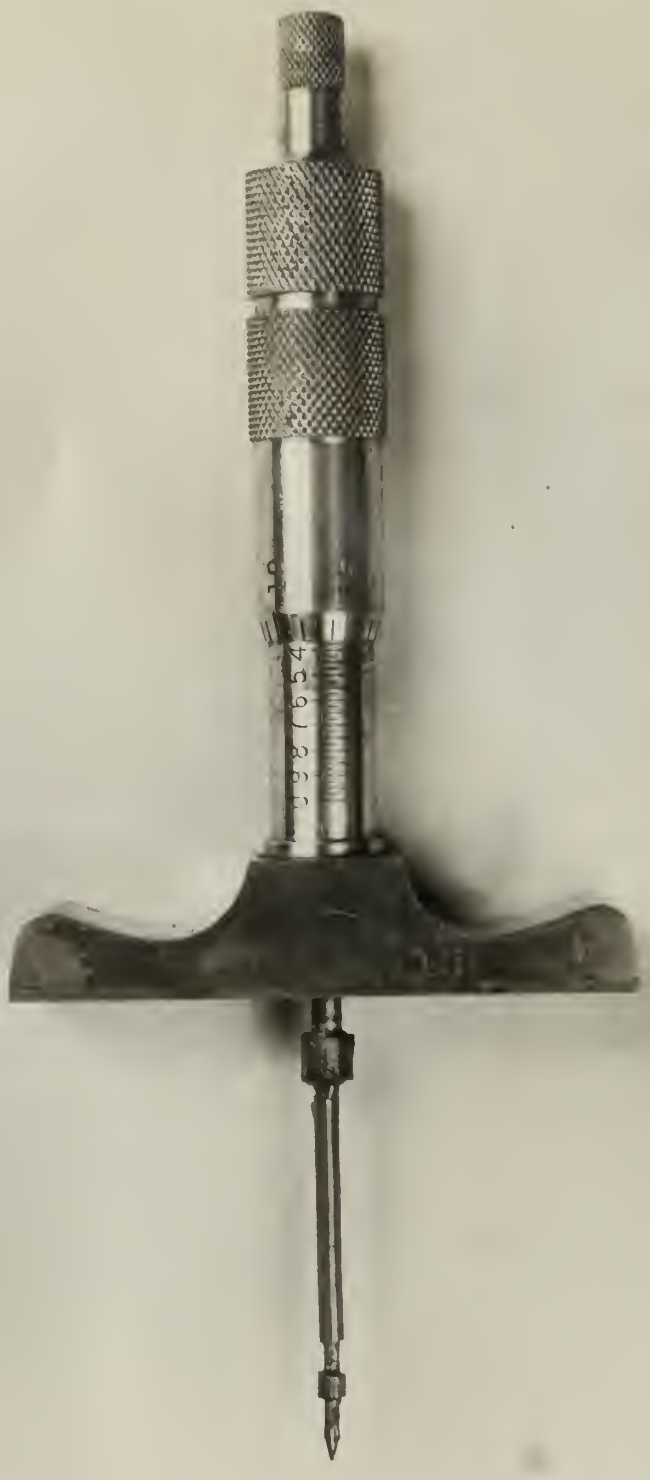

Figure 17

Micrometer Probe

is then advanced until electrical continuity is established by the probe tip touching the outer edge of the liquid film. This continuity is easily detected by the ohmmeter. The insulation on the shaft of the probe prevents completion of the circuit by the film on the near wall of the tube, through which the probe extends.

Pressure readings in the test section were made with a standard U tube manometer with air in the tubing between the manometer and the pressure tap. Surface tension forces at the interface between the liquid on the walls of the test section and the air in the tubing, plus the tendancy of the liquid to be drawn from the test section into the tubing when changing the pressure level, made these readings somewhat difficult. Uncertainties of measured pressure levels were only evident at low air flow rates, when the surface tension forces were of a comparable magnitude to the pressure forces. Modifications have been made to correct this by using a single manometer tube, with the connecting tubing completely filled with liquid. This requires that a zero reading be taken with no flow in the test section, but eliminates all interfaces in the pressure measuring apparatus. However, all data presented here were made with the original system. Pressure readings plotted as straight lines for all but the very low air flow rates, and appear to be fairly reliable.

The test section discharges to a closed separating tank, whose purpose is to separate the liquid from the air. The air suction line is connected to the top of the tank through a standard pipe Tee inside

the tank. The air flow must traverse several sharp changes in direction, thereby separating any liquid droplets which might be entrained. A liquid recirculating pump is connected to the bottom of the separating tank through a flexible hose.

No attempt was made to measure the air flow rates in these preliminary investigations. Such measurements could be easily made by installing a rotameter or some positive displacement measuring device in the air suction line. It is felt that these measurements, which would enable determination of friction factors, would be highly desirable for future experimental work.

The liquid flow rate is measured by an orifice installed in the supply line. The pressure drop across this orifice is measured by a water over mercury manometer. This system was calibrated in place by time - weight measurements. Calibration data and curves are given in Appendix B. Liquid temperature readings are obtained from a thermometer placed in the settling tank at the top of the test section.

Auxiliary equipment consists of a pump to recirculate the liquid through the system, and necessary piping. For the preliminary experimental program included in this thesis, water was the only liquid tested and therefore, connections were made to a water main as a source. A line sketch of the equipment is shown in Figure 18. Figure 19 is a photograph of the set-up, showing the test section assembly and separating tank on the right, with the micrometer probe in place.

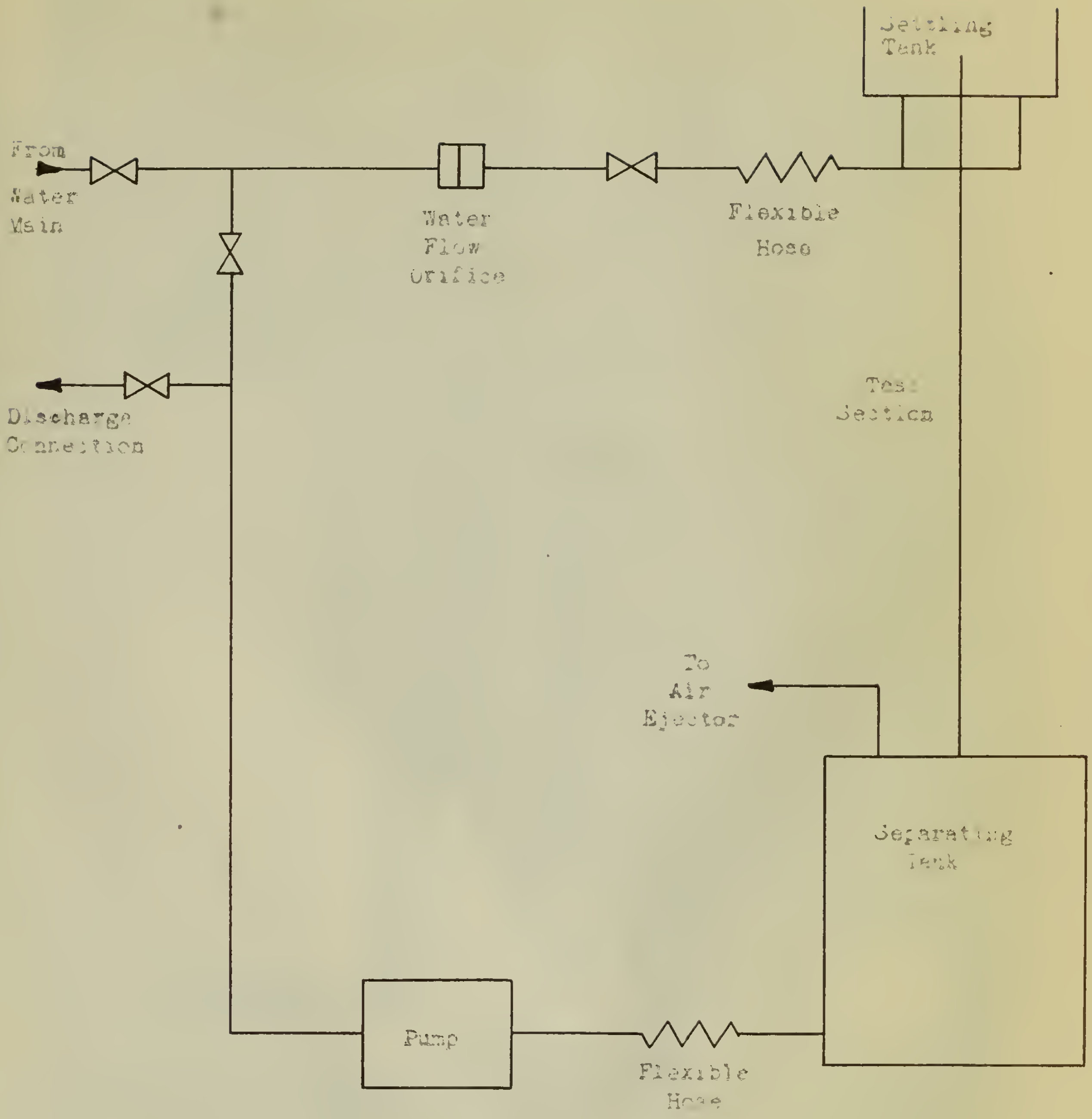

FIGURE 19

Schematic of Experimental Apparatus

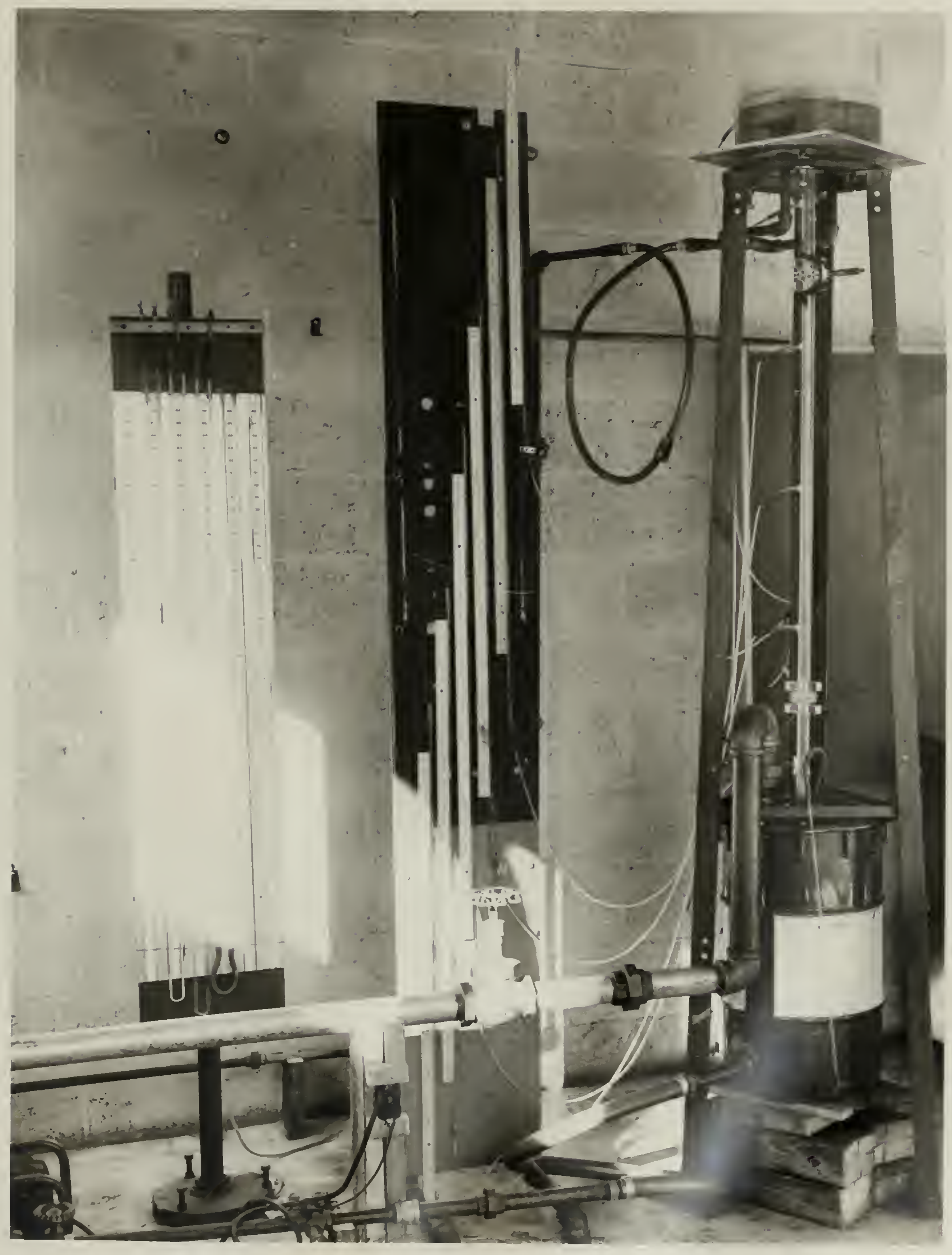

Figure 19

Experimental Apparatus

Since it was anticipated that vibrations would quite possibly be critical in affecting the steadiness of the flow, flexible hoses were installed in the piping from the separating tank to the pump and in the supply piping just before the settling tank. The test section was thus isolated from vibrations in the piping system and pump.

SECTION C - FILM THICKNESS

Film thickness measurements have been made in the manner described in Section B, Part II. Since we are dealing with a round tube rather than a flat plate, it would be worthwhile to investigate the equations applicable to this case and compare them with those derived for the flat plate in earlier sections.

Consider the control volume, whose cross section is shown shaded in Figure 20. This control volume is an annular ring around the tube.

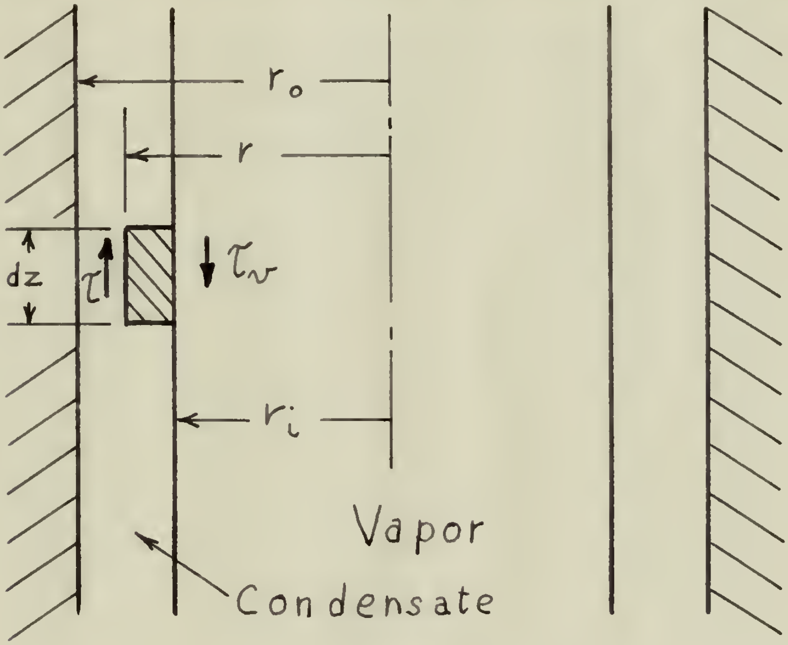

FIGURE 20

Since there is no condensation, momentum terms may be neglected, and the force balance for the control volume is given as

$$\tau 2\pi r dz + \frac{dp}{dz} dz \pi (r^2 - r_i^2) - \frac{g}{g_o} \rho \pi (r^2 - r_i^2) dz - \tau_v 2\pi r_i dz = 0 \tag{64}$$

After some simplification and rearrangement, this reduces to

$$\tau = \frac{g}{g_o} \rho \frac{1}{2} \frac{(r^2 - r_i^2)}{r} + \tau_v \frac{r_i}{r} - \frac{1}{2} \frac{dp}{dz} \frac{(r^2 - r_i^2)}{r} \tag{65}$$

Since momentum terms do not enter, it is possible to use the expression for dp/dz of Equation (61) with the second term = 0

$$\frac{dp}{dz} = \frac{g}{g_o} \rho_v - \frac{2\tau_v}{r_i} \tag{66}$$

Substituting this in Equation (65), we get

$$\tau = \frac{g}{g_o} (\rho - \rho_v) \frac{(r^2 - r_i^2)}{2r} + \tau_v \frac{r}{r_i} \tag{67}$$

In solving for dp/dz from conditions in the vapor core of the tube and then applying this dp/dz to the equations for shear stress in the liquid film, the assumption has been made that no change in the pressure gradient occurs in a radial direction. This assumption is quite good, and almost exact for thin liquid films.

In order to compare the distribution of shear stress given by Equation (67) with that previously derived for the flat plate, it is necessary to substitute $r_i = r_o - x_o$ and $r = r_o - x$. These substitutions are identically true from the geometry and merely serve to shift the zero axis from the tube centerline to the tube wall. Making the

substitutions and simplifying, we have

$$\tau = \frac{g}{g_0}(\rho - \rho_v)\left[\frac{r_0(x_0 - x)}{r_0 - x} - \frac{(x_0^2 - x^2)}{2(r_0 - x)}\right] + \tau_v \frac{r_0 - x}{r_0 - x_0} \tag{68}$$

If the liquid film is thin, $r_o \gg x$ and $r_o \gg x_o$. For this condition considerable simplification may be made, resulting in the following shear stress distribution.

$$\tau = \frac{g}{g_0}(\rho - \rho_v)(x_0 - x) + \tau_v \tag{69}$$

This expression is identical to Equation (2), which was derived for the flat plate, and forms the basis for the development of the predicted heat transfer coefficients.

In the experimental program, the maximum film thickness measured was of the order of .025 inches. This represents 5% of the tube radius. By substituting these values in Equation (68), it is easily shown that the maximum error which is introduced by the simplifying assumption that the film is thin is only 5.5%. This maximum error will occur when considering the wall shear stress and will only be apparent when the vapor shear stress forces are large compared to the gravity forces. In this case, the film thicknesses are much smaller than .025 inches.

Having verified that the flat plate equations for shear stress are approximately true for the case of a vertical tube, it is now possible to utilize the flat plate equations to predict the film thickness as a function of τ_v^*. For laminar flow, Equation (22) applies. For a given Reynolds Number, by assuming various values of x_o^* and

solving for τ_w^*, we are able to plot x_o^* as a function of τ_w^*. Similarly, for the case of turbulent flow in the liquid film, for a given Reynolds Number, a trial and error solution of Equation (49) will yield a value of x_o^+. From the definition of x_o^+, Equation (38), the wall shear stress can be found in terms of the film thickness, x_o. By equating this expression for wall shear stress to that from the force balance, Equation (3), a formula for x_o^* in terms of τ_w^* is obtained. This has been done for both laminar and turbulent films at the Reynolds Numbers for which film thickness readings were obtained, and forms the basis for the theoretical curves shown on the plots of measured data.

The procedure used in obtaining measured values of film thickness is as follows. Liquid was recirculated with the pump, and the flow rate adjusted to give the Reynolds Number desired. The pump was used on all of these runs, rather than water directly from the water main as it was found that fluctuations in city water pressure made it impossible to obtain steady flow rates. With the water flow rate constant, the throttling valve on the air suction line was adjusted to give various levels of pressure drop through the test section. At each of these values of pressure drop, film thickness readings were taken with the micrometer probe, following the procedure described in Section B, Part II. Before each series of runs, film thickness readings were taken through all three of the probe ports in the group being worked with to insure that film thicknesses were equal around the circumference

of the tube and that the flow was evenly distributed. The raw data and computations for these runs are included in Appendix C and are shown plotted in Figures 21 through 27.

The static pressure level at points in the test section was plotted against distance, and a straight line curve drawn through these points. The slope of this curve was then taken as the pressure gradient in the z-direction. This pressure gradient could then be easily converted to the vapor shear stress, τ_v^*, from the formula

$$\tau_v^* = \frac{g_0}{g} \frac{1}{(1-\rho_v/\rho)\left(\frac{\nu^2}{g}\right)^{1/3}} \frac{r_0}{2} \frac{dp}{dz} \tag{70}$$

where r_0 is the radius of the tube.

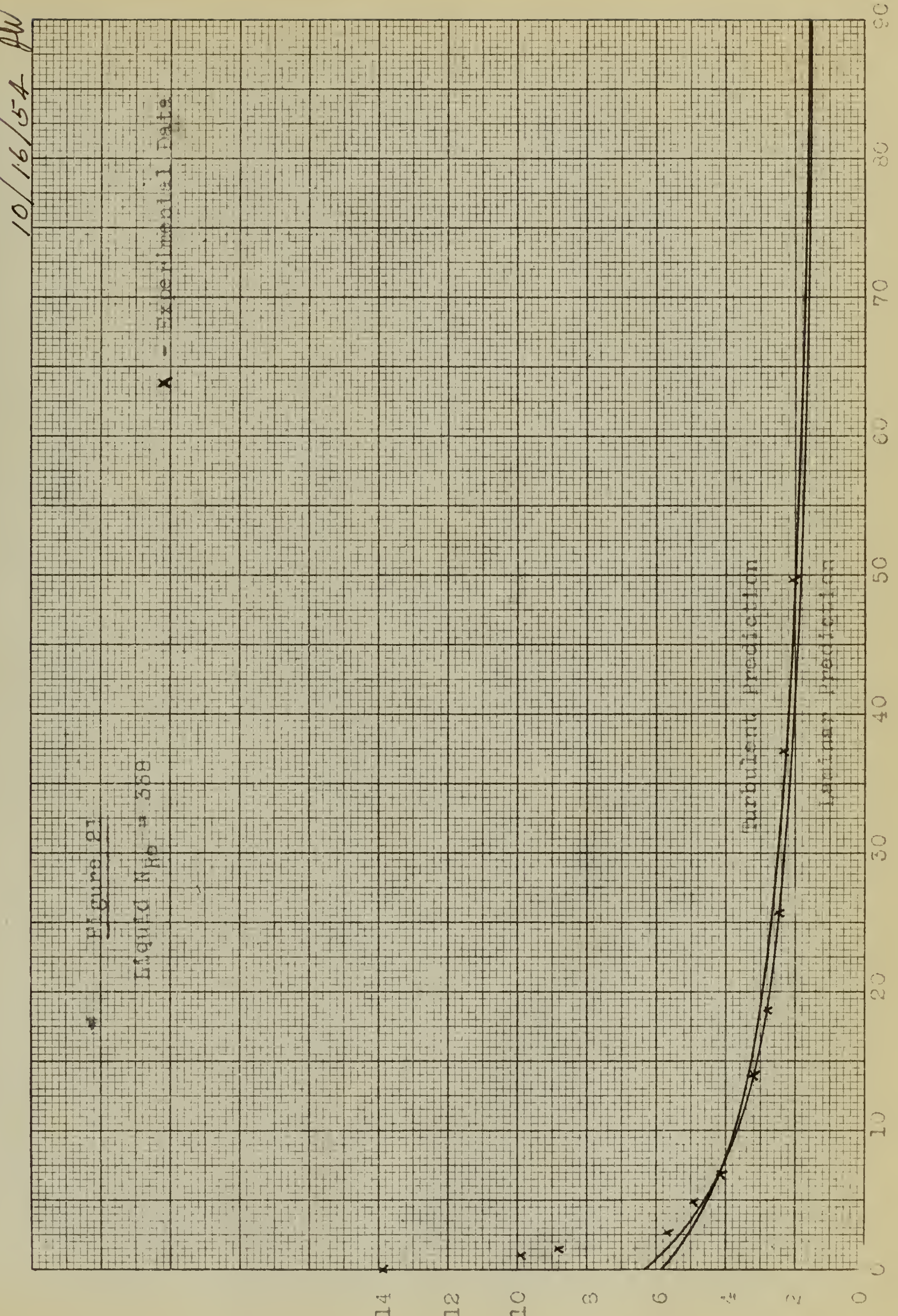

Figure 21

Liquid $N_{Re} = 568$

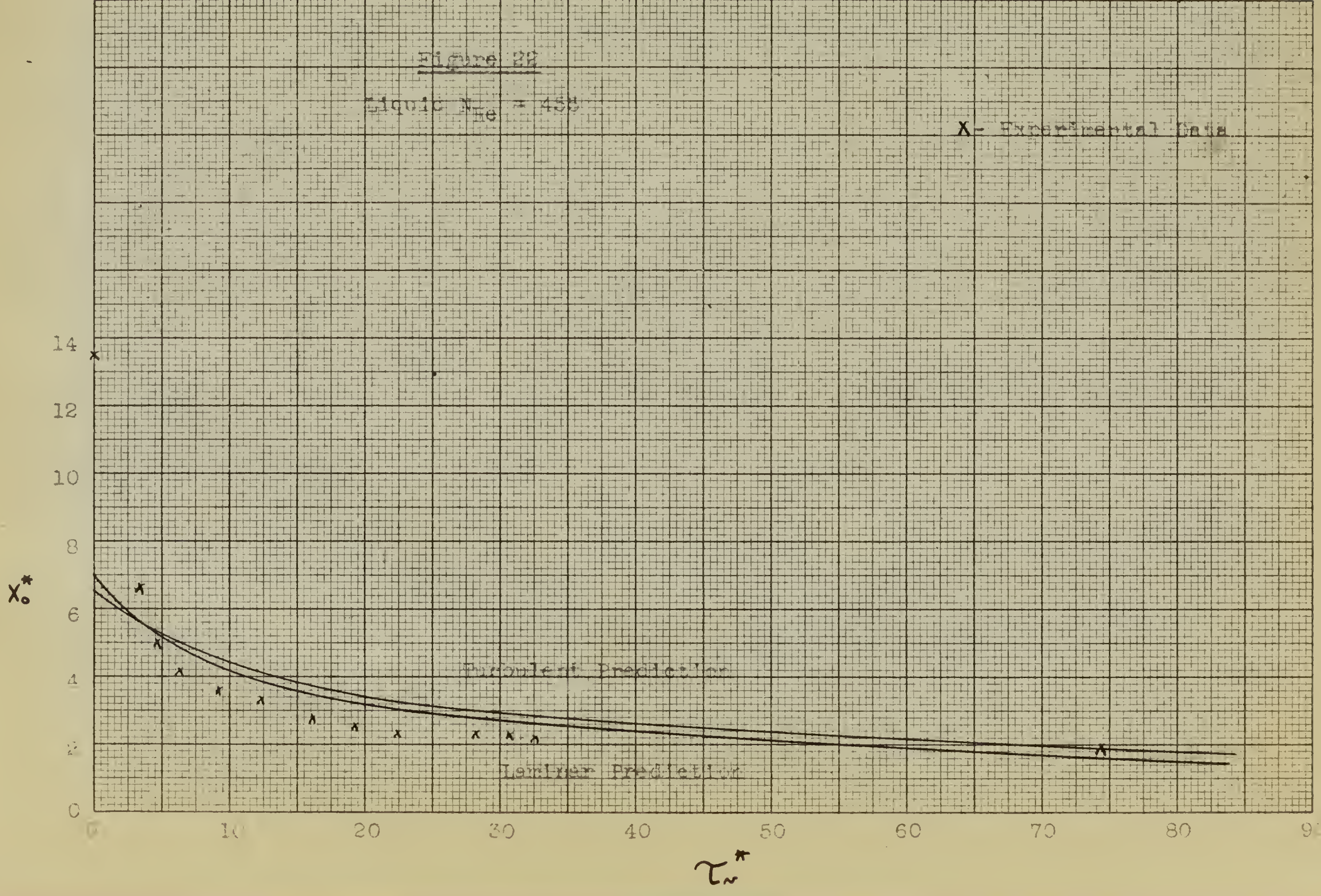

Figure 22

Liquid N_{Re} = 458

10/9/54 JW

10/16/54 JW

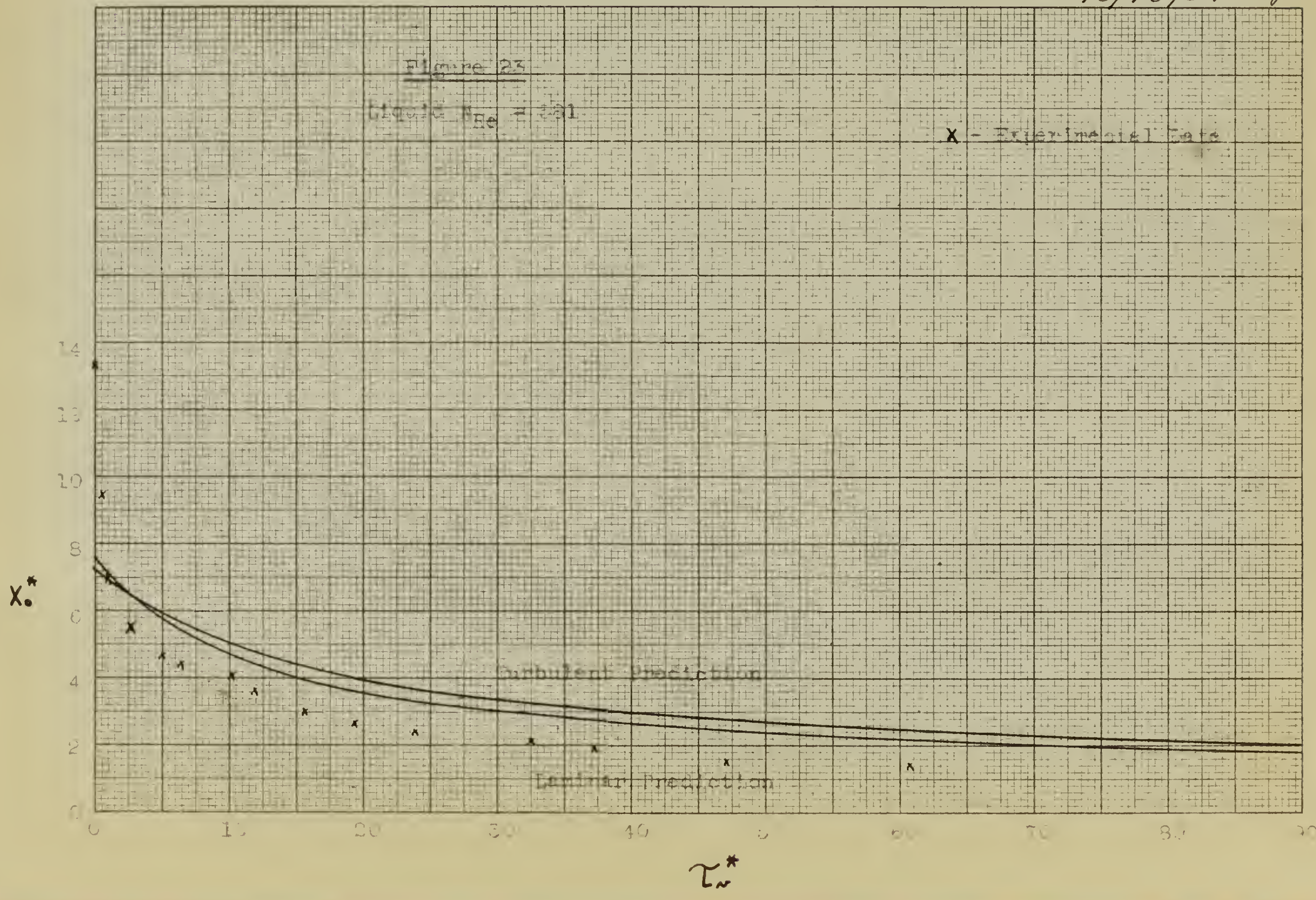

Figure 23

Liquid N_{Re} = 231

10/9/54 JW

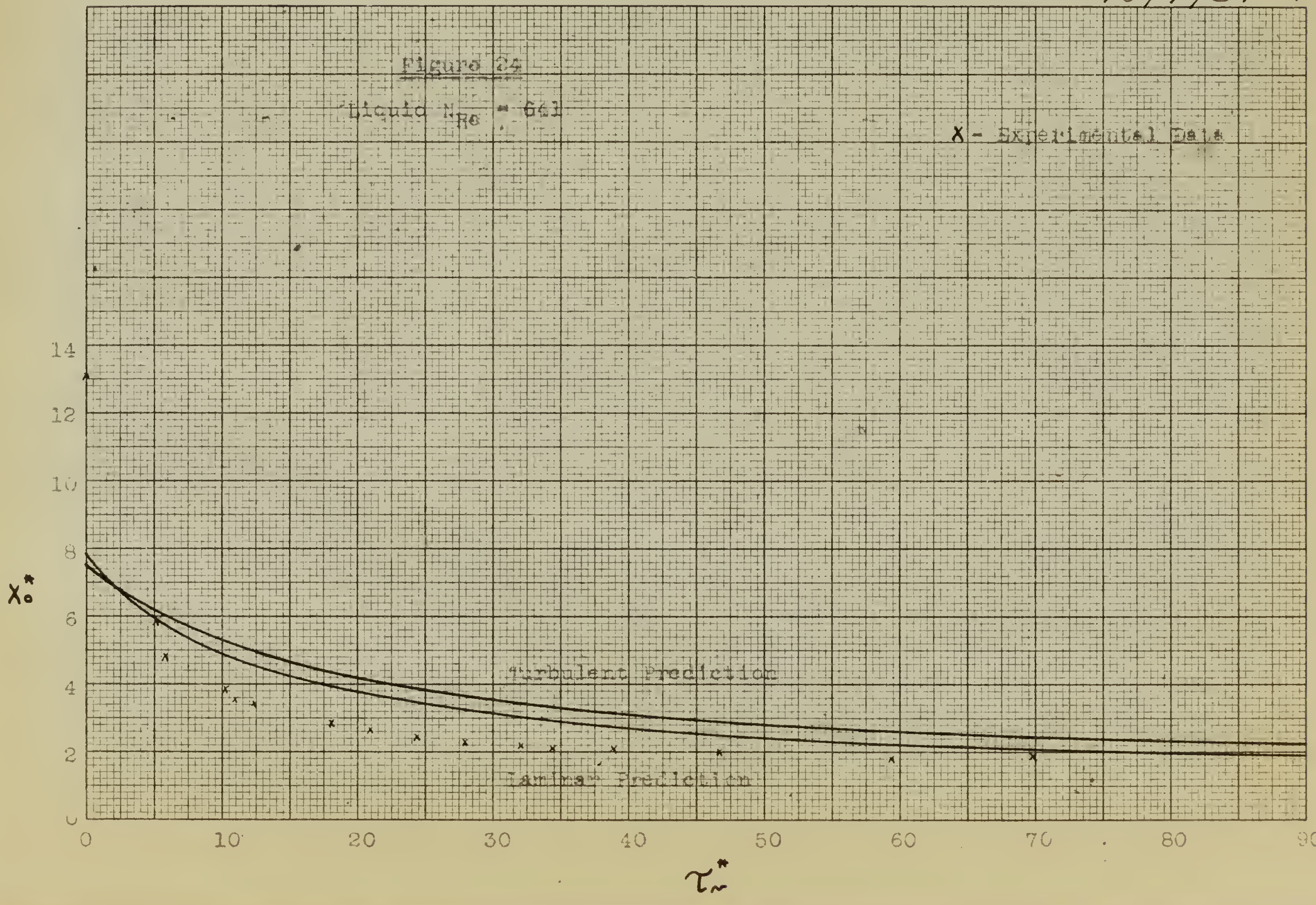

Figure 24

10/16/54 JW

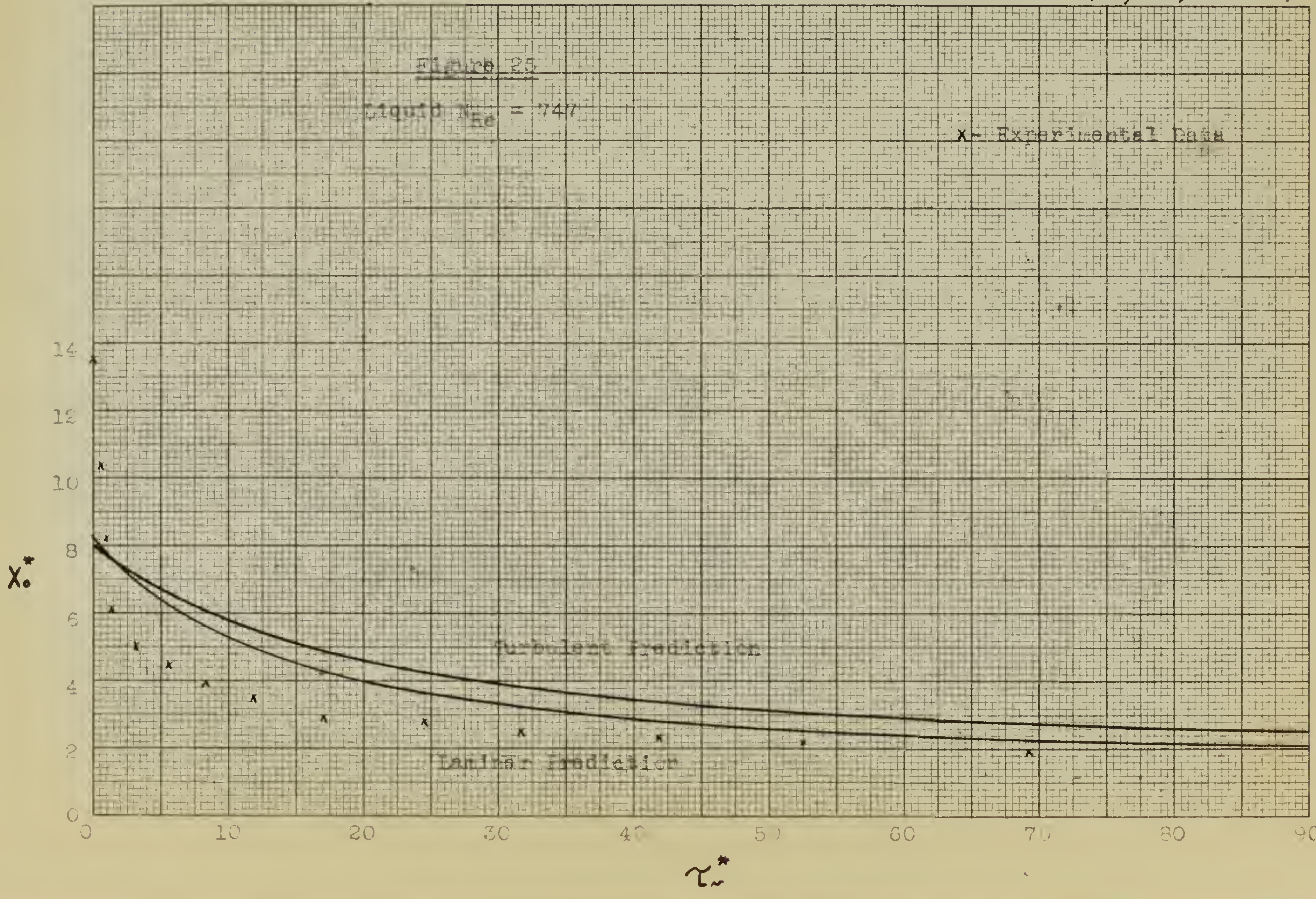
Figure 25

10/9/54 JW

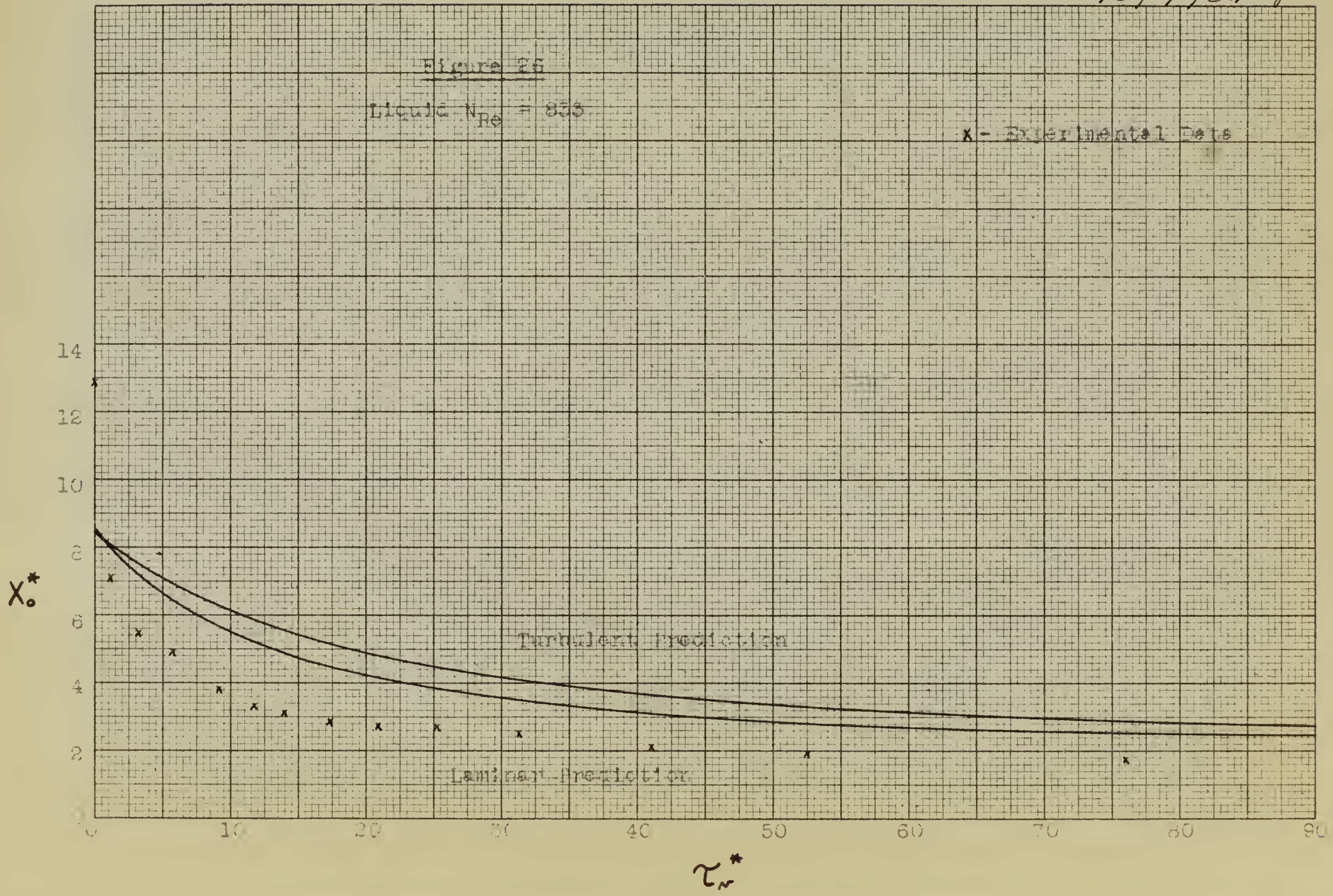

Figure 26

Liquid N_{Re} = 833

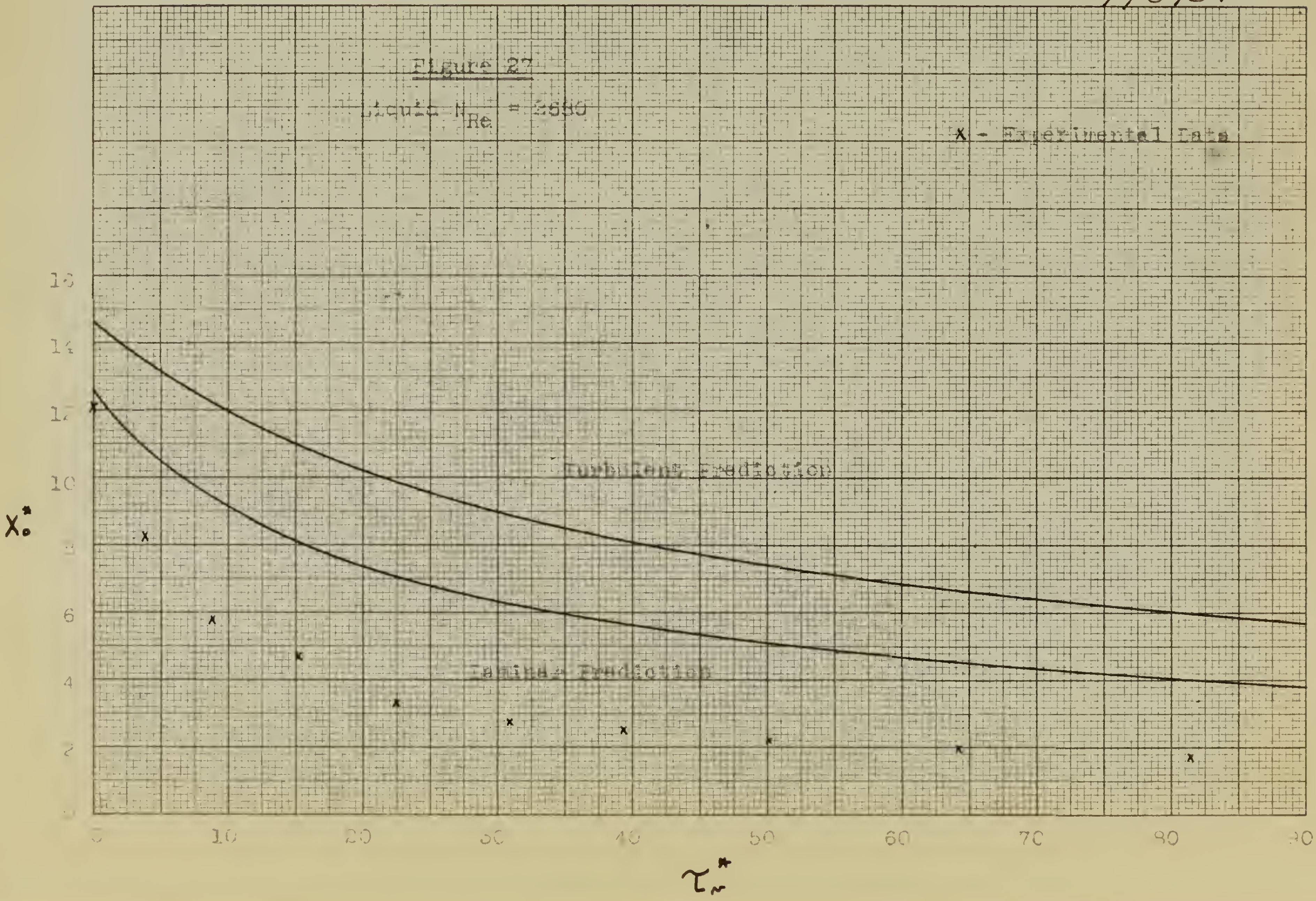

Figure 27

Liquid $N_{Re} = 2550$

9/3/54 JW

DISCUSSION OF FILM THICKNESS MEASUREMENTS

Inspection of the plotted results of the film thickness measurements, Figures 21 to 27, reveals several interesting facts. First, the shapes of the curves of x_o^* versus τ_w^* correspond closely with the shapes of the theoretical curves. In general, the values of measured film thickness lie below the predicted values, this deviation becoming more noticeable at higher liquid Reynolds Numbers. The measured values for $\tau_w^* = 0$ are consistently higher than predicted. At high values of τ_w^*, experimental values of x_o^* agree well with theoretical values. There appears to be rather sharp change in curvature of the measured values at values of τ_w^* in the neighborhood of 5 to 10.

For $\tau_w^* = 0$, visual observations revealed that rather large surface waves were present on the interface of the liquid layer. These waves made film thickness measurements, using the micrometer probe and electrical continuity technique, somewhat uncertain. The ohmmeter registered alternate breaking end making of contact between these surface waves and the probe. In taking the readings, an attempt was made to obtain a mean wave height reading, but this procedure is admittedly a crude one, as surface tension forces tended to maintain contact between the probe tip and the liquid surface. Therefore, it is not surprising that these readings were high, it being believed that thicknesses, as measured, were actually somewhat nearer the crests of the waves than the mean height.

For all values of τ_w^* greater than about 5, the large, slow moving

surface waves were replaced by much smaller and more rapidly moving irregularities. Indications on the ohmmeter gave quite sharp cut-off points for contact of the probe with the surface. It is felt that film thickness readings for the higher values of τ_r^* are accurate to within .0005 inches. This is based on the sharp cut-off points and the consistency of the readings on several runs under identical conditions.

The fact that measured values of x_o^* lie below the predicted curves leads to the conclusion that the velocity distribution is actually something other than that assumed. Although the theoretical turbulent curves lie above the laminar curves, it is believed that, for the higher values of τ_r^*, the film is essentially in turbulent motion. This conclusion is based on the appearance of the film and on some preliminary results obtained with a hot wire anemometer in the liquid film. The fact that the velocity distribution may be something other than the universal distribution of Prandtl-Nikuradse is not altogether surprising. The use of this velocity distribution is certainly an over extension of their work, which was derived from measurements of full pipe flow. However, the actual values of film thickness are at least within a few percent of the predicted results.

It is believed that the change in curvature of the measured values of film thickness is due to the damping out of the large surface waves. This corresponds to visual observations. The general character of the flow, as observed through the transparent test section was as follows: For $\tau_r^* = 0$, the flow was mainly clear with relatively large and regular surface waves. The frequency of these waves was low and fairly

constant, being of the order of 8 cycles per second. As the air flow was increased, these large surface waves were damped out until, at around $\tau_w^* = 5$, the flow appeared quite clear and transparent. For yet higher values of τ_w^*, very small surface waves were formed, with a relatively high frequency. It is estimated that the height of these waves was less than .0005 inches. It is felt that these small waves are directly connected with the onset of turbulence in the liquid film. It is to be noted in this respect, that these small waves could be attained without any air flow at all, but required very high liquid Reynolds Numbers. No measurements of this point were obtained, the flow rate being beyond the capacity of the liquid flow manometer. It is estimated that liquid Reynolds Numbers of the order of magnitude of 6,000 to 8,000 are required to attain this condition.

On the basis of the film thickness measurements, no definite information could be deduced as to the onset of turbulence, as affected by a vapor shear stress. However, the equations predicting film thickness proved to be approximately correct. It may be concluded from this information that the assumed velocity distribution is adequate for the purpose of predicting heat transfer coefficients. It may also be concluded that the equations derived for a flat plate will be equally applicable to vertical tubes, as long as the film thickness is small compared to the tube radius.

SECTION D - PRELIMINARY RESULTS OF HOT WIRE ANEMOMETER

In Part I the criteria for determining the transition point of the liquid film from laminar to turbulent flow were proposed. These criteria, although based on some experimental work, are far from being verified, especially in the region of appreciable vapor shear stresses. In fact, no experimental work has been found that can shed light on this phenomenon of transition, as affected by a vapor shear stress. This section will discuss the preliminary work for determining the transition point by means of a hot wire anemometer. No quantitative information has been obtained, but work along these lines is currently in progress and should become available in the near future, reference (16).

The instrument is a standard hot wire anemometer, manufactured by the Flow Corporation of Cambridge, Massachusetts. It is being used in compressor blade cascade studies in the Gas Turbine Laboratory at M. I. T. The element is a .0003 inch diameter tungsten wire, supported by a long shaft. By inserting the shaft through one of the probe ports on the test section, the wire can be introduced into the liquid film on the far side of the test section. With currents of approximately 150 milliamps, good indications can be obtained on an oscilloscope. With the relatively high current, the wire burns out almost instantly if exposed to air. This has been the source of some difficulty, and it may be necessary to modify the wire element or lower the current to prevent this.

At low liquid Reynolds Numbers, the flow appears to be quite

susceptible to unsteadiness caused by vibrations. Preliminary runs were made while a large air compressor was running in the same building, approximately 100 feet away. Very regular velocity fluctuations were observed at low Reynolds Numbers, which died out as the liquid flow was increased. The runs were then repeated at night, when the compressor was not running, and these fluctuations were absent.

For the case of no shear stress, laminar flow in the liquid film existed up to Reynolds Number of 6,000 to 8,000. A trip wire was inserted around the nozzle throat at the entrance to the test section. With this trip wire, occasional turbulent fluctuations were observed at the maximum flow rate that the liquid flow manometer could measure. It is believed that stable laminar flow exists up to Reynolds Numbers of 6,000. This observation has at present not been verified.

With air flowing in the test section, a consistently turbulent flow could be attained with lower liquid Reynolds Numbers. However, as was evident from the film thickness measurements, the film is extremely thin for the regions of appreciable vapor shear stress, and difficulty was encountered in keeping the hot wire completely in the water film. It may be necessary to use a more viscous fluid in order to get film thicknesses of sufficient magnitude with which to work.

On the basis of the very sketchy work done with this technique, little of a quantitative nature can be concluded. However, the technique appears to be a powerful one. Turbulent indications are quite marked on the oscilloscope trace, although a lower background noise level would be desireable to enable more exact determination of the

transition from completely laminar conditions. It is felt that, once the minor problems have been solved, the hot wire anemometer will yield the answer to the transition question.

SECTION E - RECOMMENDATIONS FOR FUTURE EXPERIMENTAL WORK

In view of the present lack of knowledge concerning the behavior of a falling liquid film from a fluid dynamics point of view, it is recommended that the first experimental efforts be directed along this channel.

Specifically, it is felt that it would be desirable to fully investigate the transition criteria. This should be done with at least three liquids of widely varying viscosity. Consideration should be given to varying surface tension also. This recommendation is based on the fact that, in this type of fluid flow, these forces may quite possibly be the only significant ones in the radial direction. It is worthy of comment that a surface tension ratio was the correlating factor in the friction factors presented in reference (11).

In working with other fluids, it would be desirable to verify the film thickness measurements presented in this thesis. By gathering sufficient information, equations more adequately describing the velocity distribution in the turbulent regions should be developed.

Much more information concering friction factors in two phase cocurrent flow is needed. As previously pointed out, this can be easily obtained from the present set-up by adding a meter to measure air flow rates.

After the hydrodynamics of the liquid film have been sufficiently defined, the analysis should be modified to include any new or better information that may have been discovered. Finally the analysis should

be directly checked by investigation of an experimental condenser, in which provisions should be made to determine point values and mean values of the condensing side heat transfer coefficients.

APPENDICES

APPENDIX A - NUMERICAL EVALUATION OF ANALYTIC EQUATIONS

Laminar Portion

For this portion of the condensate film, the significant Equations are (18), (22), and (26).

$$z^* = (x_o^*)^4 + \frac{4}{3}\,\tau_v^*\,(x_o^*)^3 \tag{18}$$

$$\frac{N_{Re}}{(1-\rho_v/\rho)} = \frac{4}{3}\,(x_o^*)^3 + 2\,\tau_v^*\,(x_o^*)^2 \tag{22}$$

$$\frac{h_m}{k}\left(\frac{\nu^2}{g}\right)^{1/3} = \frac{4}{3}\,\frac{(x_o^*)^3}{z^*} + 2\,\tau_v^*\,\frac{(x_o^*)^2}{z^*} \tag{26}$$

For given values of τ_v^* assume various values of x_o^* lower than the transition point, which is given by either Equation (29) or (32). For the assumed values of x_o^*, both z^* and $N_{Re}\,\frac{1}{(1-\rho_v/\rho)}$ may be evaluated directly. $\frac{h_m}{k}\left(\frac{\nu^2}{g}\right)^{1/3}$ may now be found from the given values and the computed values of z^*.

Turbulent Portion

For computation purposes, Equation (58) may be rearranged into the more convenient form

$$\frac{h_m}{k}\left(\frac{\nu^2}{g}\right)^{1/3} = \frac{N_{Re}}{(z^* - z_t^*) + z_t^*} \tag{58a}$$

The evaluation of this equation entails a numerical integration procedure and is best followed by listing the steps involved.

Step 1 - For given values of τ_v^* and N_{Pr}, assume various values of x_o^* greater than that at the transition point.

Step 2 - Evaluate M from Equation (45a).

Step 3 - Evaluate $x_o^+ = x_o^* \sqrt{(x_o^* + \tau_v^*)(1 - \rho_v/\rho)}$. At this point in the computations it was necessary to assume that $(1 - \rho_v/\rho) = 1$.

Step 4 - Calculate F_2 from Equation (47).

Step 5 - Calculate F_1 from Equation (51).

Step 6 - Form the product, $F_1 F_2 \left[\frac{M}{x_o^+}\right]^{1/3}$.

Step 7 - Plot this product as a function of x_o^+.

Step 8 - At various values of x_o^+, take the area under this curve with a planimeter or by other suitable graphical means. This area is taken from the transition point, x_{ot}^+, to the selected values of x_o^+.

Step 9 - Calculate $(z^* - z_t^*) = \frac{4}{N_{Pr}} \frac{1}{(1-\rho_v/\rho)^{4/3}} \int_{x_{ot}^+}^{x_o^+} F_1 F_2 \left[\frac{M}{x_o^+}\right]^{1/3} dx_o^+$

Step 10 - Add to the result of step 9 the distance to the transition point, z_t^*, found in the laminar calculations.

Step 11 - Calculate N_{Re} from Equation (59).

Step 12 - Now $\frac{h_m}{k}\left(\frac{\nu^2}{g}\right)^{1/3} = \frac{N_{Re}}{z^*}$

Where z^* is the result of step 10.

Step 13 - Plot $\frac{h_m}{k}\left(\frac{\nu^2}{g}\right)^{1/3}$ versus z^* and N_{Re}. There will result a double series of curves with τ_v^* and N_{Pr} as parameters.

The results of the above calculations are contained in Table I and are shown plotted in Figures 7 through 12.

TABLE I

ANALYTIC VALUES OF HEAT TRANSFER COEFFICIENTS

$N_{Pr} = .01$

x_o^+	z^*	N_{Re}	$\frac{h_m}{k}\left(\frac{\nu^2}{g}\right)^{1/3}$
$\tau_w^* = 0,\quad z_t^* = 14,900$			
50	24,580	2,302	.09365
100	80,500	5,544	.06887
200	265,700	12,744	.04796
300	530,500	20,464	.03857
400	857,700	28,544	.03328
600	1,662,900	46,244	.02781
800	2,626,500	62,844	.02393
1000	3,668,500	80,844	.02204
$\tau_w^* = 2.5,\quad z_t^* = 7420$			
50	20,460	2,302	.1125
100	72,460	5,544	.07651
200	248,860	12,744	.05121
300	502,620	20,464	.04071
400	817,820	28,544	.03490
600	1,595,420	46,244	.02899
800	2,528,620	62,844	.02485
1000	3,574,620	80,844	.02262
$\tau_w^* = 5,\quad z_t^* = 2815$			
50	18,415	2,302	.1250
100	68,015	5,544	.08151
200	237,615	12,744	.05363
300	481,615	20,464	.04249
400	786,415	28,544	.03630
600	1,539,215	46,244	.03004
800	2,442,015	62,844	.02573
1000	3,463,615	80,844	.02334

$N_{Pr} = .01$

x_o^+	z^*	N_{Re}	$\frac{h_m}{k}\left(\frac{\nu^2}{g}\right)^{1/3}$
$\tau_v^* = 10$	$z_t^* = 80.9$		
30	5,681	1,125	.1980
50	16,481	2,302	.1397
100	62,081	5,544	.08930
200	219,681	12,744	.05801
300	447,681	20,464	.04571
400	730,881	28,544	.03905
600	1,445,281	46,244	.03200
800	2,308,081	62,844	.02723
1000	3,276,081	80,844	.02468
$\tau_v^* = 20$	$z_t^* = 61.5$		
30	4,862	1,125	.2314
50	13,662	2,302	.1685
100	52,062	5,544	.1065
200	190,862	12,744	.06677
300	396,862	20,464	.05156
400	856,062	28,544	.04351
600	1,301,662	46,244	.03553
800	2,083,662	62,844	.03016
1000	2,972,462	80,844	.02720
$\tau_v^* = 50$	$z_t^* = 40.2$		
30	3,240	1,125	.3472
50	9,640	2,302	.2388
100	38,040	5,544	.1457
200	144,040	12,744	.08848
300	305,240	20,464	.06704
400	512,040	28,544	.05575
600	1,035,640	46,244	.04465
800	1,675,240	62,844	.03751
1000	2,408,000	80,844	.03357

$N_{Pr} = 1$

x_o^+	z^*	N_{Re}	$\frac{h_m}{k}\left(\frac{\mu^2}{g}\right)^{1/3}$
$\tau_w^* = 0$, $z_t^* = 14,900$			
50	19,196	2,302	.1199
100	36,996	5,544	.1499
200	73,856	12,744	.1726
400	146,976	28,544	.1942
600	218,536	46,244	.2116
800	288,336	62,844	.2179
1000	356,836	80,844	.2266
$\tau_w^* = 2.5$, $z_t^* = 7420$			
50	12,892	2,302	.1785
100	27,192	5,544	.2039
200	57,272	12,744	.2225
400	117,712	28,544	.2425
600	177,192	46,244	.2610
800	235,632	62,844	.2667
1000	293,172	80,844	.2758
$\tau_w^* = 5$, $z_t^* = 2815$			
50	9,387	2,302	.2452
100	22,367	5,544	.2479
200	49,987	12,744	.2549
300	78,047	20,464	.2622
400	106,087	28,544	.2691
600	161,647	46,244	.2861
800	216,287	62,844	.2906
1000	270,167	80,844	.2992

$N_{Pr} = 1$

x_o^+	z^*	N_{Re}	$\frac{h_m}{k}\left(\frac{\nu^2}{g}\right)^{1/3}$
$\tau_w^* = 10,\ z_t^* = 80.9$			
15	1,021	379	.3714
30	3,561	1,125	.3159
50	7,601	2,302	.3029
100	18,921	5,544	.2930
200	43,521	12,744	.2928
300	68,961	20,464	.2967
400	94,641	28,544	.3016
600	145,741	46,244	.3173
800	196,181	62,844	.3203
1000	246,161	80,844	.3254
$\tau_w^* = 20,\ z_t^* = 61.5$			
15	862	379	.4399
30	2,882	1,125	.3904
50	6,182	2,302	.3724
100	15,662	5,544	.3540
200	36,882	12,744	.3455
300	59,202	20,464	.3457
400	81,982	28,544	.3482
600	127,902	46,244	.3616
800	173,862	62,844	.3615
1000	219,662	80,844	.3680
$\tau_w^* = 50,\ z_t^* = 40.2$			
15	560	379	.6769
30	1,960	1,125	.5740
50	4,260	2,302	.5404
100	11,100	5,544	.4995
200	27,080	12,744	.4706
300	44,620	20,744	.4586
400	62,840	28,544	.4542
600	100,440	46,244	.4604
800	139,020	62,844	.4521
1000	177,840	80,844	.4546

$N_{Pr} = 10$

x_o^+	z^*	N_{Re}	$\frac{h_m}{k}\left(\frac{\nu^2}{g}\right)^{1/3}$
$\tau_r^* = 0$, $z_t^* = 14{,}900$			
50	16,564	2,302	.1390
100	22,652	5,544	.2447
200	33,972	12,744	.3751
300	44,524	20,464	.4596
400	54,580	28,544	.5230
600	73,596	46,244	.6283
800	91,668	62,844	.6856
1000	108,900	80,844	.7424
$\tau_r^* = 2.5$, $z_t^* = 7420$			
50	9,935	2,302	.2317
100	15,567	5,544	.3561
200	26,023	12,744	.4897
300	35,799	20,464	.5716
400	45,151	28,544	.6322
600	62,927	46,244	.7349
800	79,687	62,844	.7886
1000	95,855	80,844	.8434
$\tau_r^* = 5$, $z_t^* = 2815$			
50	5,985	2,302	.3846
100	11,265	5,544	.4921
200	21,241	12,744	.6000
300	30,689	20,464	.6668
400	39,729	28,544	.7185
600	56,873	46,244	.8131
800	73,153	62,844	.8591
1000	88,849	80,844	.9099

$N_{Pr} = 10$

$\tau_w^* = 10$, $z_t^* = 80.9$			
x_o^+	z^*	N_{Re}	$\frac{h_m}{k}\left(\frac{\nu^2}{g}\right)^{1/3}$
15	777	379	.4880
30	2,137	1,125	.5264
50	4,049	2,302	.5685
100	8,849	5,544	.6265
200	18,129	12,744	.7030
300	27,049	20,464	.7566
400	35,617	28,544	.8014
600	51,849	46,244	.8919
800	67,289	62,844	.9339
1000	82,289	80,844	.9824
$\tau_w^* = 20$, $z_t^* = 61.5$			
15	606	379	.6257
30	1,686	1,125	.6673
50	3,238	2,302	.7109
100	7,334	5,544	.7559
200	15,630	12,744	.8154
300	23,774	20,464	.8608
400	31,718	28,544	.8999
600	47,054	46,244	.9828
800	61,830	62,844	1.0164
1000	76,158	80,844	1.0615
$\tau_w^* = 50$, $z_t^* = 40.2$			
15	392	379	.9673
30	1,128	1,125	.9973
50	2,248	2,302	1.0240
100	5,304	5,544	1.0452
200	11,768	12,744	1.0829
300	18,384	20,464	1.1131
400	25,024	28,544	1.1407
600	38,272	46,244	1.2083
800	51,280	62,844	1.2255
1000	64,032	80,844	1.2626

APPENDIX B - CALIBRATION OF WATER FLOW ORIFICE

TABLE II

lbs	sec.	lb/sec	Temp °F	GPM	inches Hg
5	76.6	.0653	73	.471	2.08
10	63.0	.1589	73	1.142	12.03
10	71.6	.1398	73	1.007	9.48
10	79.4	.1260	73	.908	7.63
10	160.5	.0623	73	.449	1.95
10	171.0	.0585	79	.421	1.65
10	112.5	.0889	79	.640	3.78
10	90.4	.1107	79	.797	5.86
10	245.3	.0407	79	.294	.77
10	79.4	.126	79	.909	7.48
10	69.7	-	79	1.054	9.98
10	58.9	-	79	1.222	13.97
10	52.6	-	79	1.370	17.55
10	54.3	-	79	1.329	16.47
10	49.8	-	79	1.449	19.65

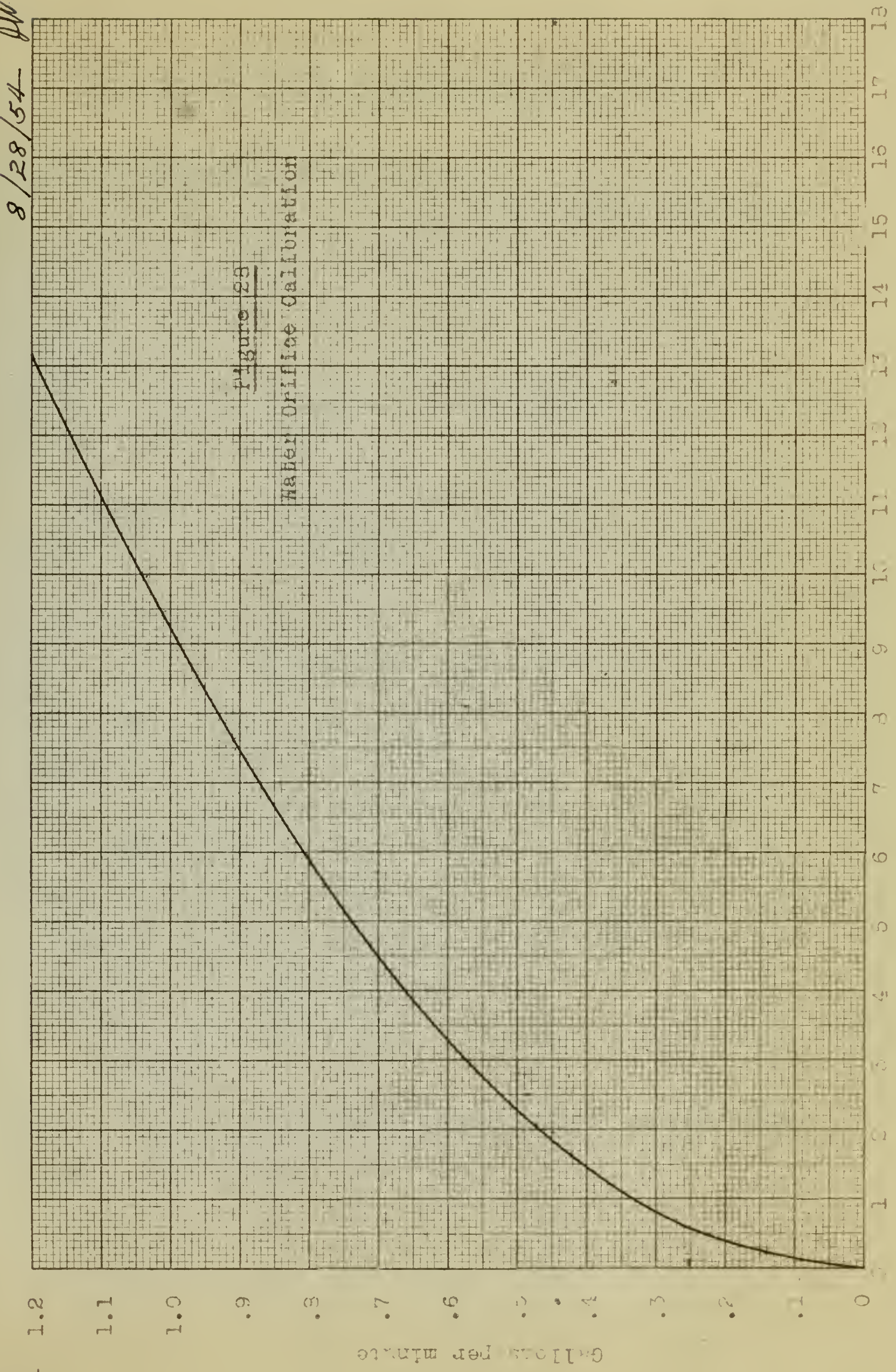

Figure 23

Water Orifice Calibration

8/28/54 JW

APPENDIX C - DATA AND CALCULATIONS FOR FILM THICKNESS

Theoretical Predictions of Film Thickness

Laminar - The laminar predictions result directly from Equation (22), which may be rearranged in the form

$$\tau_w^* = \frac{N_{Re} - \frac{4}{3}\left(x_0^*\right)^3}{2\left(x_0^*\right)^2}$$

For a given N_{Re}, the plot is made by assuming values of x_0^* and solving for τ_w^* .

Turbulent - The turbulent predictions result from the following procedure: First, consider Equation (49), which relates N_{Re} and x_0^+,

For $x_0^+ > 30$

$$\frac{\Gamma}{\rho\nu} = N_{Re}/4 = (-64 + 3\, x_0^+ + 2.5\, x_0^+ \ln x_0^+)$$

For $5 < x_0^+ < 30$

$$\frac{\Gamma}{\rho\nu} = N_{Re}/4 = (12.55 - 8.05\, x_0^+ + 5\, x_0^+ \ln x_0^+)$$

For a given N_{Re}, this equation is solved by trial and error for x_0^+. Now, by eliminating τ_0 between the definition of x_0^+, Equation (38), and the force balance, Equation (3), τ_w^* may be expressed in terms of x_0^+ and x_0^*,

$$\tau_w^* = \frac{1}{(1 - \rho_v/\rho)} \; \frac{\left(x_0^+\right)^2}{\left(x_0^*\right)^2} - x_0^*$$

With the value of x_0^+ determined by the N_{Re}, and by assuming various values of x_0^*, τ_w^* can be solved for.

The above procedures for both the laminar and turbulent films will yield the predicted film thicknesses shown plotted in Figures 21 to 27.

Measured Values of Film Thickness

Measured data is contained in Table III. Pressure readings were plotted and the straight line slopes taken to give dp/dz. From Equation (71), by neglecting ρ_v compared to ρ, τ_w^* can readily be computed. Similarly x_o^* can be found from its definition and the measured values of x_o. Calculations are also included in Table III.

TABLE III

LIQUID N_{Re} = 338

Water Orifice: 0.10 in. Hg.

GPM .093

Water Temp: 73.5° F.

Water Viscosity: 1.953×10^{-5} lb-sec/ft^2

N_{Re} 338

$(g/\mu^2)^{1/3}$ 568 1/in.

Probe Wall Reading: .5265

inches H_2O below atm.						$\frac{\text{in. } H_2O}{\text{ft}}$			inches	
p_1	p_2	p_3	p_4	p_5	p_6	dp/dz	τ_w^*	Film Probe Rding	$x_o \times 10^3$	x_o^*
0	0	0	0	0	0	0	0	.502	24.5	13.90
0	0	.16	.22	.24	.35	.090	1.06	.5095	17.0	9.65
0	0	.20	.35	.42	.54	.120	1.42	.511	15.5	8.80
0	0	.41	.42	.80	1.7	.220	2.60	.5165	10.0	5.68
0	.07	.55	1.3	1.5	2.0	.418	4.94	.5178	8.7	4.94
.03	.45	1.0	1.85	2.15	2.85	.588	6.95	.5192	7.3	4.15
.45	1.4	2.9	3.7	4.4	5.15	1.175	13.90	.5209	5.6	3.18
1.5	2.7	4.5	5.9	7.3	8.2	1.575	18.63	.5216	4.9	2.78
2.7	4.25	6.9	8.75	10.5	11.7	2.175	25.70	.5221	4.5	2.55
4.5	6.6	10.2	13.1	15.4	17.1	3.150	37.30	.5223	4.2	2.38
6.9	9.9	14.9	18.5	21.6	24.3	4.200	49.60	.5229	3.6	2.04
11.35	16.1	23.55	29.2	34.3	38.9	6.330	74.90	.5231	3.4	1.93

Liquid N_{Re} = 455

Water Orifice: 0.20 in. Hg.

GPM .140

Water Temp: 70°F.

Water Viscosity: 2.034 X 10^{-5} lb-sec/ft^2

N_{Re} 455

$(g/\nu^2)^{1/3}$ 551 1/in

Probe Wall Reading: .526

inches H_2O below atm.						$\frac{\text{in. } H_2O}{\text{ft}}$			inches	
p_1	p_2	p_3	p_4	p_5	p_6	dp/dz	τ_w^*	Film Probe Rding	$x_o \times 10^3$	x_o^*
0	0	0	0	0	0	0	0	.5015	24.5	13.5
.10	.21	.11	.7[illegible]	.94	1.46	.30	3.45	.514	12.0	6.6
.12	.14	.80	.72	1.33	1.79	.40	4.60	.517	9.0	4.96
.32	.54	.83	1.87	2.13	2.88	.55	6.31	.5185	7.5	4.14
.28	.99	1.55	2.77	3.08	4.12	.80	9.19	.5195	6.5	3.58
.61	1.39	2.60	4.11	4.62	5.64	1.08	12.35	.520	6.0	3.31
1.44	2.46	[illegible].15	5.[illegible]7	6.62	7.76	1.40	16.09	.521	5.0	2.76
2.04	3.07	5.4[illegible]	7.22	8.33	9.44	1.68	19.23	.5214	4.6	2.54
2.85	4.12	7.06	9.20	10.84	11.95	1.95	22.4	.5218	4.2	2.32
3.65	5.05	8.40	10.5[illegible]	12.43	13.79	2.45	28.2	.5218	4.2	2.32
3.68	5.22	8.74	11.31	13.20	14.79	2.68	30.7	.5219	4.1	2.26
4.0	5.85	9.5	12.1	14.20	15.9	2.82	32.5	.522	4.[illegible]	2.20
11.8	15.5	23.4	28.8	34.6	38.6	6.47	74.4	.5225	3.5	1.93

Liquid N_{Re} = 581

Water Orifice: 0.30 in. Hg.

GPM .177

Water Temp: 71° F.

Water Viscosity: 2.010×10^{-5} lb-sec/ft^2

N_{Re} = 581

$(g/\nu^2)^{1/3}$ 556 1/in.

Probe Wall Reading: .5265

inches H_2O below atm.						$\frac{\text{in. } H_2O}{\text{ft}}$			inches	
p_1	p_2	p_3	p_4	p_5	p_6	dp/dz	τ_v^*	Film Probe Rding	$x_o \times 10^3$	x_o^*
0	0	0	0	0	0	0	0	.5025	24.0	13.35
0	.08	.15	.11	.37	.30	.058	.67	.5095	17.0	9.45
0	.08	.50	.28	.41	.32	.090	1.04	.5129	12.6	7.0
0	.08	.75	.35	1.0	1.1	.220	2.55	.5167	9.8	5.45
0	.08	.8	1.45	2.0	2.1	.430	4.99	.5181	8.4	4.66
0	.30	1.1	1.55	2.2	2.8	.553	6.41	.5186	7.9	4.39
0	.65	1.5	2.5	3.35	4.0	.875	10.14	.5192	7.3	4.05
.15	1.0	2.1	3.35	4.3	5.0	1.025	11.89	.520	6.5	3.61
.50	1.5	2.95	4.55	5.45	6.35	1.35	15,65	.5211	5.4	3.00
.95	2.25	4.0	5.9	7.2	8.1	1.675	19.41	.5217	4.8	2.67
1.5	3.0	4.0	6.4	9.0	10.0	2.050	23.8	.5218	4.3	2.39
3.05	5.15	8.85	11.4	13.6	15.5	2.800	32.5	.5227	3.8	2.11
4.0	6.35	10.55	13.4	15.7	18.1	3.200	37.1	.5232	3.3	1.836
6.7	10.25	16.1	20.3	24.4	28.1	4.050	47.0	.5239	2.6	1.446
9.7	14.5	22.2	27.9	33.3	38.0	5.225	60.6	.5240	2.5	1.39

Liquid N_{Re} = 641

Water Orifice: 0.40 in. Hg.

GPM .207

Water Temp 66.5° F.

Water Viscosity: 2.132×10^{-5} lb-sec/ft^2

N_{Re} 641

$(g/\nu^2)^{1/3}$ 533 1/in.

Probe Wall Reading: .526 in. (Port 2)

inches H_2O below atm.						$\frac{\text{in. } H_2O}{\text{ft}}$		inches		
P_1	P_2	P_3	P_4	P_5	P_6	dp/dz	τ_w^*	Film Probe Rding	$x_o \times 10^3$	x_o^*
0	0	0	0	0	0	0	0	.5015	24.5	13.1
0	0	.04	.32	.84	1.31	.47	5.20	.515	11.0	5.86
0	.19	1.0	.85	1.3	2.55	.52	5.73	.517	9.0	4.80
0	.8	1.6	2.15	3.4	4.4	.92	10.27	.5188	7.2	3.84
0	1.30	2.1	2.6	4.0	5.2	.98	10.92	.5194	6.6	3.52
0	1.5	2.85	3.25	4.9	6.25	1.12	12.40	.5196	6.4	3.41
.85	2.25	4.1	5.0	6.85	8.4	1.62	18.00	.5207	5.3	2.82
1.65	3.05	5.5	6.65	8.85	10.55	1.88	20.9	.5211	4.9	2.62
2.0	3.80	6.5	7.8	10.45	12.2	2.20	24.4	.5215	4.5	2.40
2.5	4.75	7.65	9.35	12.25	14.25	2.52	28.0	.5218	4.2	2.24
3.2	5.45	9.0	11.0	14.15	16.5	2.88	32.0	.5219	4.1	2.18
3.75	6.1	10.3	12.2	15.4	18.2	3.10	34.4	.5222	3.8	2.02
4.5	7.05	11.5	14.2	17.5	20.4	3.50	38.9	.5222	3.8	2.02
5.85	9.0	14.2	18.7	21.6	25.0	4.20	46.6	.5223	3.7	1.97
7.8	11.6	18.05	23.6	27.5	31.8	5.35	59.4	.5227	3.3	1.76
9.7	14.1	21.7	27.4	32.9	37.3	6.28	69.7	.5225	3.5	1.87

Liquid N_{Re} = 747

Water Orifice: 0.50 in. Hg.

GPM .233

Water Temp: 69° F.

Water Viscosity 2.060×10^{-5} lb-sec/ft^2

N_{Re} 747

$(g/\mu^2)^{1/3}$ 546 1/in.

Probe Wall Reading: .5262

inches H_2O below atm.						$\frac{\text{in. } H_2O}{\text{ft}}$			inches	
P_1	P_2	P_3	P_4	P_5	P_6	dp/dz	τ_w^*	Film Probe Rding	$x_o \times 10^3$	x_o^*
0	0	0	0	0	0	0	0	.5015	24.7	13.5
0	0	.03	.27	.21	.08	.05	.57	.5071	19.1	10.43
0	0	.05	.52	.34	.08	.09	1.02	.5111	15.1	8.25
0	0	.03	.75	1.08	.71	.152	1.34	.5150	11.2	6.11
0	0	.22	.72	1.09	1.3	.275	3.13	.517	9.2	5.02
0	.08	.69	1.17	1.98	2.31	.492	5.61	.518	8.2	4.48
0	.34	1.10	1.96	2.51	3.31	.725	8.35	.519	7.2	3.93
0	.82	1.85	3.1	4.05	4.9	1.05	11.95	.5198	6.4	3.50
.5	1.65	3.3	5.0	6.3	7.3	1.50	17.09	.5209	5.3	2.90
1.3	2.9	5.2	7.5	9.15	10.45	2.15	24.5	.5211	5.1	2.79
2.35	4.35	7.9	10.4	12.45	14.3	2.775	31.6	.5215	4.6	2.52
4.0	6.75	11.2	14.6	17.5	20.55	3.675	41.8	.5220	4.2	2.29
5.85	9.4	15.1	19.4	23.45	27.3	4.625	52.6	.5222	4.0	2.18
9.0	14.1	21.95	28.2	34.0	39.1	6.075	69.1	.5228	3.4	1.86

Liquid N_{Re} = 833

Water Orifice: 0.60 in. Hg.

GPM .260

Water Temp: 69° F.

Water Viscosity: 2.060×10^{-5} lb-sec/ft^2

N_{Re} 833

$(g/\mu^2)^{1/3}$ 546 1/in.

Probe Wall Reading: .526

inches H_2O below atm.						$\frac{\text{in. } H_2O}{\text{ft}}$			inches	
p_1	p_2	p_3	p_4	p_5	p_6	dp/dz	τ_w^*	Film Probe Rding	$x_o \times 10^3$	x_o^*
0	0	0	0	0	0	0	0	.5025	23.5	12.83
.20	0	.35	0	.63	.60	.100	1.14	.513	13.0	7.1
.3	00	.6	.85	1.5	1.6	.275	3.13	.516	10.0	5.46
.45	0	.6	1.4	2.1	2.9	.500	5.70	.517	9.0	4.91
.50	.50	1.4	2.5	3.5	4.2	.800	9.11	.519	7.0	3.82
.45	.80	2.05	3.3	4.4	5.2	1.025	11.69	.520	6.0	3.28
-	1.15	2.5	4.0	5.2	6.2	1.225	13.96	.5203	5.7	3.12
-	1.55	3.15	4.8	6.2	7.25	1.525	17.39	.5208	5.2	2.84
.65	2.05	3.9	5.8	7.4	8.7	1.825	20.8	.5209	5.1	2.78
1.1	2.60	4.85	6.95	8.95	10.25	2.20	25.1	.5210	5.0	2.73
1.65	3.5	6.2	8.8	10.85	12.45	2.75	31.3	.5215	4.5	2.46
2.85	5.25	9.05	12.2	14.6	17.1	3.60	41.0	.5222	3.8	2.08
5.15	8.2	13.55	17.5	21.3	24.9	4.625	52.6	.5225	3.5	1.91
9.45	13.45	21.35	27.6	33.0	38.0	6.575	76.0	.5228	3.2	1.75

Liquid N_{Re} = 2680

Water Orifice: 6.42 in. Hg.

GPM .832

Water Temp: 69° F.

Water Viscosity: 2.05×10^{-5} lb-sec/ft^2

N_{Re} 2680

$(g/\nu^2)^{1/3}$ 550 1/in.

Probe Wall Reading: .525

inches H_2O below atm.						in. H_2O / ft			inches	
p_1	p_2	p_3	p_4	p_5	p_6	dp/dz	$\tau_{\sim}^{*}$	Film Probe Rding	$x_o \times 10^3$	x_o^{*}
0	0	0	0	0	0	0	0	.503	22	12.1
.19	.08	.17	.27	.58	.97	.33	3.78	.510	15	8.25
.23	.27	.57	1.1	2.40	3.19	.77	8.79	.5145	10.5	5.78
.30	1.10	1.95	3.65	4.7	6.2	1.33	15.22	.5165	8.5	4.67
.30	2.2	3.90	6.1	7.8	9.9	1.97	22.7	.519	6	3.30
.50	3.65	6.3	8.9	11.7	14.8	2.70	30.9	.520	5	2.75
1.10	4.4	7.9	11.3	14.6	18.5	3.43	39.3	.5205	4.5	2.48
2.05	5.7	9.65	13.7	18.0	22.8	4.37	50.1	.521	4	2.20
3.6	7.6	12.55	18.2	23.8	30.3	5.60	64.1	.5215	3.5	1.925
4.25	10.1	16.0	23.0	29.0	37.9	7.10	81.4	.522	3	1.650

APPENDIX D

BIBLIOGRAPHY

(1) Nusselt, W., "Die Oberflachenkondensation des Wasserdamfes", Zeitschrift Vereines Deutscher Ingenieure, 60, 1916, pp. 541-569.

(2) Kirkbride, C.G., "Heat Transfer by Condensing Vapor on Vertical Tubes", Trans. American Institute of Chemical Engineers, 30, 1933-34, pp. 170-186.

(3) Carpenter, F.G., "Heat Transfer and Pressure Drop for Condensing Pure Vapors Inside Vertical Tubes at High Vapor Velocities", PhD thesis, University of Delaware, 1948.

(4) Tepe, J.B., and Mueller, A.C., "Condensation and Subcooling Inside an Inclined Tube", Chemical Engineering Progress, 43, May 1947, p. 267.

(5) Colburn, A.P., "Problems in Design and Research on Condensers of Vapours and Vapour Mixtures", General Discussion on Heat Transfer, Sept. 1951, published by the Institute of Mechanical Engineers, pp. 1 - 11.

(6) Rohsenow, W.M., "Heat Transfer and Temperature Distribution in Laminar Film Condensation", paper presented before A.S.M.E., Dec. 1954.

(7) Colburn, A.P., Millar, L.L., Westwater, J.W., "Condenser Subcooler Performance and Design", Trans. American Institute of Chemical Engineers, 38, 1942, pp. 447-464.

(8) Colburn, A.P., "Calculation of Condensation with a Portion of the Condensate Layer in Turbulent Motion", Trans. American Society of Chemical Engineers, 30, 1933-34, pp. 187-193.

(9) Carpenter, E.F. and Colburn, A.P., "The Effect of Vapor Velocity on Condensation Inside Tubes", General Discussion on Heat Transfer, Sept. 1951, published by the Institute of Mechanical Engineers, pp. 20 - 26.

(10) Seban, R.A., "Remarks on Film Condensation With Turbulent Flow", Trans. American Society of Mechanical Engineers, 76, 1954, pp. 299-303.

(11) Bergelin, Kegel, Carpenter, and Gayley, "Co-Current Gas-Liquid Flow in Vertical Tubes", Fluid Mechanics and Heat Transfer Institute, Berkeley,California, 1949, published by the American Society of Mechanical Engineers, pp. 19-28.

(12) McAdams, W.H., "Heat Transmission", 3rd Edition, McGraw-Hill, 1954, pp. 245.

(13) Monrad, C.C. and Badger, W.L., Trans. American Institute of Chemical Engineers, 24, 1930, pp. 84-119.

(14) Von Karman, Th, "Analogy Between Fluid Friction and Heat Transfer", Trans. American Society of Mechanical Engineers, 61, 1939, pp. 205-210.

(15) Wurster, A., in "Discussion", Trans. American Institute of Chemical Engineers, 38, 1942, pp. 464-468.

(16) Klingaman, David, S.M. Thesis, Naval Architecture and Marine Engineering Department, M.I.T., in preparation.

(17) Hebbard, G.M. and Badger, W.L. "Steam Film Heat Transfer Coefficients for Vertical Tubes", Industrial and Engineering Chemistry, 26, 1934, pp. 420-424.

(18) Cooper, C.M., Drew, T.B. and McAdams, W.H., "Isothermal Flow of Liquid Layers", Industrial and Engineering Chemistry, 26, 1934, pp. 428-431.

(19) Jakob and Erk, "Heat Transfer with Condensing Superheated and Saturated Steam", Forschungsarbeiten, V. d. I. No. 310.

(20) Baum, S., "Heat Transfer Coefficients in a Falling Film Heater" - M.S. Thesis, 1936, Chemical Engineering Department, M. I. T.

(21) Bays, G.S. and Blenderman, L.M., "Heat Transfer Coefficients in a Falling Film Condenser", M.S. Thesis, 1935, Chemical Engineering Department, M. I. T.

(22) Bays, G.S., "Heat Transfer in Falling Film Heaters", Sc.D. Thesis, 1936, Chemical Engineering Department, M. I. T.

(23) Bays, G.S., and McAdams, W.H., "Heat Transfer Coefficients in Falling Film Heaters", Industrial and Engineering Chemistry, 29, 1937, pp. 1240-1246.

(24) Fentress, C.D., "Heat Transmission in a Vertical Falling Film Condenser", M. S. Thesis, 1935, Chemical Engineering Department, M. I. T.

(25) Leavitt, S.T., "Overall Heat Transfer Coefficients From the Dropwise Condensation of Steam in a Falling Film Condenser", B.S. Thesis, 1935, Business and Engineering Administration Department, M. I. T.

(26) McAdams, W.H., Drew, T.B., and Bays, G.S., "Heat Transfer to Falling Film Heaters", Trans. American Society of Mechanical Engineers, 62, 1940, pp. 627-631.

(27) Rohsenow, W.M., Webber, J.H. and Ling, A.T., "Effect of Vapor Velocity on Laminar and Turbulent Film Condensation", paper presented before American Society of Mechanical Engineers, Dec. 1954.

Thesis
W33 Webber 28996
Effect of vapor velocity
on film condensation.

Thesis
W33 Webber 28996
Effect of vapor velocity on
film condensation.

thesW33
Effect of vapor velocity on film condens

3 2768 001 95139 5
DUDLEY KNOX LIBRARY